DANISH METEOROLOGICAL INSTITUTE

SCIENTIFIC REPORT

91-3

The Geomagnetic Activity Index PC

by

Susanne Vennerstrøm

Ph.D. Thesis
Presented to

Geophysical Institute
University of Copenhagen

DMI

COPENHAGEN 1991

Available for sale and on exchange from
DMI Library
Danish Meteorological Institute
Lyngbyvej 100, DK-2100 Copenhagen Ø
Denmark

ISBN 87 7478 303 3

CONTENTS

I. INTRODUCTION

The PC-index is an index for geomagnetic activity which aims to monitor the activity in the (P)olar (C)ap. In the polar regions of the Earth's magnetosphere and ionosphere there exists a variety of different electric current systems, all of which contribute to the magnetic perturbation measured at the surface of the Earth. When constructing an index, it is therefore very important to make quite clear what type of activity it is aimed to monitor. One current system existing in the polar regions, which is well documented is the two cell equivalent current system illustrated in Figure I.1.

Figure I.1

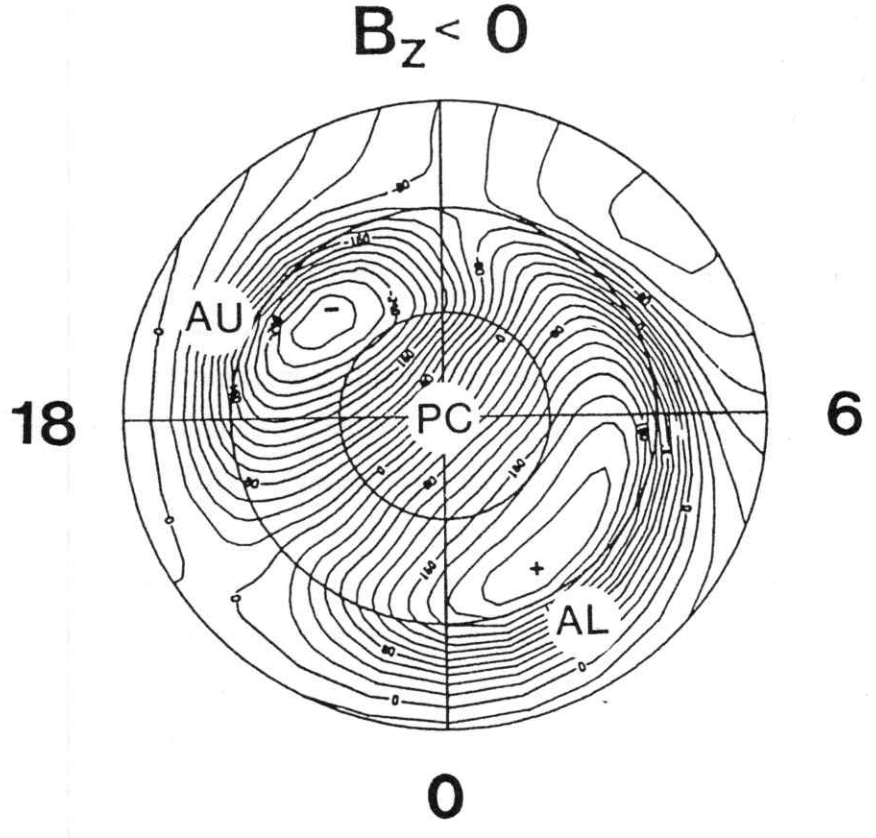

Polar diagram of the equivalent current system when $B_z<0$ and $B_y\approx0$, calculated by means of an empirical model of magnetic variations. Reproduced from Friis-Christensen et al. [1985].

It consists of a sunward current across the polar cap and two antisunward currents, the eastward and westward electrojets, in the auroral region. The eastward and westward electrojets are presently being monitored by the auroral zone magnetic activity indices AU and AL, by a ring of observatories in the auroral zone.

In 1979 Troshichev et al. [1979] proposed to make an index which should monitor the sunward equivalent current crossing the polar cap. A station in the polar cap which is located very close to the pole will, although the Earth is rotating under the two cell pattern, all the time be located under the sunward part of the current system. The idea was, therefore, to base the index on measurements from a single near pole station. The station Thule, which is run by the Danish Meteorological Institute and located in the Greenlandic village Qaanaaq at 86.5 degrees geomagnetic invariant latitude, fulfills the requirement of being close to the pole. The station Vostok, at -83.3 degrees and run by the Arctic and Antarctic Research Institute in Leningrad, does the same in the southern hemisphere. We have examined the magnetic perturbations at these two stations (Vennerstrøm and Friis-Christensen [1987], Troshichev et al. [1988], Vennerstrøm et al. [1990]) and proposed an algorithm for such an index. Here we report mainly on the results from Thule.

It is well known that the interplanetary magnetic field (IMF) plays an important role in the generation of electric currents in the polar regions of the ionosphere and magnetosphere, and especially the southward component of the IMF is known to be effective in generating the two cell system. We have, therefore, examined the correlation between the IMF and the magnetic perturbation at the near pole station Thule and find linear correlation coefficients as high as 0.7 - 0.8. This result ensures that the station measures a parameter fundamental to the current system. When designing an index, it is not enough to make clear what current system it aims to monitor. It is equally important to examine how other current systems influence or disturb the index. In the polar region two other current systems are known to exist which are closely related to the IMF: The cusp current, which is mainly controlled by the east-west component of the IMF, and a current system observed at very high latitudes within the polar cap, which is controlled by the northward component of the IMF. We have therefore also investigated the relationship between the perturbation in Thule and the east-west and northward components of the IMF, and conclude that both components contribute

significantly to the perturbation. These current systems can therefore disturb the PC-index significantly. Fortunately they are mainly observed during summer. During winter, they are only in very rare cases large enough to give a significant contribution to the magnetic perturbation on ground.

The sources to magnetic perturbations in the near pole region are believed partly to be due to ionospheric Hall-currents in the polar cap, and partly to be due to distant field-aligned currents at the poleward rim of the auroral oval. The field-aligned currents at the rim of the oval are on the other hand intimately related to the ionospheric auroral electrojets. One should therefore expect some relation between the auroral electrojet indices AL, AU and AE and the PC-index, especially during winter when the ionospheric conductivity in the polar cap is at minimum. We have therefore made a statistical analysis of the relation between PC and AE, AU and AL, in order to judge to which extent PC can be used as an alternative indicator of the level of activity in the auroral electrojets, and to elucidate some of the differences between the indices. There are two major problems one encounters using AE, AU and AL, where one could imagine the PC-index could be useful:

- AE, AU and AL are only available with a time delay of several years. They are derived from data from 12 observatories, some of which are still in analogue form; and the digitizing and data quality control is a long and slow procedure. The PC-index, on the other hand, is derived from data from a single station and can therefore be calculated and published very quickly.

- The auroral electrojet indices can only be derived for the northern hemisphere auroral oval. The geography of the Antarctic continent makes it impossible to place a ring of observatories in the auroral regions in the southern hemisphere. The PC-index, however, could be derived for both the northern and southern hemisphere.

We have examined the linear correlation between PC and AE, AL and AU and find a surprisingly high correlation coefficient R. The correlation is best with AE and during winter, where we on the basis of 15 minute averages find R = 0.8-0.9. We find that this correlation is sufficiently high to ensure that the single station index PC actually measures

something global and not mainly local phenomena. We conclude that the PC-index can be used during winter and equinox as a fast available indicator of the "global" activity in the auroral oval. Apart from being available years before AE, PC could also be computed for periods in the past where AE for different reasons is not available.

Finally we have examined long-term variations of the PC-index within the last solar cycle from 1975-85. We find that the long-term variations of PC is very similar to the long-term variation of other indices such as AE and the midlatitude index A_p. An analysis of the long-term variations of the solar wind parameters furthermore shows that the southward component of the IMF and the solar wind velocity is effective in generating geomagnetic activity on long, as well as on short, time-scales.

II. SOLAR WIND CONTROL OF NEAR POLE MAGNETIC VARIATIONS

II.1 The main controlling factor

The interplanetary magnetic field (IMF) is known to be intimately related to the generation of electric currents in the polar region of the ionosphere and magnetosphere. The nature of this relationship is, however, not yet clear, although it seems to be widely accepted that magnetic merging plays an important role.

Consequently, several statistical analyses have been made trying to relate measurements of the IMF with various geomagnetic indices (see e.g. Baker et al., 1983 and the many references therein), and it has been thoroughly demonstrated that the southward component of the IMF B_s sets up a two cell convection and equivalent current pattern in the polar regions, the strength of which is approximately proportional to the magnitude of B_s.

This two cell pattern is, in merging theories, explained by Dungey's classical picture: Merging on the closed field lines on the dayside, cross polar flow on open field lines, reconnection in the tail, and return flow on closed field lines in the auroral regions.

B_s is known to give the main contribution to the strength of the two cell currents, but also the solar wind velocity and the east-west component of the IMF has been found to give a contribution. Consequently, several parameters have been proposed to describe the essence of the generation mechanisms, all of which includes the southward component of the IMF: B_z, vB_z, vB_s, v^2B_s, $vB_T\sin^2(\theta/2)$, vB_T, and $v(B_z^2+B_y^2+B_x^2)\sin^4(\theta/2)$, where v is the solar wind velocity, B_y the azimuthal, B_z the vertical and B_s the southward component of the IMF, B_T is equal to $(B_z^2+B_y^2)^{\frac{1}{2}}$, and θ is the angle between the IMF and the Earth magnetic field at the subsolar point of the magnetopause (assumed to be northward). The last parameter is the ϵ parameter defined in Akasofu [1979].

Troshichev and Andrezen [1985] investigated the relationship between most of these IMF-parameters and the magnetic activity in the near pole region in the southern hemisphere. This was the first statistical investigation of a PC-index based on a single near pole station, and we shall, therefore, describe their results in some detail. The statistical method used was a linear correlation analysis, and the geomagnetic parameter was the so-called MAGPC-index derived from the near pole station Vostok at Antarctica. The MAGPC-index was computed by projecting the measured horizontal perturbation onto the 03 - 15 MLT meridian. The idea was to get a measure of the cross polar cap current in the two cell equivalent current system, and in order to take into account that the two cell system is skewed compared to the noon-midnight meridian, the 03 - 15 meridian was selected for projection instead of the dawn-dusk meridian. The analysis was limited to summer data. They divided their data into two groups according to the sign of B_z. For B_z negative they found a reasonably high correlation for most IMF-parameters, the best being obtained with the parameters vB_z and $vB_T\sin^2(\theta/2)$, giving a linear correlation coefficient R close to 0.6. When B_z was positive, a very poor correlation was found for all IMF-parameters. Here the best correlation was obtained with $vB_T\sin^2(\theta/2)$ giving R = 0.3. The numbers quoted are daily averages. The time-scale used was 15 minute averages, and a time delay of 20 minutes was introduced between the IMF measurements and the response in Vostok.

The station Thule has the advantage over Vostok that we have a larger data base, including digital data from all seasons, almost unbroken from 1975 till now. We can therefore use Thule data to get a more extensive and profound analysis of the relation between near pole magnetic variations and the IMF. In Troshichev and Andrezen [1985] only data during summer, where the near pole region is almost completely sunlit, was used. Here we include data from all year, but since the ionospheric conductivity in the near pole region to a high extent is created by solar UV-radiation, we expect the correlation and also the size of the response in Thule to a given size of the IMF to vary throughout the year. We therefore divide the data according to month of the year. Troshichev and Andrezen [1985] found that the correlation varied with local time of the station, so, following their analysis, we divide the data according to hour of local time. We also use the same

time-scale (15 min averages) and the same time delay (20 minutes) between the variations in the solar wind and Thule.

One way to try to single out a specific type of magnetic activity is to project the total measured perturbation onto the direction, in which this type of activity typically is observed. Applying this method here, means that we should project the measured perturbation onto a direction, perpendicular to the direction in which the cross polar cap current in the two cell pattern is typically flowing. In Troshichev and Andrezen [1985] this is done by choosing a specific meridian onto which to project, namely, the 03 - 15 MLT meridian. In this work we use the statistical analysis itself to define the direction. We simply choose the direction that gives the highest correlation with the IMF-parameter under consideration. This enables us to let the direction vary both with local time of the station and with season. For each month and each hour of local time, we project the measured horizontal perturbation on to various directions, with a projection angle varying from -90 to 90 degrees in 5 degree intervals.

The projection procedure can be described by the following formula:

$$\Delta F = \Delta H \sin\gamma \pm \Delta D \cos\gamma$$
$$\gamma = \lambda \pm Dec + UT + \varphi$$

When $\pm$ is indicated + must be used for the southern hemisphere and - for the northern hemisphere. (H,D) are the two components of the horizontal perturbation. H is directed northward along the local magnetic meridian and D is perpendicular to H pointing eastward. (ΔH, ΔD) are the deviations of H and D from quiet level. Dec is the declination, UT is universal time and λ is the longitude of the station. Expressed like this φ will represent the angle between the dawn-dusk meridian and the projection direction. We then perform the computation, letting φ vary from -90 to 90 degrees in 5 degree intervals, for each hour of local time and each month separately. For each computation we derive the linear correlation coefficient R, and for each month and each hour of local time we then choose the direction which gives the highest correlation with the given IMF-parameter. The resultant directions is thus a function of both month, local time and given IMF-parameter.

Table II.1 lists the coefficients of correlation for different IMF-parameters averaged over month and local time. Since the sign of B_z is known to be important, we have performed the regression for all B_z, B_z negative and B_z positive separately. The IMF data used was IMP-8 measurements during the IMS-period 1977-80. Each coefficient of correlation R(LT, month) is based on roughly 125 data points (all B_z), so the averages given in the table is based on around 36,000 data points.

Table II.1 Average coefficient of correlation, R

Parameter	All B_z	$B_z<0$	$B_z>0$
B_z	-0.71	-0.64	-0.45
vB_z	-0.71	-0.71	-0.45
vB_s	0.74	0.71	
v^2B_s	0.75	0.73	
$vB_T\sin^2(\theta/2)$	0.77	0.74	0.56
ϵ	0.72	0.67	0.55

It is seen that using this method we obtain higher correlations than Troshichev and Andrezen [1985], but their general results are confirmed: All parameters involving the southward component give a good correlation, and the correlation coefficients are higher for B_z negative than B_z positive. It is seen that the correlation is increasing, when the solar wind velocity and the azimuthal component is included in the parameter. The highest correlation is thus obtained with the parameter $vB_T\sin^2(\theta/2)$ derived by Kan and Lee [1979] for the merging electric field.

The size of the response on ground to a given IMF is, as we shall see, both seasonal and diurnal dependent, but the maximal coefficient of correlation R is found to be rather uniform. Figure II.1 shows a contour plot of R as function of UT and month. It is seen that R $\approx$ 0.75 - 0.80 at all local times and all months except for a small minimum with R = 0.7 at noon during midsummer (geographic local noon in Thule is around 16.30 UT).

Figure II.1

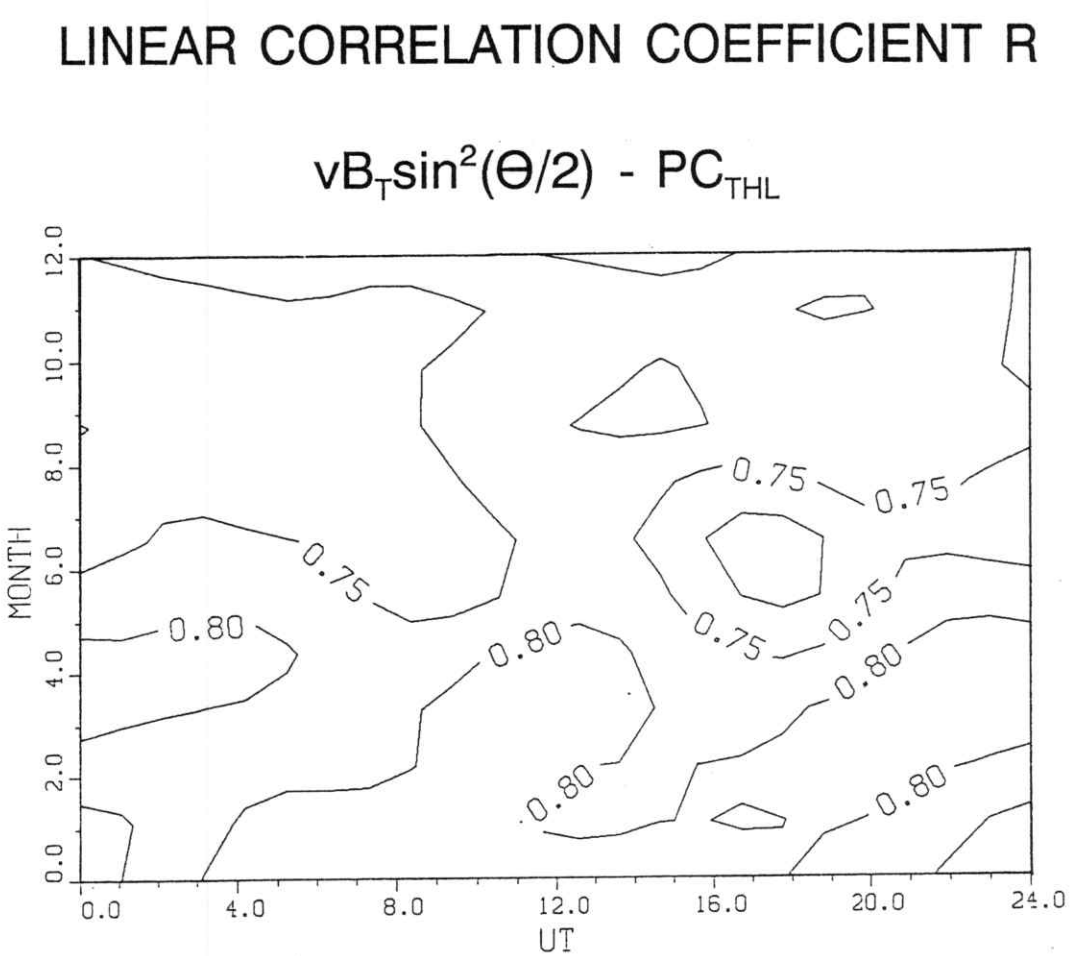

Contour diagram of the linear correlation coefficient between the IMF-parameter $vB_T\sin^2(\theta/2)$ and the horizontal magnetic perturbation in Thule projected onto the direction that maximizes the correlation.

Figure II.2 shows the directions that give maximum correlation with various IMF-parameters. The diagrams are MLT-invariant latitude, and the angle φ of formula II.1 is indicated at the figure. It is seen that the directions varies throughout the day, but rather similarly for all parameters.

Figure II.2

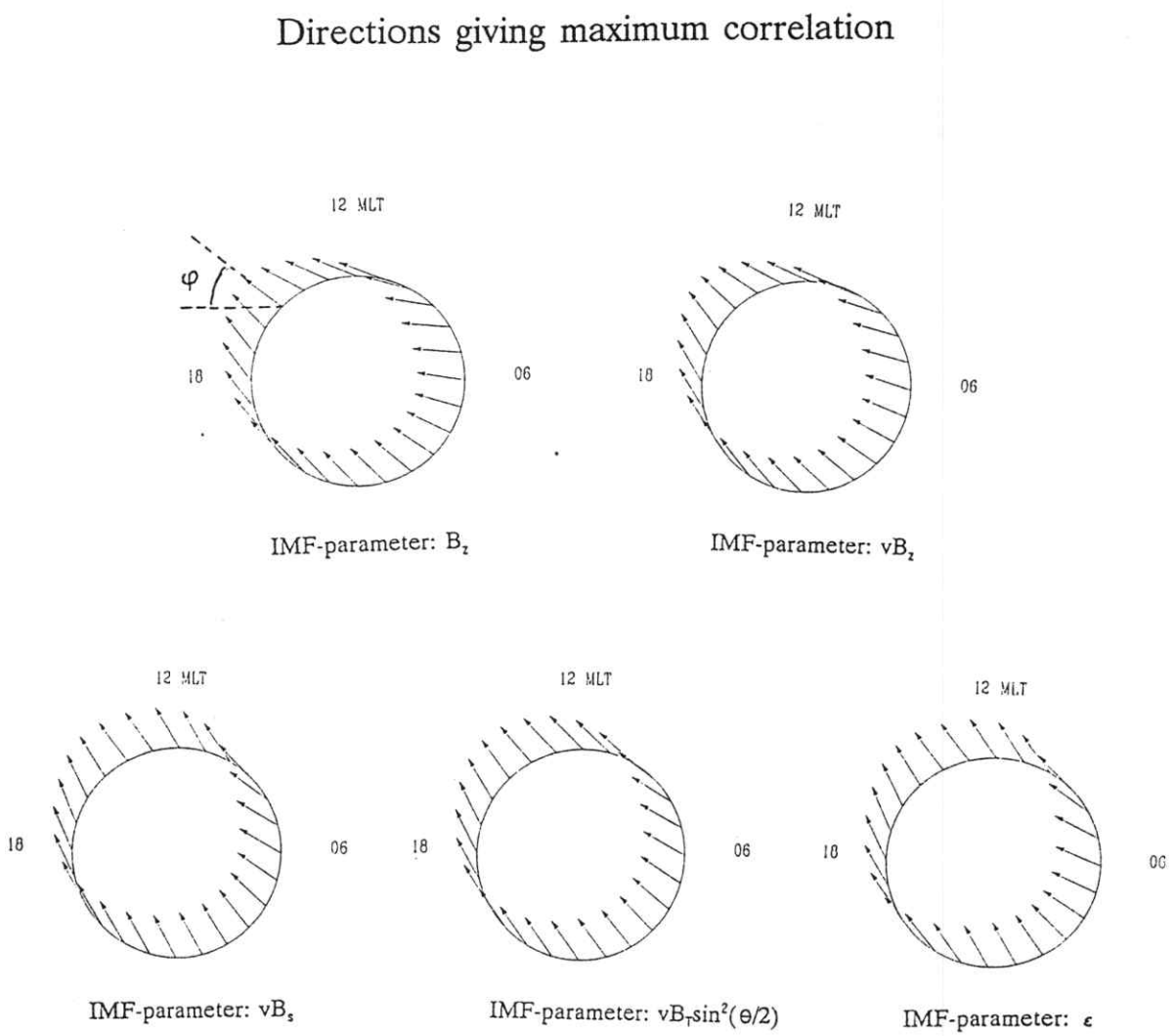

Polar diagrams (invariant latitude-MLT) showing the directions onto which the horizontal perturbation in Thule should be projected to obtain maximum correlation with various IMF-parameters.

Figure II.2 only shows the results from April, but the trend is the same for all months. The largest deviation is found for the parameters B_z and vB_z, i.e. those parameters where the correlation with the *northward* component as well as with the southward component is included in the derivation of the angles. In Table II.2 we list the diurnal and seasonal averages of the optimal angles. The results are given for B_z negative and positive separately, as well as for all B_z-values.

Table II.2 Average optimal angle φ (deg.)

Parameter	All B_z	$B_z<0$	$B_z>0$
B_z	33	46	-164
vB_z	34	48	-169
vB_s	46	48	
v^2B_s	46	46	
$vB_T\sin^2(\theta/2)$	48	45	36
ϵ	45	45	34

It is clear from this table that the IMF *conditions*, i.e. the sign of B_z is far more important than which specific IMF-parameter is being used. Looking at the column showing all B_z-values, we only find significant differences for B_z and vB_z, and these differences disappear if we only look at the B_z negative cases.

We thus conclude that the sign of B_z is the most important factor in the IMF control of near pole magnetic variations. When B_z is southward, we find a good correlation with all parameters that includes B_s, whereas when B_z is northward, the correlation is poor for all

parameters. The high correlation obtained for B_z southward indicates that it is possible to define a PC-index that monitors the currents generated by B_s, by using the projection method at a single near pole station. The poor results for B_z northward, on the other hand, rules out the possibility to monitor the polar cap current, controlled by the northward component, by this method.

II.2 The influence of IMF B_y

II.2.1 Does B_y contribute to the two cell current?

The two cell pattern is in merging theories explained by Dungey's classical picture: Merging on the closed field lines on the dayside, cross polar flow on the open field lines, and return flow on the closed field lines in the auroral region. If one analyzes the merging concept in connection with the solar wind-magnetosphere interaction a bit further, however, two important aspects are noted:

1. The earth magnetic field at the magnetopause and the IMF does not have to be completely antiparallel for merging to occur (see e.g. Sonnerup [1974]).

2. There is a possibility that merging also occurs at other parts of the magnetopause than the subsolar region, which means that we can expect merging in regions, where the earth magnetic field is not strictly northward [Crooker, 1979].

Both of these aspects mean that not only the southward component B_s but also the azimuthal component B_y should play a role in generating the two cell current pattern. This influence should show up in two ways. The relative size, and especially the sign of B_z and

B_y, should control the location of the merging line at the magnetopause, and thereby control the *direction* of the resulting cross polar cap flow in the ionosphere. The magnitude of B_y should, however, also influence the *magnitude* of flow; the larger $|B_y|$ the larger flow.

Several observations (e.g. Friis-Christensen et al. [1985]) have indicated that near pole magnetic perturbations change direction with the IMF B_y component, and recently also satellite observations of the ionospheric electric field confirm this trend (Heppner and Maynard [1987]).

The effect of $|B_y|$ on the size of the perturbations have been less obvious and more controversial. The first observational indication was found by Nishida and Maezawa [1971] in a study of the correlation between the IMF and the magnetic variations in the near pole station Alert for selected days. They found that the parameter $(B_z^2+B_y^2)^{\frac{1}{2}}\sin^2(\theta/2)$ had a good correlation with typical variations in the two cell activity. They found a correlation that was just as good as that of B_z. In Vennerstrøm and Friis-Christensen [1987] this point was investigated by examining the relationship between a MAGPC-index in Thule and the solar wind parameters B_z, B_y and v. The MAGPC-index was obtained by projecting the horizontal perturbation onto the 03 -15 MLT meridian, like in Troshichev and Andrezen [1985]. In order to treat all data points in one analysis we had to correct for diurnal variations in the MAGPC-index. These variations can be seen as a varying response on ground to a constant IMF-parameter and are mainly caused by varying ionospheric conductivity, as a result of impact of solar UV radiation. The diurnal variations was removed by computing the linear regression coefficient α between the projected horizontal perturbation ΔF and B_z as a function of month and local time:

$$\Delta F = \alpha(B_z+K)$$

The corrected index named NPC was then obtained by dividing with α:

$$NPC = \Delta F/\alpha(\text{month,LT})$$

Figure II.3

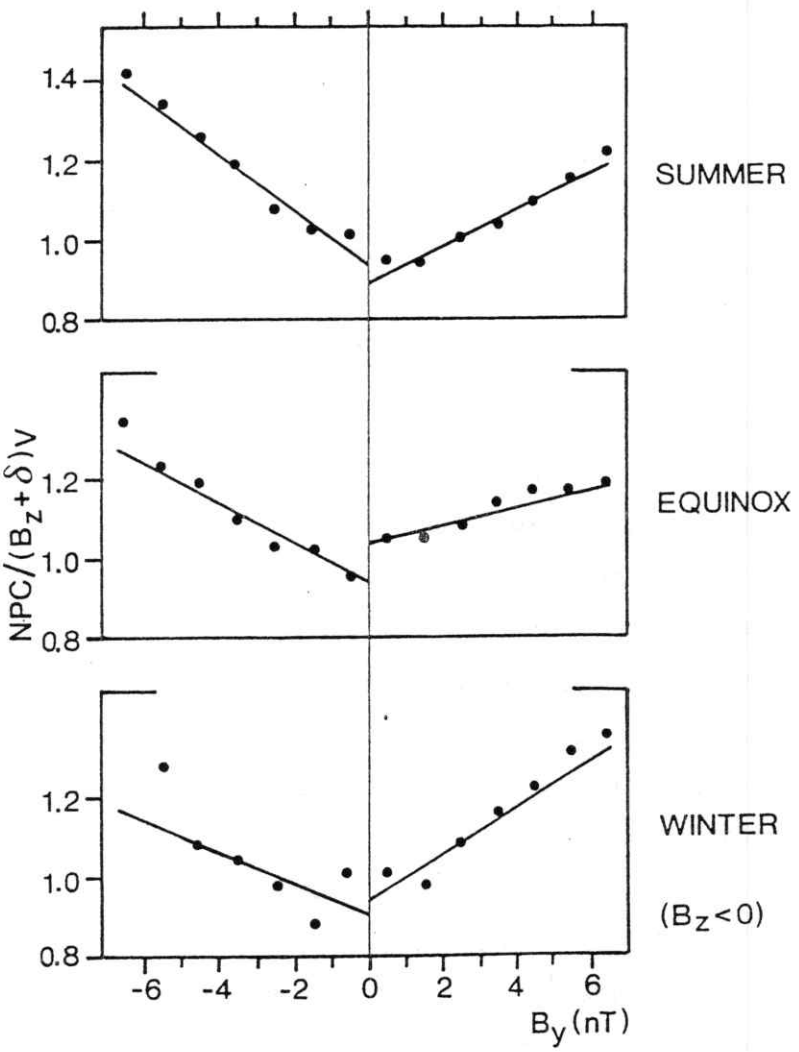

Linear regression lines of the parameter NPC/v($B_z+\delta$) versus B_y for three different seasons. The regression lines were made separately for $B_y<0$ and $B_y>0$. The points represents averages of width 1nT in B_y. The regression lines were made on the original data points. (Reproduced from Vennerstrøm and Friis-Christensen [1987]).

Figure II.4

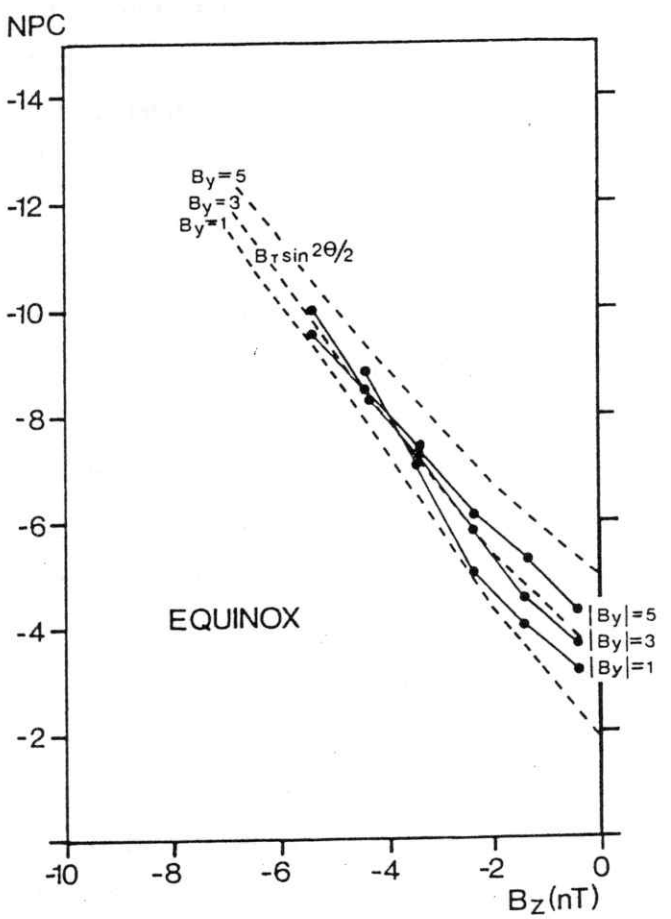

The solid lines show the corrected index NPC as a function of B_z using $|B_y|$ as a parameter. The points represent averages within a mesh of 1nT width in B_z and 2nT width in B_y. The dashed lines show the function

$$f(B_y,B_z) = a(B_z^2+B_y^2)^{\frac{1}{4}}\sin^2(\theta/2)+b$$

using B_y as a parameter. a and b were determined through a linear fit between the data with $2nT<|B_y|<4nT$ and the dashed curve marked $B_y = 3$. (Reproduced from Vennerstrøm and Friis-Christensen [1987]).

The analysis only included negative B_z values. NPC was then corrected for the influence B_z and v, by performing a linear regression between NPC/v and B_z:

$$NPC/v = K(B_z + \delta)$$

and the parameter $NPC/v \cdot (B_z + \delta)$ was computed and used in a linear correlation analysis with B_y. Since we expect the sources to near pole magnetic perturbations to change with season, the data was divided into summer, equinox, and winter. The results are reproduced in Figure II.3. It is clear from this that there is a $|B_y|$-effect on the MAGPC-index for all seasons.

This effect was investigated further by plotting NPC as a function of B_z using $|B_y|$ as a parameter. The results are reproduced in Figure II.4. On top of the data is plotted the function $f(B_y,B_z) = B_T \sin^2(\theta/2)$ also using $|B_y|$ as a parameter. It is seen that the $|B_y|$-effect is larger in the theoretical expression than in the data; and also that the $|B_y|$-effect seems to vanish at large negative values of B_z. It was therefore concluded that a $|B_y|$-effect on the MAGPC-index existed but was only about half the size of the effect in the theoretical expression $B_T \sin^2(\theta/2)$. It was further noted that, at least in that data-set, the effect seemed to vanish for large negative B_z.

One problem of the analysis of the MAGPC-index is, that it does not take into account, that the direction of the flow is changing with the sign of B_y. The MAGPC-index is computed by projecting the measured perturbation onto a fixed direction, assumed to be the flow direction. If the flow therefore change direction with growing B_y, the examination of the MAGPC-index would tend to underestimate the contribution from B_y. This point have been examined, using the procedure of optimization of correlation, by dividing the data according to the sign of B_y. The result is shown in Figure II.5, where the optimal directions for the two parameters vB_z and $vB_T \sin^2(\theta/2)$ is seen in respectively the left and right panel. The solid lines indicate the results for B_y positive and the dashed lines the result for B_y negative.

Figure II.5

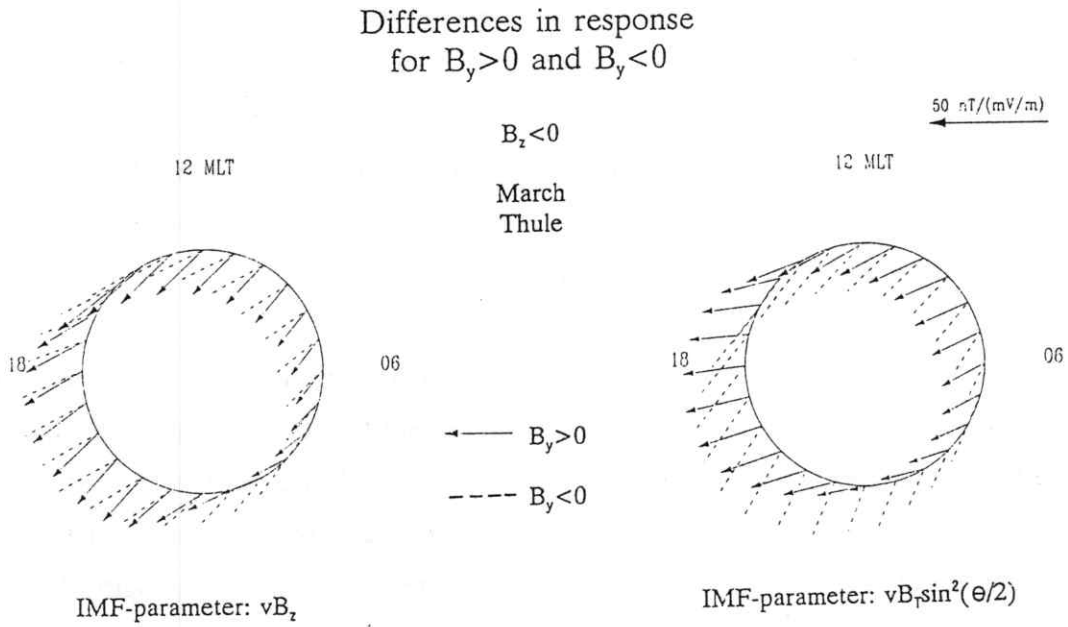

Polar diagrams showing the directions onto which to project the horizontal perturbation in Thule to obtain maximum correlation with the IMF-parameters vB_z (left) adn $vB_T\sin^2(\theta/2)$ (right). The solid vectors indicate the directions obtained for B_y positive, and the dashed lines the directions for B_y negative. The size of the vectors is a measure of the size of the response in Thule to a given size of the IMF-paramter. The results shown are for March, but the trend described in the text is similar for all months.

It is seen that the result is different for the two parameters vB_z and $vB_T\sin^2(\theta/2)$. For $vB_T\sin^2(\theta/2)$, the optimal angle is deflected westward for B_y positive and eastward for B_y negative, and the resulting patterns are in good accordance with the results found for the ionospheric electric field by Heppner and Maynard [1987]. When the parameter vB_z, however, is used in the optimization procedure, the deflections are smaller and in the opposite direction. Here the deflection is westward for B_y negative and (mainly) eastward for B_y positive. We believe the reason is that B_y gives a real contribution to the total current, but in different directions for B_y positive and negative. The main difference between vB_z

and $vB_T\sin^2(\theta/2)$ is that B_y is included in the latter. Therefore, when $vB_T\sin^2(\theta/2)$ is used, the optimization procedure will tend to find a direction that includes the contribution from B_y. When vB_z is used, the procedure will only take the B_z contribution into account, and instead of taking the B_y contribution into account, it will do the opposite, namely, find a direction that minimizes the "disturbing" influence of B_y. This means that it will have a tendency to pick directions perpendicular to the B_y contribution. When $vB_T\sin^2(\theta/2)$ is used, both the contribution from B_z and B_y is taken into account and the optimal directions, therefore, come close to the actual directions of the current.

There has been speculation on whether B_y gives a real contribution to the currents, or whether it merely influences the structure of the current system, without influencing the strength of the currents. We believe that both the effect of $|B_y|$ on the MAGPC-index and the above results prove that B_y gives a real contribution to the currents. If the role of B_y merely was to change the direction of the current pattern, the strength of which was determined by vB_s, the results of Figure II.5 for vB_z would be similar to the results for $vB_T\sin^2(\theta/2)$ and reflect the actual directions of the flow, instead of producing opposite deflections.

To investigate the effect of B_y further, we have computed the directions for optimal linear correlation with B_y, i.e. we have followed the procedure described in section II.1, but instead of using vB_z or $vB_T\sin^2(\theta/2)$, we have simply used B_y as IMF-parameter. Knowing, from the above analysis, that the direction is different for B_y positive and negative we have divided the data accordingly. The results are seen at Figure II.6 in a diagram similar to the previous figures. Like in Figure II.5 the size of the vectors is a measure of the size of the response.

Figure II.6

Response to B_y

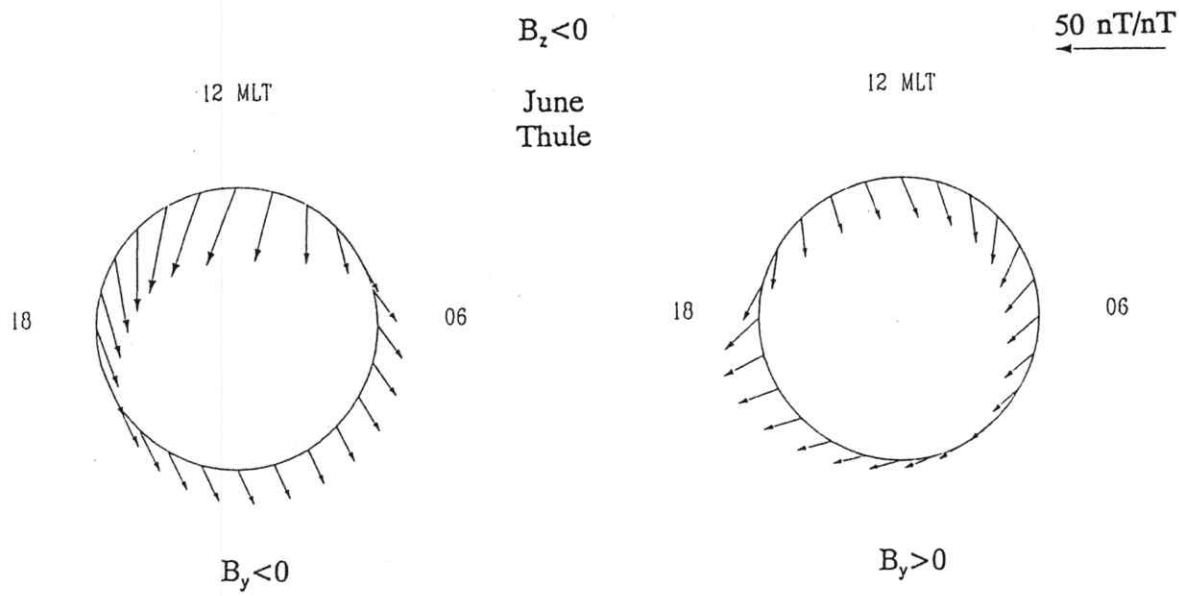

Polar diagrams showing the directions onto which to project the horizontal perturbation in Thule to obtain maximum correlation with IMF B_y. The left panel is for B_y negative and the right panel for B_y positive. Only data points where B_z was negative was included in the computation. The size of the vectors indicates the size of the response on ground to a given size of B_y. The results are for midsummer.

Figure II.7

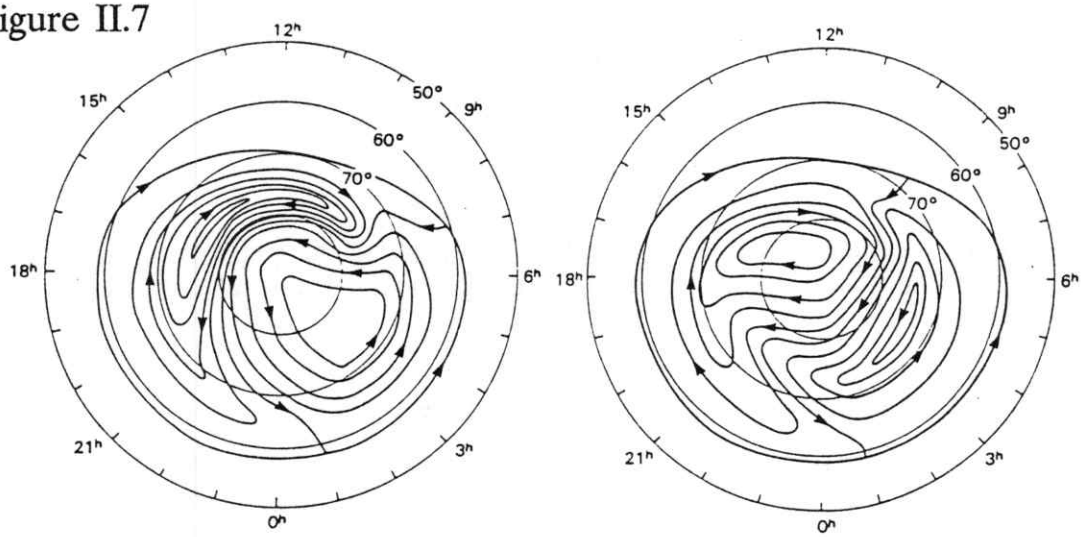

Empirical electric potential pattern for IMF weakly northward and $B_y<0$ and $B_y>0$. The patterns have been obtained from satellite electric field measurements by Heppner and Maynard [1987].

For comparison Figure II.7 shows the empirical electric field models by Heppner and Maynard [1987], for the case that B_z is relatively close to zero. It is seen that the coincidence with the B_y-response in the near pole region is very good.

Figure II.8

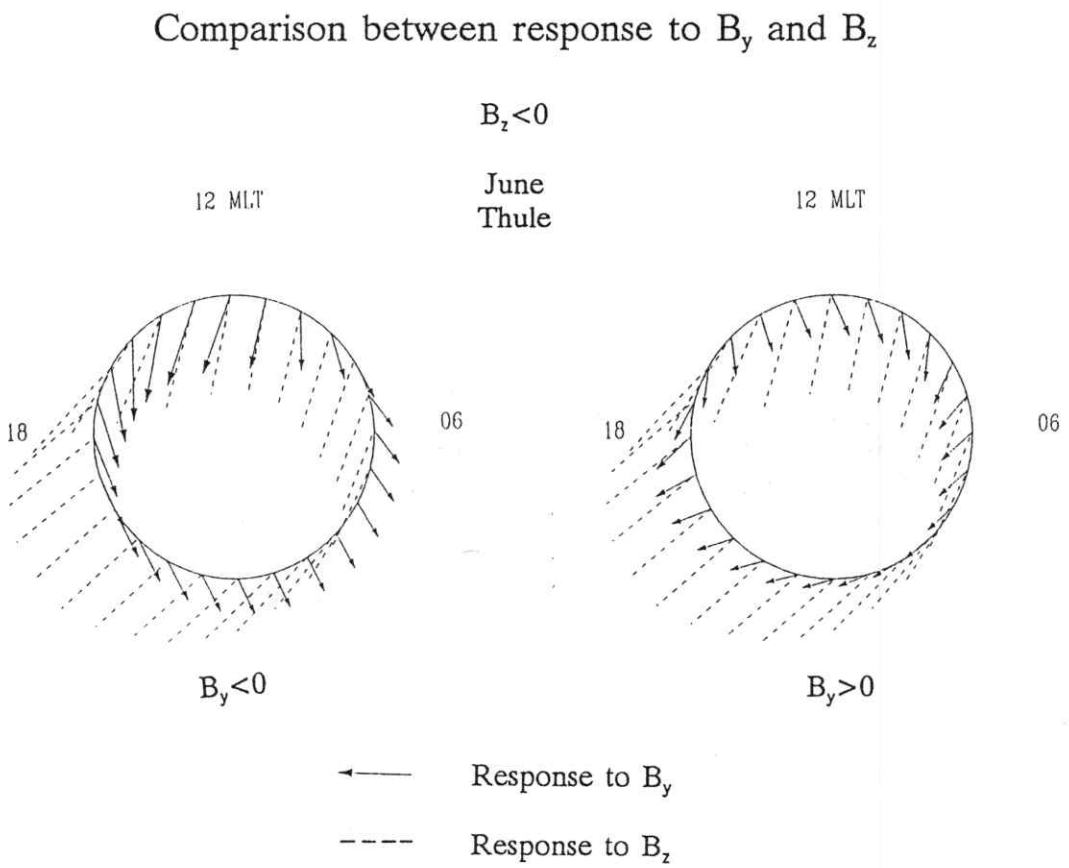

Polar diagrams similar to Figure II.6 but comparing the response to B_y (solid lines) with the response to B_z (dashed lines). The results are for midsummer.

In Figure II.8 we compare the B_y-response with the response to B_z. The dashed vectors indicate the optimal directions for correlation with B_z, and again the size of the vectors is a measure of the size of the response. It is seen that the response to B_y is about half the size of the response to B_z. This is more than was found for the influence of B_y on MAGPC, but the figure also indicates why. The MAGPC-index is obtained by projecting the magnetic perturbations onto the 03-15 MLT meridian, but especially the response to

B_y negative has maximum at large angles to this, especially at the night-side and during winter. In Vennerstrøm and Friis-Christensen [1987] we found:

$$\left[\frac{\Delta MAGPC}{\Delta B_y} \Big/ \frac{\Delta MAGPC}{\Delta B_z}\right]_{\substack{B_z = -1 \\ B_y = 3}} \approx 0{,}3$$

while we here in the linear approximation find ≈ 0.5 for the same ratio by comparing the slopes of the regression on B_z and B_y. When taken from the theoretical expression $B_T \sin^2(\theta/2)$ this ratio is ≈ 0.7 (Vennerstrøm and Friis-Christensen [1987]).

In the examination of the MAGPC-index and in Figure II.8 only B_z negative cases are taken into account. We have calculated the optimal direction and regression lines for the B_z positive case also, with the surprising result that they are very similar to the B_z negative case. Figure II.9 shows the B_z positive case which can be compared with the B_z negative case in Figure II.6.

Figure II.9

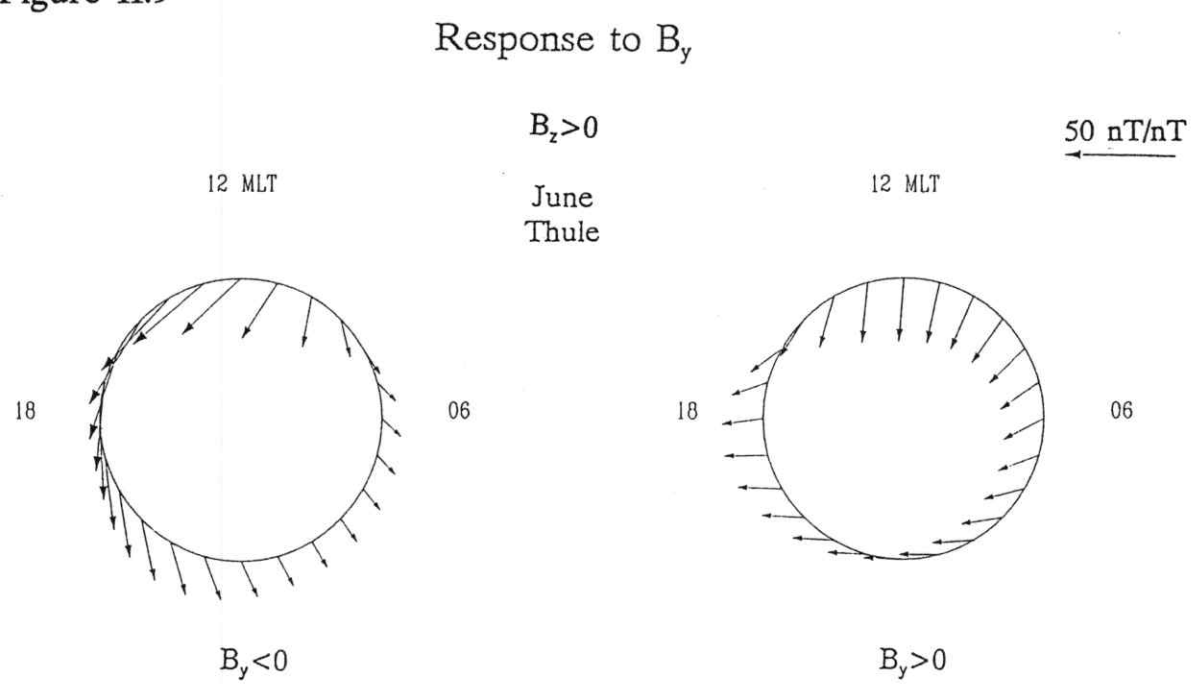

Polar diagrams similar to Figure II.6 but for $B_z>0$.

We have earlier concluded that the sign of B_z is the most important factor in the IMF-control of near pole magnetic variations, but from the comparison of Figures II.6 and II.9 we must conclude, however, that concerning the response to B_y the sign of B_z is only of secondary importance. In the examination of the MAGPC-index we found that the effect of $|B_y|$ was largest for small values of B_z. To check this for the B_y-response reported here we have repeated the calculation of optimal correlation, but now dividing the data into three intervals: $B_z<-2nT$, $-2nT<B_z<2nT$ and $B_z>2nT$. Table II.3 lists the average optimal direction φ_y, the average coefficient of correlation R_y and the average slope of the regression line α_y for different B_z intervals.

Table II.3 Average parameters computed for different IMF conditions

	φ_y		R_y		α_y	
	$B_y>0$	$B_y<0$	$B_y>0$	$B_y<0$	$B_y>0$	$B_y<0$
$B_z<-2nT$	22	-24	0.41	-0.60	8	-10
$-2nT<B_z<2nT$	58	-15	0.44	-0.58	6	-7
$B_z>2nT$	47	-13	0.57	-0.64	7	-7

We had expected that the slope and correlation was largest for $-2nT<B_z<2nT$, but instead it is seen that the response is rather similar for all B_z-intervals. So the conclusion that the $|B_y|$-effect is largest for small B_z is not confirmed by this method of calculation.

The largest known effect of B_y on high-latitude magnetic perturbations is the so called DPY current, an east - west flowing Hall-current observed in the polar cusp, especially

during summer (Svalgaard [1973], Friis-Christensen and Wilhjelm [1975]). We find it reasonable to believe that the B_y-effect, observed in the near pole region, is part of the DPY-current system, although it is not a DPY-current in the traditional sense. The optimal directions found for the B_y-response in Thule could be compatible with an ionospheric closure of the DPY-current across the polar cap. One interpretation is that both the DPY-current and the $|B_y|$-effect found in Thule is caused by merging on a skew merging line as described by Kan and Lee [1979]. The rather good quantitative agreement between the "crude" theoretical expression $B_T\sin^2(\theta/2)$ and the observations in Thule makes this interpretation tempting.

II.2.2 Seasonal asymmetry in the effect of B_y

In the last section we found that the MAGPC-index increases with increasing $|B_y|$, as illustrated by Figure II.3. By close inspection of the same figure, it can, however, also be seen that there is a small seasonal asymmetry in the response to B_y. During winter B_y positive gives a stronger contribution to PC than B_y negative, and visa versa during summer. Such an asymmetry was first discovered by Murayama et al. [1980] who examined the B_y dependence of AL for different tilt angles of the earth's axis. They found a clear seasonal asymmetry in AL, like the one just described for MAGPC. In interpreting their results, Murayama et al. [1980] observed that if one assumes that the merging is taking place preferably where the fields are antiparallel, the merging will be on the dawnside when B_y is negative during summer, and also on the dawnside when B_y is positive during winter, because of the tilt of the earth's axis. In other words, under these assumptions, they found an increase in AL when the merging was taking place on the dawnside. It has later been suggested that this was so simply because the garden hose angle of the IMF causes the merging in general to be stronger on the dawnside than on the duskside, either directly, because the B_x component changes the direction of the IMF with respect to the earth field (Heelis [1984]), or through draping of the IMF (Crooker et al. [1985]).

Figure II.10

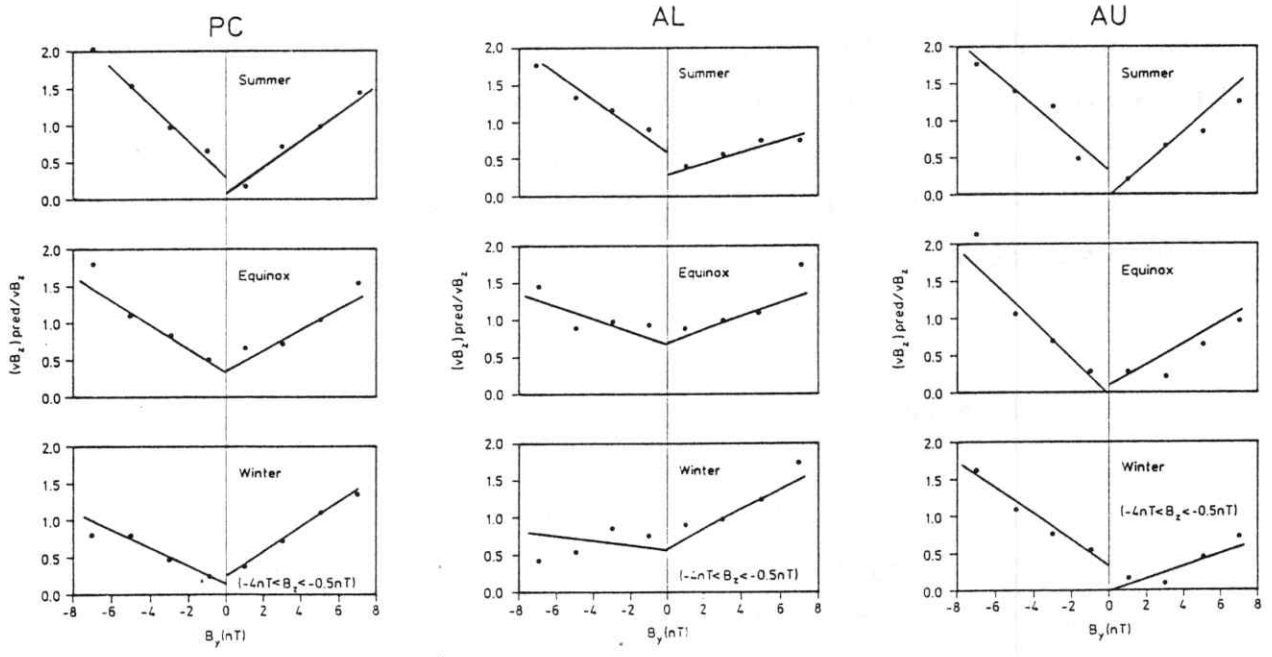

Linear regression lines of the parameter $(vB_z)_{pred}/vB_z$, where $(vB_z)_{pred}$ is computed from the three indices PC, AL, and AU, versus B_y. The points represent averages within a mesh of 2nT width in B_y. The regression lines were made on the original data points. Only data points with B_z<-0.5nT were included in the computation.

In order to clarify this question, we have repeated Murayama et al.'s computations for AL, using our data base, and have extended the investigation with a similar computation for AU, and of course for PC. The analysis starts by eliminating the larger influence from vB_z. We compute the parameter $(vB_z)_{pred}/vB_z$ where $(vB_z)_{pred}$ is the "predicted" value of vB_z determined from one of the indices AL, AU or PC. The predicted value is computed by assuming a linear relationship between vB_z and the index in question, e.g.:

$$AL = a \cdot vB_z + b$$

a and b are then determined from a correlation analysis using the whole data base, but taking into account that they can vary with season and time of the day. For each index the parameter $(vB_z)_{pred}/vB_z$ is then examined as a function of B_y. Using this method, it is necessary to limit the investigation to negative B_z cases, because AL and AU do not respond to positive B_z. Murayama et al. [1980] did not divide the data according to the sign of B_y but made one regression line covering both B_y positive and negative. Using this method, all attention is paid to the asymmetry between B_y positive and negative, and it is not possible to see any effect of $|B_y|$. Since we know that at least PC respond to $|B_y|$, we did not follow Murayama et al. at this point, but made our first analysis separately for B_y positive and negative. The results are shown at Figure II.10.

It is seen that all three indices respond to $|B_y|$, although the effect is rather weak in AL. In AU, however, it is just as strong as in PC. With regard to the asymmetry in AL, we find the same results as Murayama et al. The effect of B_y negative is strongest during summer and the effect of B_y positive is strongest during winter. The same trend, although weaker is seen in PC, but *not in AU*. For AU the effect of B_y negative is strongest during *all year*. The asymmetric effect is seen more easily on Figure II.11 where the regression lines covering both signs of B_y are shown.

We find that our results contradict an interpretation of the results of Murayama et al. in terms of merging site asymmetries. We believe that the eastward electrojet and the polar cap are better representatives for dayside merging processes than the westward electrojet, which is dominated by nightside processes such as strong substorm intensifications. If the seasonal asymmetry in AL, therefore, was caused by dayside merging asymmetry, this should be seen even more clearly in PC and AU. As mentioned in the introduction, we must expect some effect of the nightside processes to be present also in PC, because the field-aligned currents at the poleward rim of the auroral oval contributes considerably to the magnetic perturbation in the polar cap, especially during winter. This explains, in our opinion, why the seasonal asymmetry in AL also can be seen in PC.

Figure II.11

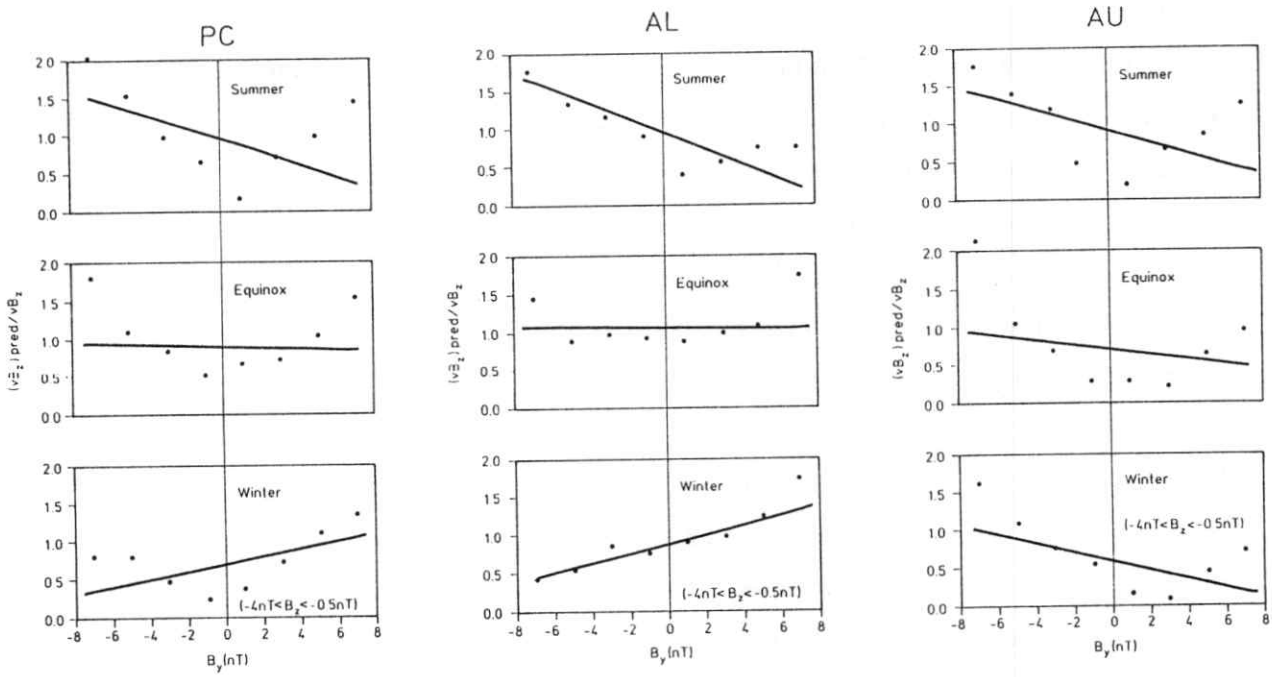

The same as in Figure II.10, but here the regression lines cover both B_y positive and negative simultaneously.

An effect of B_y positive during winter was described by Friis-Christensen and Wilhjelm [1975], and in Figure II.12 we have reproduced some of their results. The figure shows average magnetic disturbance vectors rotated 90°, from standard geomagnetic observatories during winter, when B_y is positive and B_z is negative. To eliminate the effect of B_z, the average perturbation for $B_y \simeq 0$ has been subtracted. It is obvious from the figure that we are dealing with a nightside effect which is localized to the westward electrojet. We believe that this disturbance is identical to what Murayama et al. observe with AL during winter, and also, that it is this effect that causes the slope of the regression lines on Figure II.9 to be larger for $B_y>0$ than for $B_y<0$ during winter.

Figure II.12

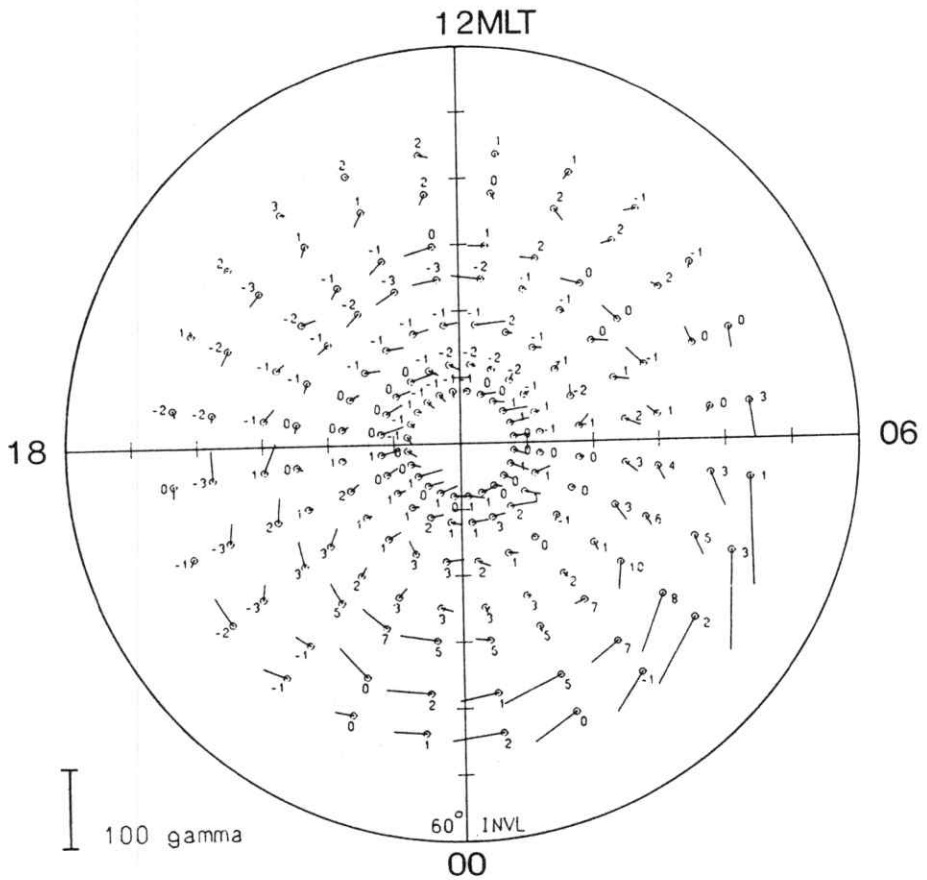

Statistical averages of the horizontal perturbation vectors over the north pole during winter, observed at standard geomagnetic observatories at each hour of local time. The vectors are rotated 90° clockwise to represent corresponding equivalent current vectors. The averages were obtained under the IMF condition $B_y>1.5$nT and $B_z<-1$nT, and they are residual in the sense that the average value for $B_z<-1$nT and $-1.5\text{nT}<B_y<1.5$nT have been subtracted. (Reproduced from Friis-Christensen and Wilhjelm [1975]).

We conclude that the effect of B_y on currents in the polar region is very complicated and may consist of contributions from several different cources. The results shown here could indicate that the $B_y<0$ condition in some way enhances the effectivity of the dayside process, while the $B_y>0$ condition do the same for the nightside processes.

III. SOURCES TO MAGNETIC ACTIVITY IN THE POLAR CAP

The skewed equivalent currents crossing the polar cap in the two cell system are thought to have two main sources: 1) Ionospheric Hall currents in the polar cap, and 2) distant field-aligned currents at the poleward rim of the oval. One way to establish which source is dominant is to compare the horizontal magnetic perturbation with a direct measurement of the electric field in the polar cap ionosphere. If the magnetic perturbation on ground is caused by overhead Hall currents, the electric field and the magnetic perturbation should be pointing in the same direction.

Comparisons between ionospheric electric fields and ground magnetic perturbations have been made through a variety of methods: Barium release experiments [Heppner et al., 1971; Mikkelsen et al., [1975], satellite probes [Heppner, 1972, 1977; Heppner and Maynard, 1987], payloads containing magnetometers and electric field probes [Ungstrup et al., 1975; Olesen et al., 1976], and recently also by the use of incoherent scatter radar technique [Friis-Christensen, 1986; Clauer and Friis-Christensen, 1988]. Generally it is found that the electric field and magnetic perturbation are roughly parallel in daylight, but that the magnetic perturbation is deflected somewhat westward when it is dark. The overall conclusion is that during sunlit conditions the dominant source is ionospheric Hall currents, while the distant field-aligned currents are dominant in darkness [Primdahl and Spangslev 1977].

This was to be expected, since the ionospheric conductivity in the polar cap is created mainly by solar UV-radiation [Gizler et al., 1976, Primdahl and Spangslev, 1977]. When the sun is below the horizon, the conductivity becomes too low to support any substantial ionospheric current. The fact that the conductivity in the polar cap is controlled mainly by solar UV-radiation, also means that the polar ionospheric conductivity, as a whole, is far from being uniform in darkness, because the conductivity in the auroral oval is much higher than in the polar cap. From theoretical considerations, we know that when the conductivity is not uniform, the magnetic effect from the field-aligned currents are not

cancelled completely by the effect from the Pedersen currents. Assuming a ring-shaped auroral oval, Vasyliunas [1970] further pointed out that the equivalent current would be deflected westward in the polar cap. During sunlit conditions, on the other hand, where the conductivity is much more uniform, the contribution from the Hall-current should be the most important.

Unfortunately there has not, to our knowledge, been made any comparison between the electric field and magnetic perturbation at latitudes as high as Thule and Vostok, which most of the time lies close to the day/night terminator. Mozer et al., [1974] did make electric field measurements above the near pole stations Thule and Resolute Bay by means of balloon-borne electric field probes during a limited period of time, but he decided that the relationship between the ground magnetic perturbation and the ionospheric electric field was too complex to be elucidated by his measurements.

Figure III.1 shows averages of the horizontal magnetic perturbation in Thule and Vostok for the IMS-period in the years 1977-80. In Vostok the diurnal variation of the five most quiet days was used as reference level, while in Thule a constant baseline, determined from quiet winter days was used. The data was sorted according to IMP-8 satellite measurements of the solar wind, so that only periods were included, where the IMF had a southward component. Several investigators have analyzed the time lag between variations of the IMF and the geomagnetic variations. The result varies between approximately 20 minutes and around 60 minutes, depending on the general level of activity, and depending on which satellite and geomagnetic parameter is used (see e.g. Baker et al., [1983] and references therein). Using the same data set as in the present paper, Troshichev et al. [1988] found that a time delay of about 20 minutes gives the best correlation between IMF and PC, and a 20 minutes time delay has therefore also been used here. The perturbations were divided into three seasons and are presented in an invariant latitude - magnetic local time diagram. When a station is located very close to the pole, there can be a large difference between geographic local noon, where the solar UV-radiation is at maximum, and magnetic local noon. This is especially true for Vostok, where geographic local noon is close to 4 MLT.

Figure III.1

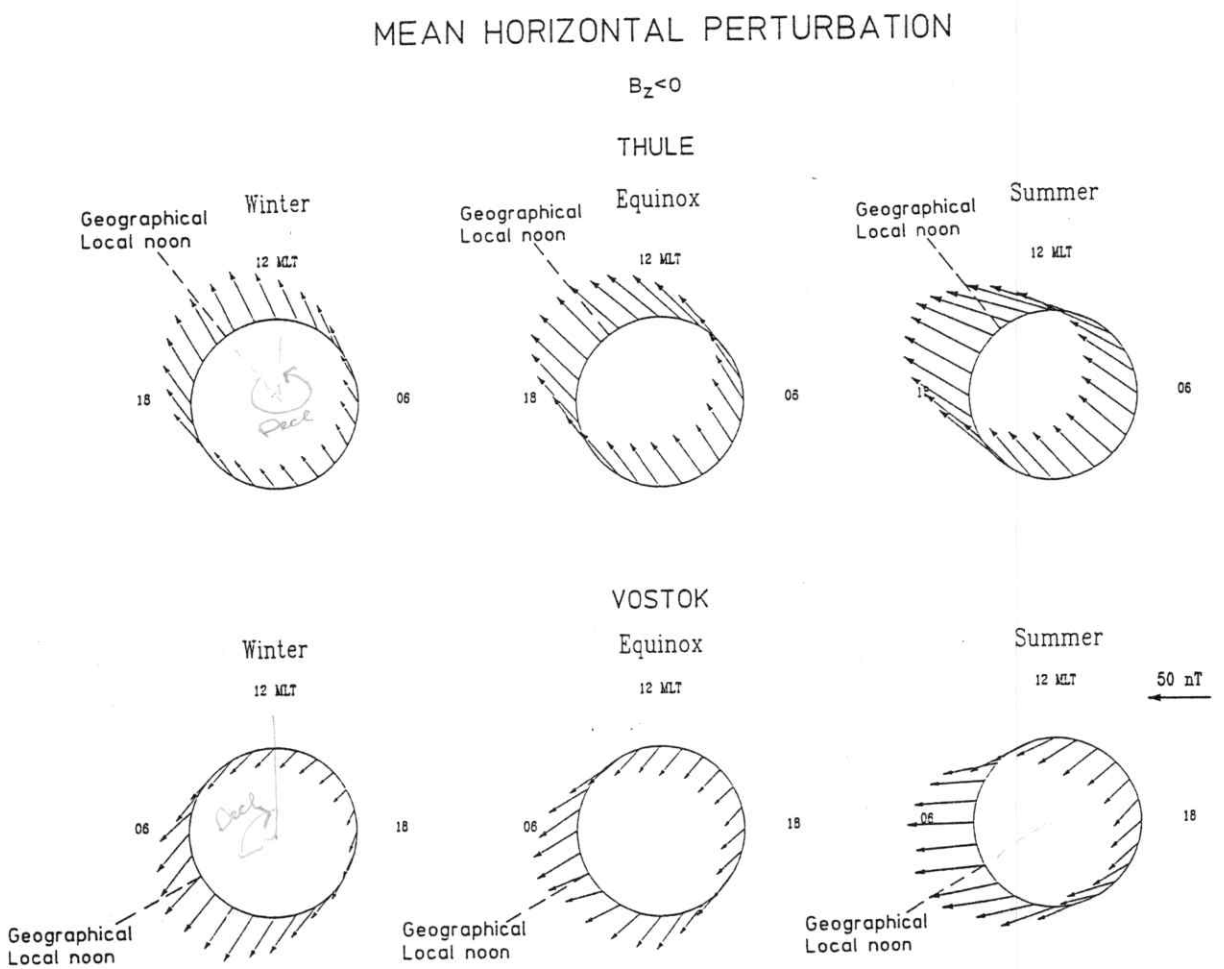

Hourly horizontal magnetic perturbation in Thule and Vostok averaged during southward IMF through the years 1977-80. The data are divided in three parts according to local season and are presented in an invariant latitude - magnetic local time diagram. It is seen that both the size and the direction of the perturbation are largely controlled by the intensity of the solar UV-radiation.

The main thing worth noting in the figure is that both the size and the direction of the perturbation seem to be largely controlled by the intensity of the solar UV-radiation. The size of the perturbation decreases clearly from summer to winter, and from geographic

local noon to midnight. The direction is roughly dawn-dusk at summer near geographic local noon corresponding to antisunward convection, but becomes more and more skewed as one approaches winter or local midnight.

Mozer et al., [1974] measured the electric field above Thule on five equinox days. On the average, they found it to be skewed only 15 degrees from the dawn-dusk meridian in an invariant latitude - MLT diagram, and it is therefore tempting to interpret the westward deflection of the magnetic perturbation from the dawn-dusk direction as a rough measure of the extent to which distant field-aligned currents contribute. An exact solution of the problem would require detailed knowledge of the conductivity and electric fielddistributions. But from the above simple considerations, we would expect the Hall-currents and distant field-aligned currents to be of roughly equal importance, with a strong seasonal effect on their relative contribution. During winter, practically no ionospheric currents can exist in the low conductivity in the dark near pole region [Primdahl and Spangslev 1977], and the distant sources have to be dominant. During summer, when the near pole region is sunlit, both sources seem to be present. At the dayside the Hall-currents probably dominate, but at the nightside the field-aligned currents also seem to give a substantial contribution.

In the dayside cusp region there exists, during summer, a well documented current system named the DPY current, which is mainly controlled by B_y (Svalgaard [1973], Friis-Christensen and Wilhjelm [1975]). The horizontal magnetic disturbance associated with this current system normally has its maximum below about 82 degrees invariant latitude. At latitudes as high as Thule and Vostok, it is mainly detected by its effect on the Z-component, but a small effect on the horizontal component can be detected even here, as described thoroughly in the previous section.

When the IMF becomes strongly northward the equivalent currents in the polar cap undergo dramatic changes. The auroral oval contracts, and the electrojets become very weak, so the equivalent currents discussed above disappear. Simultaneously, a new equivalent current system is formed within the polar cap, with quite different character and

direction. This was first discovered in 1976 [Maezawa, 1976; Kuznetsov and Troshichev, 1977], and is often referred to as "reversed convection events". Later, more detailed ground based analysis have shown that this current system exists primarily in the dayside part of the near pole region and is mixed, or closely associated, with the DPY-current [Friis-Christensen, 1983; Friis-Christensen et al., 1985]. The associated field-aligned currents have also been measured directly by satellite, and have been named "NBZ-currents" [Iijima et al. 1984]. More recently, the associated electric field structure have been measured by satellite, but interpreted as a deformed two cell system [Heppner and Maynard, 1987], rather than as separate convection cells.

Figure III.2 shows hourly averages of the horizontal magnetic perturbation in Thule for IMF $B_z > 2$ nT. The data was divided according to the sign of B_y, so that the upper panel shows the results for $B_y>0$, and the lower panel the results for $B_y<0$. The dotted lines show the directions of optimal correlation with $vB_T\sin^2(\theta/2)$ used in the derivation of PC. It is seen that the size of the perturbation is very dependent on season. During winter, the perturbation almost disappears, indicating that the low conductivity in the dark polar cap prevents the polar cap and cusp currents from being formed. During summer on the other hand, it is obvious that these currents can have a seriously disturbing influence on the PC-index. The direction of the average perturbation is very different for B_y positive and negative, so the currents controlled by B_y must be rather dominating when B_z is positive.

Figure III.2

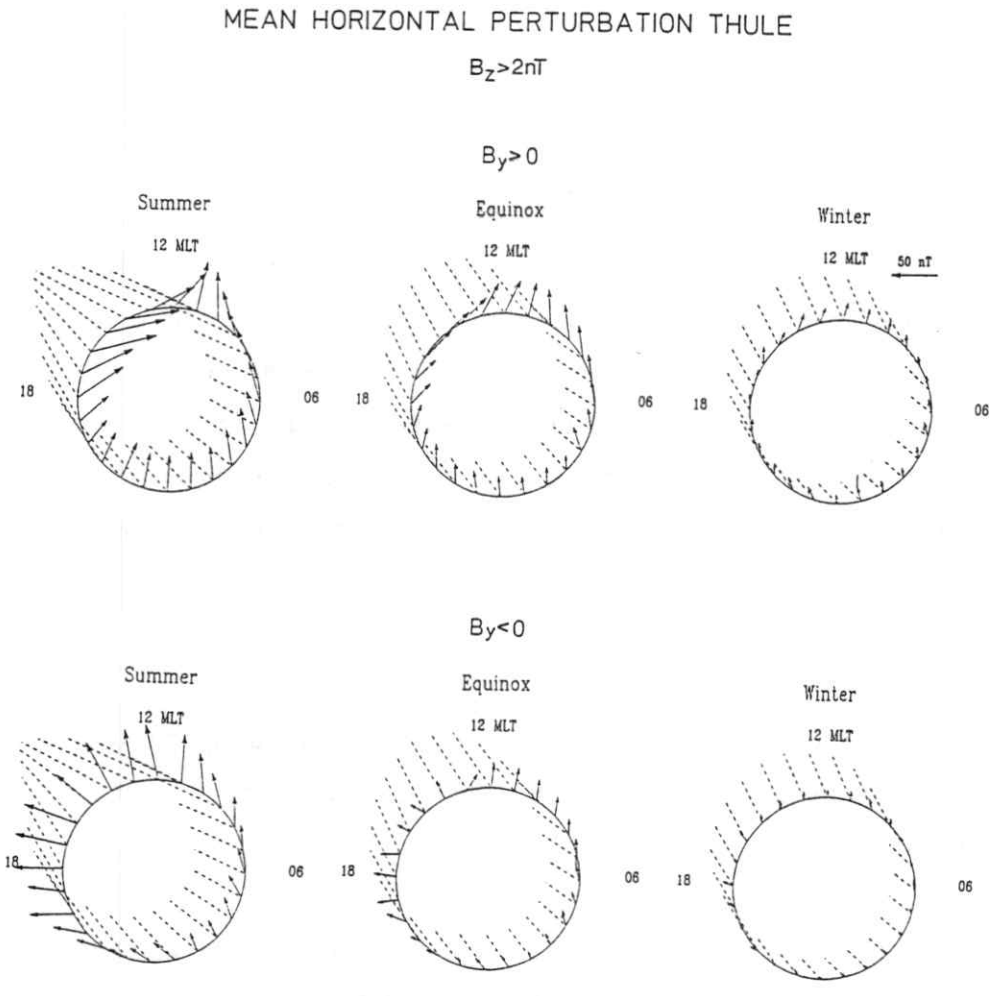

Hourly horizontal perturbation in Thule averaged during strongly northward IMF through the years 1977-80. The top panel is for $B_y>0$ and the bottom for $B_y<0$. The dashed vectors indicate the directions onto which the horizontal perturbation is projected in the derivation of the PC-index. It is seen that the polar cap current system developing during strongly northward IMF in the summer can have a seriously disturbing influence on the PC-index.

IV. THE PC-INDEX

IV.1 The algorithm

The first to define an index, PC, for magnetic activity in the polar cap was Fairfield [1966]. He defined the PC-index as the maximum of the horizontal disturbances at the three stations Thule, Alert, and Resolute Bay. This index was again used by Kokubun [1971, 1972] for scientific examination of some specific events, but was never derived on a routine basis. In the preceding sections we have examined the horizontal magnetic perturbation in the near pole region, its diurnal and seasonal variation and its relationship to various solar wind parameters. We have found that several different sources contribute to the perturbation:

(1) The well-known two cell equivalent current system made up, partly by ionospheric Hall-currents, and partly distant field-aligned currents, and generated mainly by B_s and v.

(2) A current system generated by B_y which may or may not be an integrated part of the two cell system, but which can be flowing in other directions than the normal two cell current, depending on the sign of B_y.

(3) An ionospheric Hall-current system generated at very high latitudes, when B_z is northward, and existing almost exclusively during sunlit conditions. During B_z positive conditions the B_y generated current (2) is dominating the picture.

When determining an algorithm to an index for polar cap magnetic activity it is therefore very important to make quite clear what type of magnetic activity the index is supposed to monitor. In 1979 Troshichev et al. [1979] proposed a new polar cap index based on data from a single near pole station, with the clear aim of monitoring the cross polar cap part of the two cell equivalent current pattern. To achieve this, they proposed to project the measured horizontal perturbation onto the dusk-dawn meridian in order to measure the midnight-noon directed cross polar cap current. The correlation between this parameter and B_z was however not very high. In a later work, mentioned in the previous sections, the skewness of the two cell pattern was taken into account, by projecting onto the 03-15 MLT meridian instead of the dawn-dusk meridian, with a considerable improvement of the correlation as a consequence (Troshichev and Andrezen [1985]). Finally, in Troshichev et al. [1988] a third version was proposed, based on the method of optimization of the linear correlation with the IMF used in section II. Instead of projecting onto a fixed meridian, the perturbation is projected onto the direction that produces the highest correlation with the IMF as a function of local time and month. The IMF-parameter chosen to define the projection directions which are used in the algorithm is the parameter $vB_T\sin^2(\theta/2)$, simply because it gives the highest linear correlation (Table II.1).

It is important to note that this last version of PC is principally different from the foregoing, and from other geomagnetic indices, in the way that it is empirical. The algorithm is determined on the basis of an empirical analysis of the relationship with the IMF. As such, the algorithm may be subject to effects of data selection criteria. For example, the analysis is based on data from one part of the solar cycle, namely the inclining part from 1977-80, and it is therefore necessary to check whether the relationship is the same in the remaining part of the cycle. This is of course a serious disadvantage. On the other hand, the method has the advantages of a high degree of objectivity, and of improving the correlation to the generating agent of the current system, i.e. the IMF, considerably. Figure IV.1 shows a contour plot of the direction, used in the final algorithm for the index in Thule.

Figure IV.1

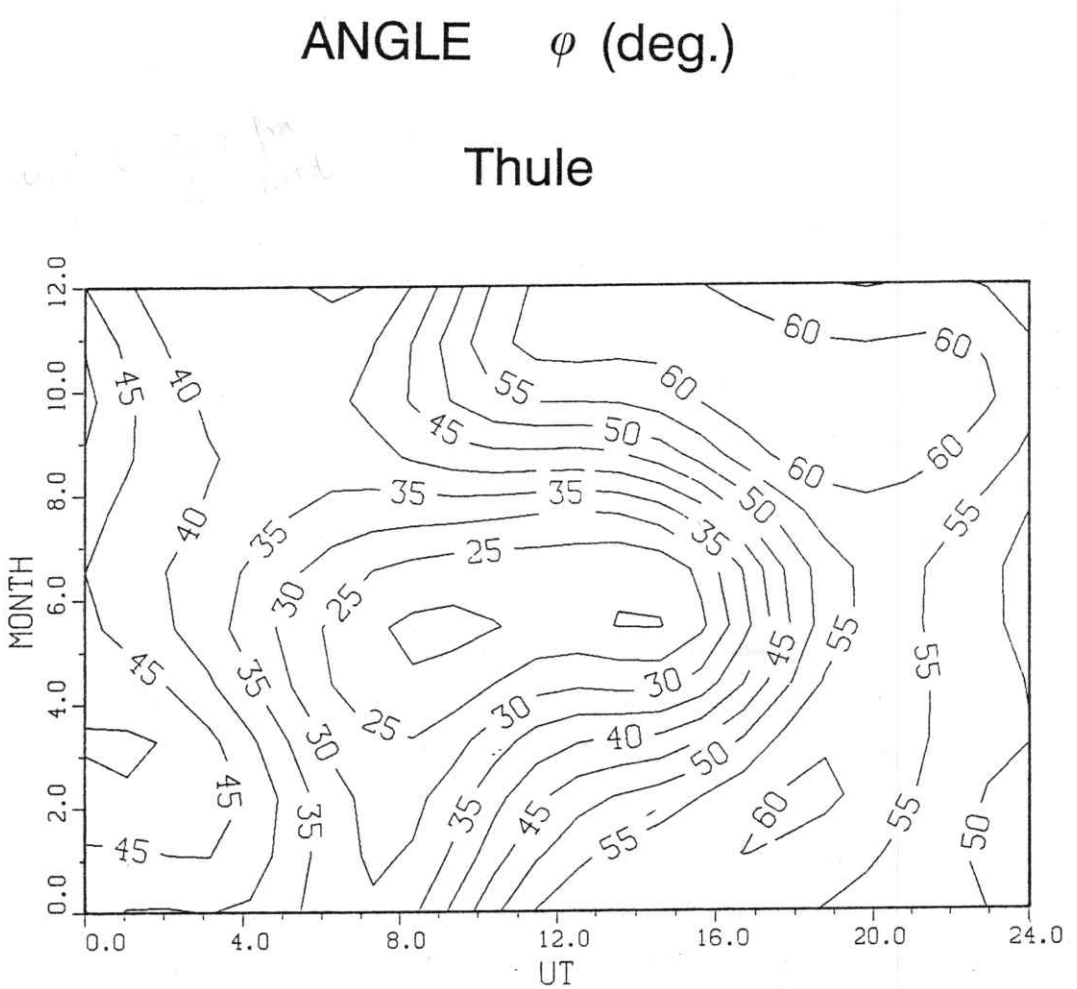

Contour plot of the angle φ (see Fig. II.2) defining the directions used for projection in the algorithm for PC in Thule.

If we turn from the directions to the size of the response on earth to a given size of $vB_T\sin^2(\theta/2)$, we find that it varies both with month, local time and the station used. If PC shall be used as a global index these variations of course have to be eliminated. One way to do it is to make use of the linear correlation analysis and normalize with respect to the solar wind. PC would thus be derived in the following way. First the measured horizontal perturbation (ΔH, ΔD) is projected onto the statistically determined optimal directions:

$$\Delta F = \Delta H \sin\gamma \pm \Delta D \cos\gamma$$

$$\gamma = \lambda \pm Dec + UT + \varphi$$

(+: Northern hemisphere; - : Southern hemisphere)

Then the linear regression coefficients (α, β) are determined and ΔF normalized:

$$\Delta F = \alpha(vB_T \sin^2(\theta/2)) + \beta$$

$$PC = \frac{(\Delta F - \beta)}{\alpha}$$

where φ, α, and β are determined from the linear correlation analysis and are functions of month and local time.

In a normal linear regression analysis the slope of the regression line α depends on the correlation. The higher the correlation the steeper the regression line. If we therefore computed the inverted regression coefficients $\tilde{\alpha}$, $\tilde{\beta}$ directly:

$$vB_T \sin^2(\theta/2) = \tilde{\alpha}\Delta F + \tilde{\beta}$$

we would obtain a different result. Since we, on one hand, in principal use the inverted formula to determine PC, and, on the other hand, know that $vB_T \sin^2(\theta/2)$ is the independent parameter, we have found it reasonable to use the, so called, orthogonal regression coefficients $\alpha_\perp$, $\beta_\perp$ in the normalization, instead of the normal correlation coefficients α, β. The orthogonal regression coefficients have the advantage of being independent of the correlation coefficient, and we thus obtain the same result disregarding the "choice" of independent parameter (see e.g. Hald [1968]).

$$\alpha_\perp = \frac{s_y^2 - s_x^2 \pm ((s_y^2 - s_x^2)^2 + 4s_{xy}^2)^{1/2}}{2s_{xy}}$$

$$s_x = \left(\frac{1}{N-1} \sum_i (x_i - \bar{x})^2 \right)^{1/2} \qquad s_y = \left(\frac{1}{N-1} \sum_i (y_i - \bar{y})^2 \right)^{1/2}$$

$$s_{xy} = \frac{1}{N-1} \sum_i (x_i - \bar{x})(y_i - \bar{y})$$

$$\beta_\perp = \bar{y} - \alpha_\perp \cdot \bar{x}$$

Figure IV.2 shows a contour plot of the orthogonal regression coefficients used in the final algorithm for PC in Thule:

Figure IV.2

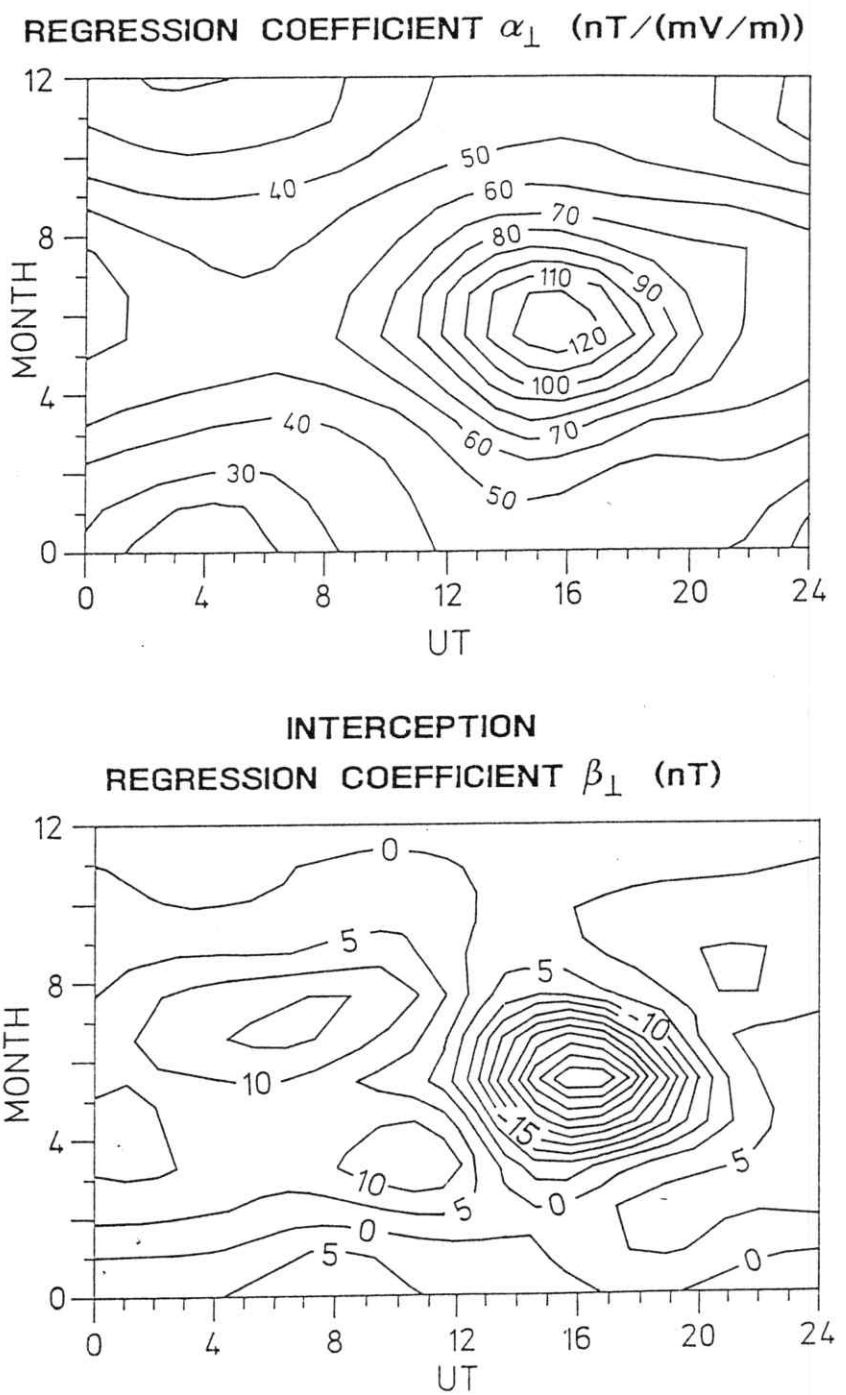

Contour plot of the regression coefficients $\alpha_\perp$ and $\beta_\perp$ used in the algorithm for PC in Thule.

Normalization with respect to a global parameter, like a solar wind parameter, has the advantage of making PC from two different stations directly comparable. It does, however, also have the effect of giving PC the unit of "solar wind" or "merging" electric field. We, therefore, want to underline that PC primarily is an index for geomagnetic activity and only in a statistical sense a measure of the parameter $vB_T\sin^2(\theta/2)$. This problem could be dealt with by multiplying by a constant scale factor expressing the average ratio between PC and some other geomagnetic index, e.g. AE, and thus give PC in units of "AE-nT". AE however is not a real global parameter since it is derived from the northern hemisphere only and from a varying number of observations; and although AE and PC, as we shall see, show a very high correlation, there are also systematic differences. The choice of unit for PC is therefore not straight forward. It seems impossible to make a choice without unpleasant side effects.

IV.2 Smoothing of the coefficients

When the normalization coefficients $\alpha_\perp$ and $\beta_\perp$ is determined empirically, they will of course be subject to statistical uncertainty. This means that there will be fluctuations in $\alpha_\perp$ and $\beta_\perp$ as functions of local time and month, which are not caused by some basic physical effect, and which therefore would not be reproduced if another data set was used in the calculation. The fluctuations are seen as sudden jumps in the normalization coefficients, which, if used directly, would result in sudden jumps in the PC-index. We have tried to overcome this problem by applying a smoothing procedure to $\alpha_\perp$, $\beta_\perp$ and φ. The smoothing is made by running the coefficients through a digital low pass filter of the binomial type, first as a function of month and then as a function of UT. The filter characteristic of binomial filters of different order is reproduced in Figure IV.3. As a function of month we have used a second order binomial filter. The exponent to the cosine is called the filter order. ν_N is the Nyquist frequency $1/(2\Delta t)$, where Δt is the sampling interval. For a variation with the period of 12 months, we would have the frequency $\nu/\nu_N = 1/6$, which is marked with a vertical line on the figure. The intersection with the filter characteristic indicates that this variation will be damped with a factor of ≈ 0.93 through filtering. Similarly a 24 hour period with $\nu/\nu_N = 1/12$ is marked.

Figure IV.3

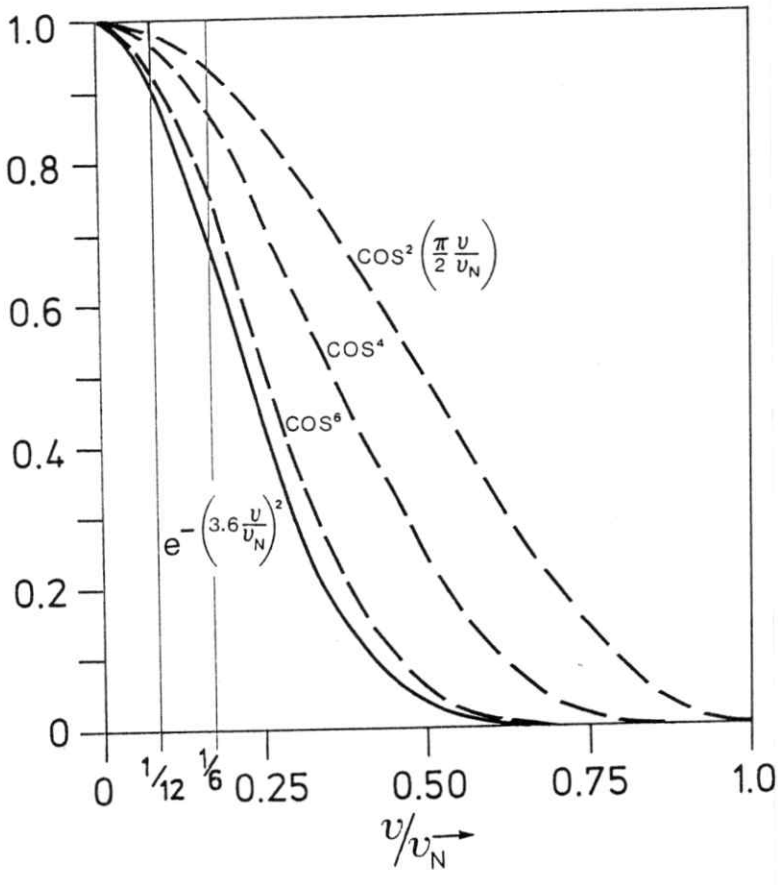

Filter characteristics for binomial filters of different order. The two vertical lines mark the frequencies for a yearly variation ($\nu/\nu_N = 1/6$), and a daily variation ($\nu/\nu_N = 1/12$).

The problem is to find a filter, which will dampen the statistical fluctuations, i.e. variations of small period, but leave the long period variations relative unchanged. If the long period variations, namely, is damped too much, strong seasonal and diurnal variations in the PC-index will be the result. This can be seen from Figure. IV.4, where the average values of PC, computed on the basis of too high a filter order, is plotted. The seasonal filter was of 6th order, and the diurnal filter of 12th order.

Figure IV.4

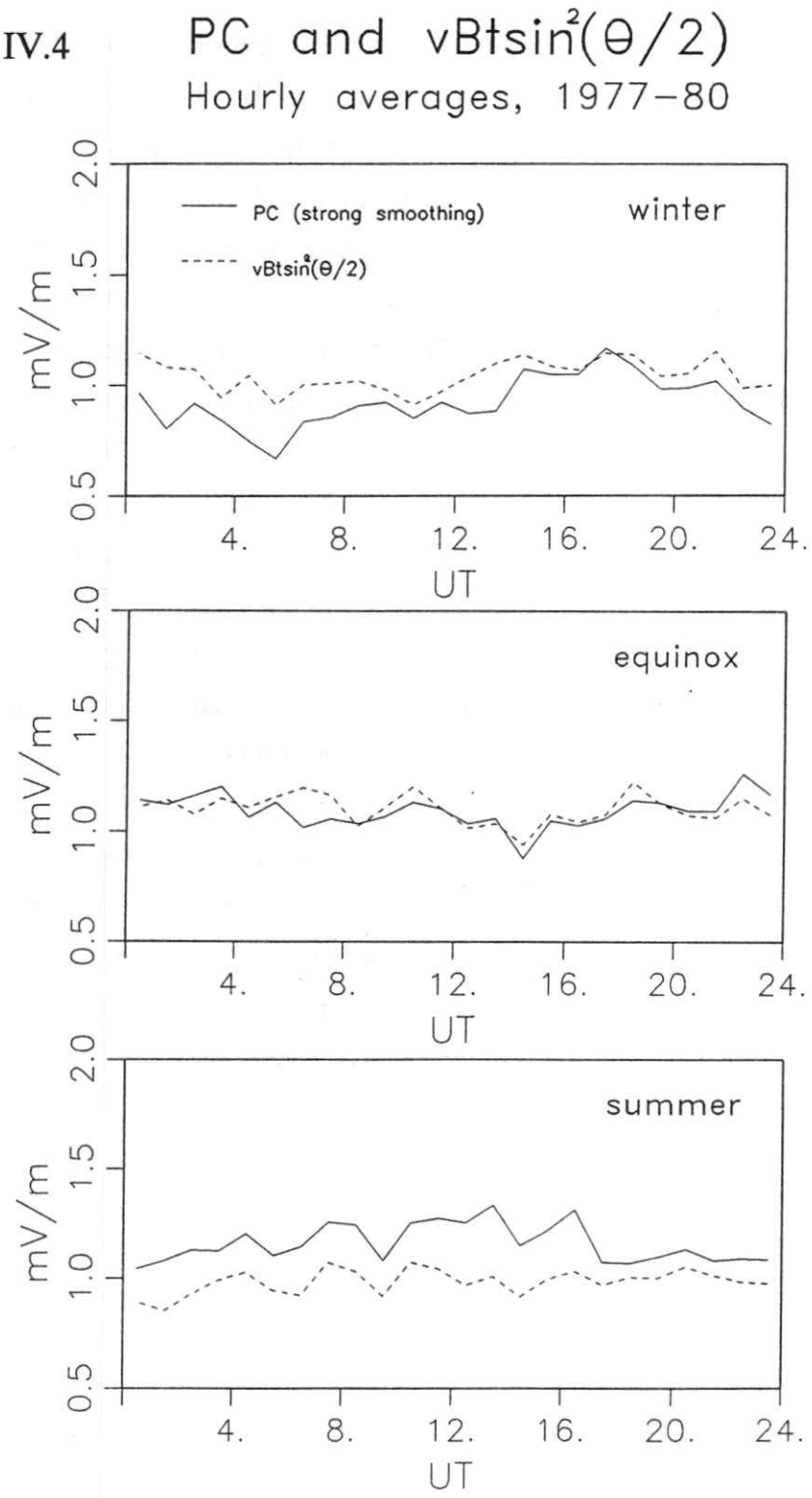

Daily and seasonal variation for PC compared to the IMF-parameter $vB_T\sin^2(\theta/2)$. Only data points that are used in the derivation of the algorithm of PC (i.e. where both IMF and Thule measurements were available), are included in the averages. A seasonal filter of 6th order and a diurnal filter of 12th order were used in the derivation of PC.

For comparison is shown averages of the solar wind parameter $vB_T\sin^2(\theta/2)$. The data set used to compute the averages in Figure IV.4 is identical to the data set used to calculate the coefficients $\alpha_\perp$ and $\beta_\perp$, so the curves for $vB_T\sin^2(\theta/2)$ and PC should, for mathematical reasons, be identical, if no smoothing was supplied. It is seen from the figure that the high order smoothing results in a strong seasonal effect: PC is higher than $vB_T\sin^2(\theta/2)$ during summer and lower during winter. There is also some diurnal variations, especially during winter. Because of this we had to choose a filter of lower order. For the seasonal variations, we chose the lowest possible filter order, namely, a second order filter. The intersection between the filter characteristic and the vertical line $\nu/\nu_n = 1/6$ at Figure VI.3 indicates that a variation with a period of a year, in this case, would be damped with a factor of ≈ 0.93. In the case of diurnal variations, smoothing is more important than in the case of seasonal variations. When PC is calculated as a function of UT, it is necessary to exchange $\alpha_\perp$ and $\beta_\perp$ in the algorithm every hour, and short-term variations in $\alpha_\perp$ or $\beta_\perp$, caused by statistical uncertainty, will create unpleasant and unreal jumps in PC. Consequently a higher order filter was chosen, namely, a 10th order filter. A variation of the period of 1 day will in this filter be damped with a factor of about ≈ 0.92. The average PC values from the final filter is seen in Figure IV.5. The results are improved considerably compared to Figure VI.4, but a small seasonal effect is seen to remain. During winter some diurnal variations also remain, but at least part of this variation is also seen in the parameter $vB_T\sin^2(\theta/2)$. The small diurnal variation during winter is therefore partly due to a data selection effect, which cannot be removed completely without choosing another set of IMF data as basis for the algorithm.

Figure IV.5

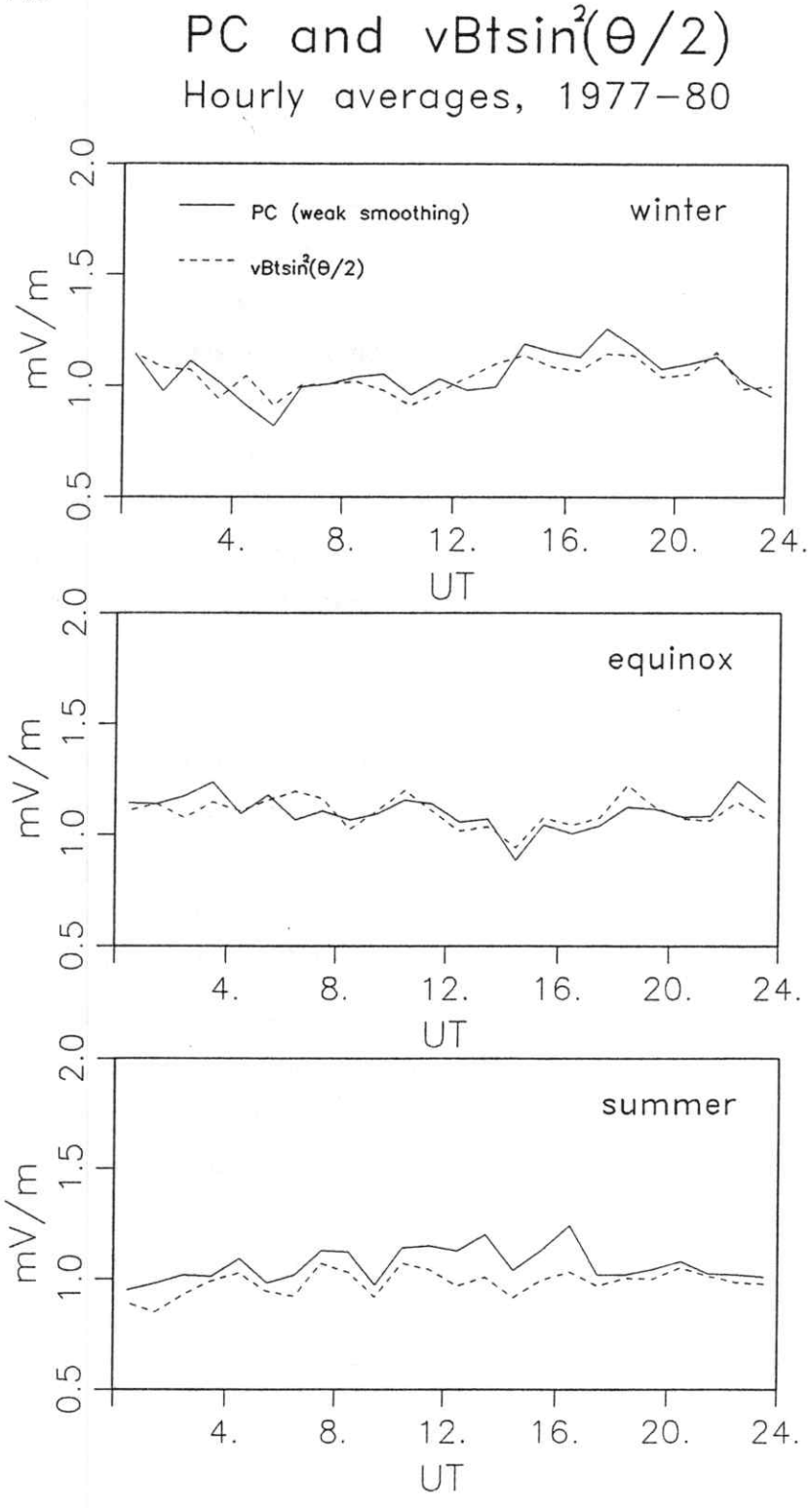

The same as Figure IV.4 but for a seasonal filter of 2nd order and a diurnal filter of 10th order.

IV.3 The algorithm and the B_y-dependence

In the preceding section, we have shown that B_y gives a significant contribution to the near pole magnetic variations, and in choosing the parameter $vB_T\sin^2(\theta/2)$ as a basis for the algorithm, we have automatically chosen to take the B_y-effect into account, to some extent. Our results, however, showed that the optimal directions are different for B_y positive and negative, and the question therefore arises, whether this should be taken into account in the algorithm. One way to do it is to compute two sets of ($\alpha_\perp$, $\beta_\perp$, φ), one for B_y positive and one for B_y negative, and use the B_y positive set for computing PC, when B_y is actually positive, and the B_y negative set, when it is negative. This would, however, require knowledge of the sign of B_y in order to calculate PC. If this knowledge should be taken from satellite measurements, it would put unacceptable strong limits on the availability of PC. One way out could be to use the well known high correlation between B_y and the *vertical* magnetic perturbation, Z, in the near pole region.

Figure IV.6 shows a contour plot of the linear correlation between B_y and the Z-component in Thule, using 15 minute averages. It is seen that the high correlation is limited to summer and dayside. At the nightside and during winter, we cannot hope to predict B_y with the necessary accuracy. To judge the effect of computing the coefficients for B_y positive and negative separately, we have made two test calculations of PC. One using exclusively ($\alpha_\perp$, $\beta_\perp$, φ) derived from B_y negative cases, regardless of the actual sign of B_y, and one using exclusively B_y positive coefficients. An example of the resulting PC-indices is shown in Figure IV.7. It appears, that the difference between the two sets of PC-indices is rather small. Based on Figures IV.6 and IV.7 we find that the uncertainty in predicting the sign of B_y is too big, and the effect on PC of the changing directions too small, to justify the introduction of a B_y dependent algorithm, which would make the index more complicated and more difficult to interpret. We therefore propose that the effect of B_y on the directions is not taken into account in deriving PC.

Figure IV.6

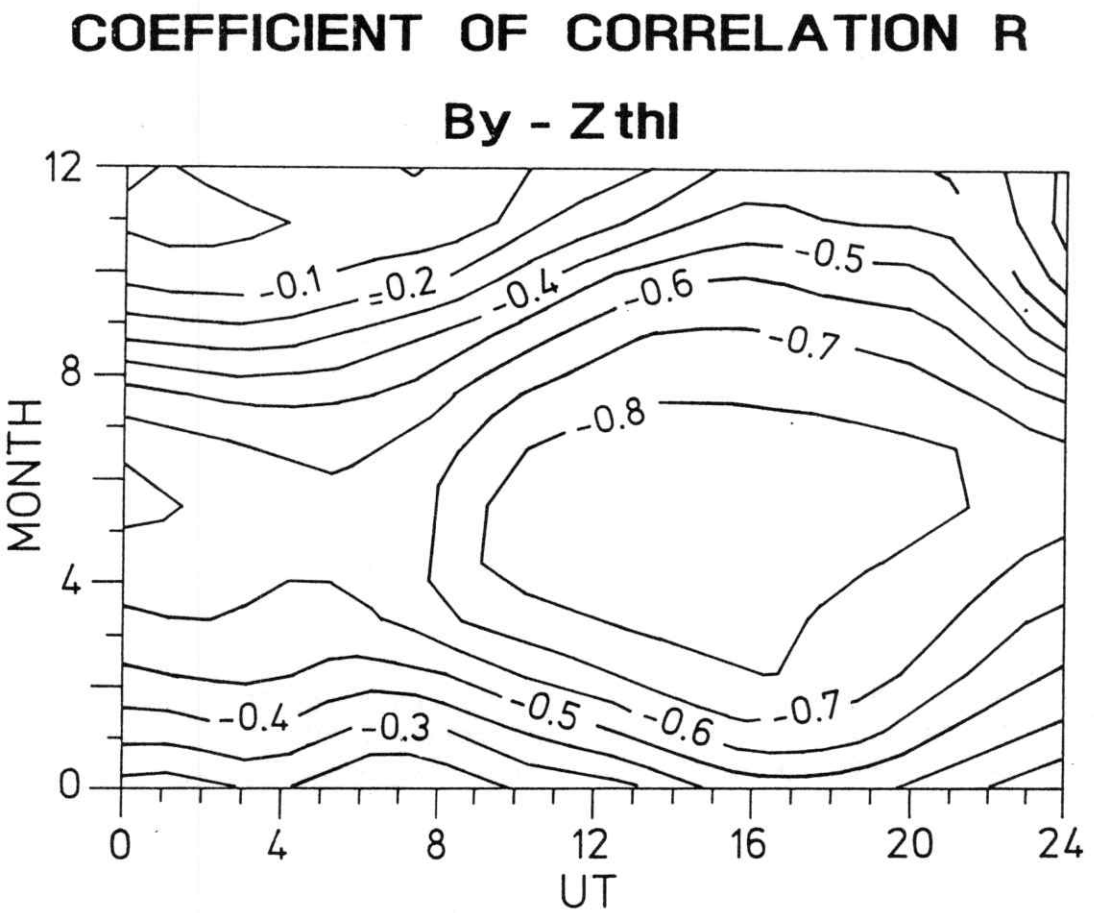

Contour plot of the coefficient of correlation between IMF B_y and the vertical magnetic perturbation Z in Thule for the years 1977-80.

Figure IV.7

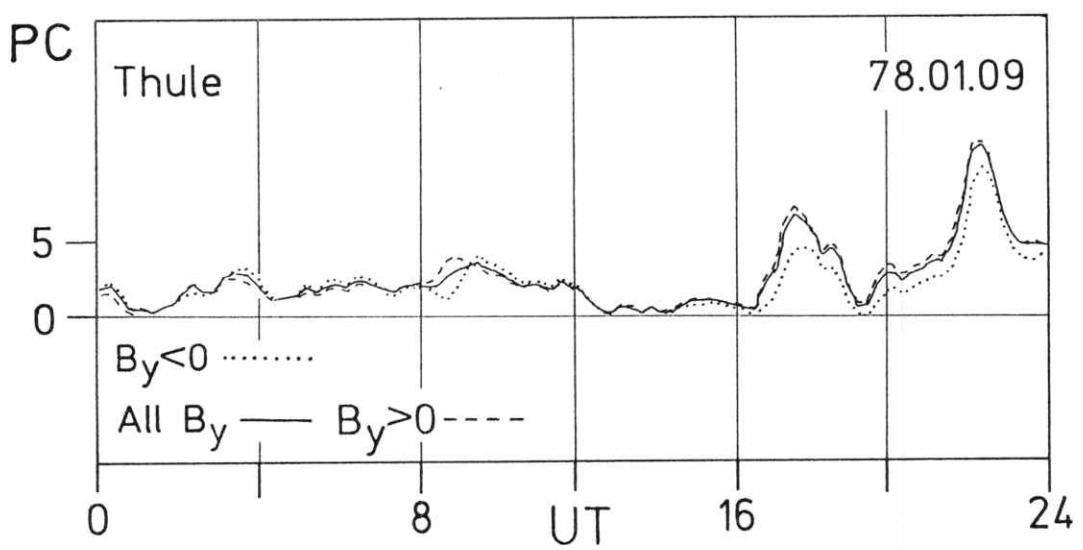

An example of PC in Thule. The solid line is the normal PC variation. The dashed lines show PC if only data points with $B_y>0$ are used in the derivation of the parameters φ, α, β. The dotted line show the same for $B_y<0$.

V. COMPARISON BETWEEN PC AND THE AURORAL ELECTROJET INDICES AE, AL, AND AU

The field-aligned currents at the poleward rim of the auroral electrojet contributes, as was discussed in the section III, substantially to the near pole magnetic perturbations. The same currents are, on the other hand, intimately related to the ionospheric electrojets. One should therefore expect some relation between the auroral electrojets and PC, especially during winter, when the ionospheric conductivity in the polar cap is at minimum.

The most widely known measure of auroral electrojet activity are the magnetic activity indices AE, AU and AL. They were introduced by Davis and Sugiura [1966] and where officially adopted by IAGA in 1969. By their wide and frequent use they have since then proved a very useful tool among scientists. They have been used frequently both in detailed descriptions of individual substorms, and as a measure of the general level of magnetic activity in the auroral oval. In this work we have used seven years of data to analyze the relation between PC and AE, AU and AL, in order to judge to which extent PC can be used as an alternative indicator of the level of activity in the auroral electrojets, and to elucidate some of the differences between the indices.

We have examined the linear correlation between PC and AE, AL and AU and find a surprisingly high correlation coefficient R. The correlation is best with AE and during winter, where we on the basis of 15 minute averages find R = 0.8-0.9. We find that this correlation is sufficiently high to ensure that the single station index PC actually measures something global and not mainly local phenomena. We have, furthermore, compared PC-variations with the current distributions derived from the model of Kamide et al. using six meridian chains of magnetometers for selected intervals, and have found that PC is sensitive, both to electrojet activity of the two cell type, and also to substorm intensifications of the westward electrojet, if they occur in the postmidnight sector, but less sensitive to substorm intensification, if they occur primarily in the premidnight sector. We conclude that the PC-index, although intended to measure only two cell activity, can be used during

winter and equinox, as a fast available indicator of the "global" activity in the auroral oval, excluding intensifications of the westward electrojet in the premidnight sector. Apart from being available years before AE, PC could also be computed for periods in the past where AE for different reasons is not available.

The auroral electrojet activity is an extremely complex phenomena, with several different sources (se e.g. Kamide and Akasofu, [1983]), and it is unthinkable that it can be accurately described by a single index like AE or PC. There is, therefore, a current trend to develope more complicated indices, which describes the currents and other physical parameters involved more accurately [Kroehl and Kamide, 1985; Akasofu et al., 1983]. These indices, however, have the limitation that they cannot easily be derived continuously, and for many periods in the past they are impossible to calculate, simply because of lack of needed data. In this connection, an index like PC will have its justification and strength.

There are several problems one encounters using AE, AU and AL, where one could imagine the PC-index could be useful:

- AE, AU and AL are only available with a time delay of several years. They are derived from data from 12 observatories, some of which is still in analogue form, and the digitizing and data quality control is a long and slow procedure. The PC-index on the other hand is derived from data from a single station, and can therefore be calculated and published very quickly.

- The auroral electrojet indices cannot distinguish between local phenomena, where the disturbance is seen only at one or two stations, and more global phenomena involving a major part of the auroral oval.

- The auroral electrojet indices can only be derived for the northern hemisphere auroral oval and especially AU show seasonal variations [Allen and Kroehl, 1975]. The magnetic perturbation at a near pole station shows of course also seasonal variations, but the PC-index could be derived simultaneously for two stations, one in each hemisphere.

- The AE-index has been criticized for not monitoring substorms accurately, especially has it been shown that the AE observatories cannot monitor substorms, when the oval contracts poleward of 72 degrees invariant latitude [Akasofu et al., 1983; Kamide and Akasofu, 1983].

V.1 Linear correlation analysis

To investigate the relationship between PC and the auroral electrojet activity, we have made a statistical analysis where we compute the linear correlation between PC and the auroral zone indices AE, AL and AU. The fact that PC is based on data from a single station, allows us to include a very large amount of data in the analysis. We have used seven years of AE, AL and AU-values from 1978-84 and PC-indices from Thule and Vostok. For Thule, digital data were available from 1975 and onwards, and we could therefore compute PC for Thule for the whole period, where the auroral zone indices where available. For Vostok, PC could be computed for the periods 1978-80 and 1983-84. The PC-index is given as 15 minute averages, and, consequently, the 1 minute samplings of AE, AL and AU, provided from World Data Centre C2 in Kyoto, were also averaged to 15 minute values.

From the above discussion, we expect the sources to the PC-index to change with season, and, at least during summer, also with local time. We therefore computed the linear correlation coefficient separately for each season, and as a function of local time. The results are shown in Figure V.1. The left panel shows the results from Thule, and the right panel the results from Vostok. The top panel is local winter, and the bottom local summer. For Thule each hourly correlation coefficient is computed on the basis of roughly 2800 data points, while the same figure for Vostok is around 1600. The correlation with AE, AU and AL are shown with different signatures.

Figure V.1

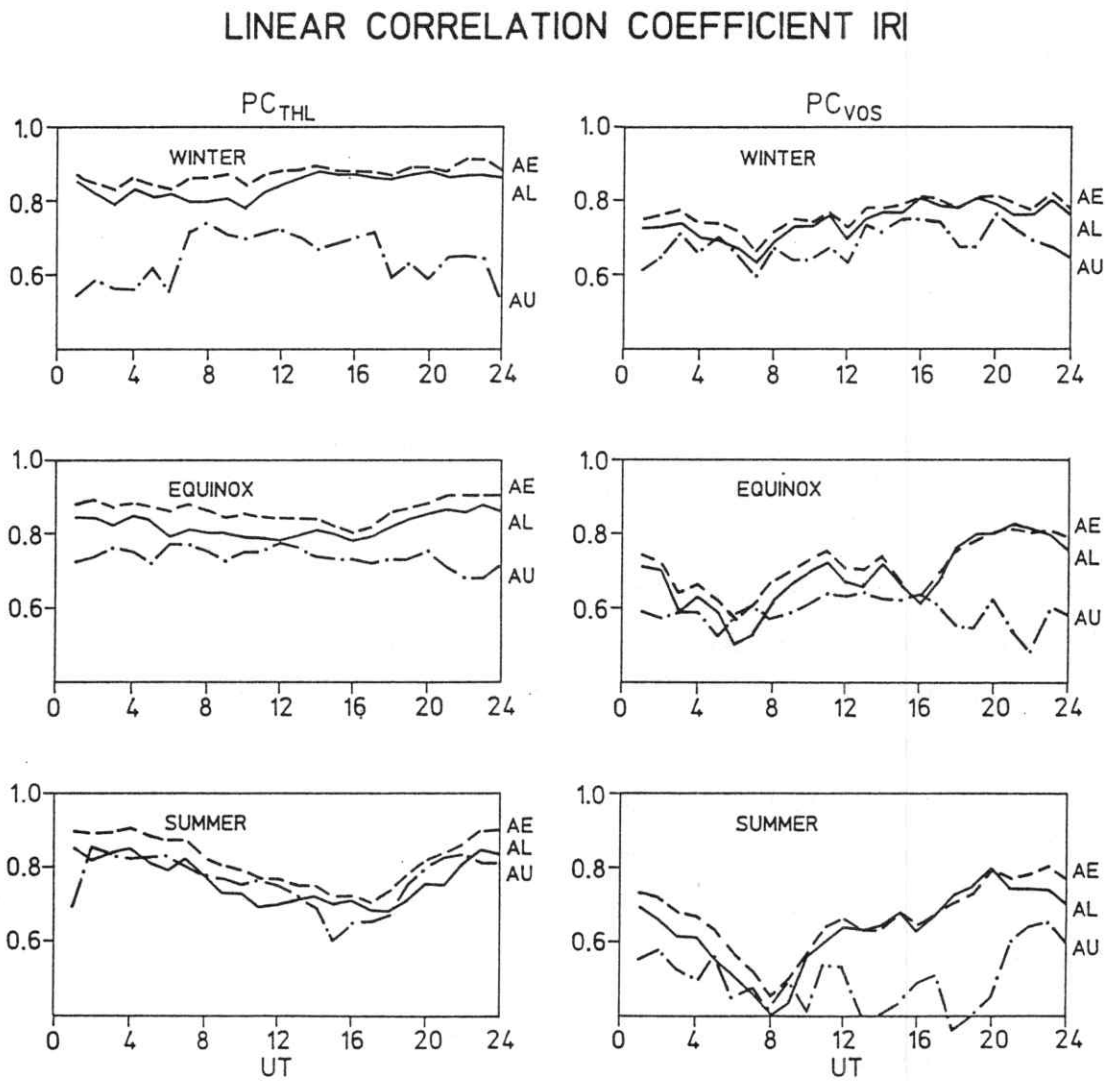

The linear correlation coefficient |R| between PC and the auroral zone indices AE, AL and AU. The results are based on all available data for the years 1978-84, and the correlation coefficient are computed separately for each season and each hour of UT. The left panel shows the results for Thule and the right panel the results for Vostok. The dashed line shows the correlation between PC and AE, the solid line the correlation between PC and AL, and the chain dotted line the correlation between PC and AU.

The first thing to note is that the best correlation is obtained with the AE-index and that it is very high, especially during local winter and equinox. The reason that AE gives the best correlation is probably that AL and AU both are designed to monitor only one of the electrojets, while AE and PC are better suited to monitor the global activity in the auroral oval. It is worth noting, however, that the correlation with AL is almost as good as that with AE.

The correlation with AU is seen to be very seasonal dependent. For Thule, the correlation with AU is rather poor during winter, and for Vostok, it is poor during local summer. The crucial factor thus seems to be the northern winter, and we therefore believe that the poor correlation is caused by a seasonal effect on the AU-index, rather than on the PC-index. Another way to check which of the indices that is causing the seasonal effect is to compare with something global, like a solar wind parameter. We have done this using the IMP-8 satellite measurements of the IMF during the IMS-period 1978-80. The results are shown in Figure V.2, where the linear correlation coefficient between the solar wind parameter vB_z and the various indices is given as a function of season. It is seen that AU shows a much stronger seasonal dependence than the other indices, with a minimum in correlation during winter, indicating that the cause is a seasonal effect on the generation of the eastward electrojet. This is in accordance with earlier investigations of the yearly variation of AU and AL, showing a strong seasonal effect in the level of AU, which is much stronger than in AL [Allen and Kroehl, 1975; Mayaud, 1980]. Having its maximum closer to noon than the westward electrojet, the eastward electrojet is more sensitive to the seasonal variations in the conductivity of the polar ionosphere [Mayaud 1980].

Not only the seasonal changes of AU, but also the seasonal changes of the sources to the PC-index show up in the correlation, although less dramatic. Both in Thule and Vostok, the correlation with AE decreases from local winter to local summer, in such a way that it stays almost constant when the station is on the nightside, but decreases significantly when the station is on the dayside.

Figure V.2

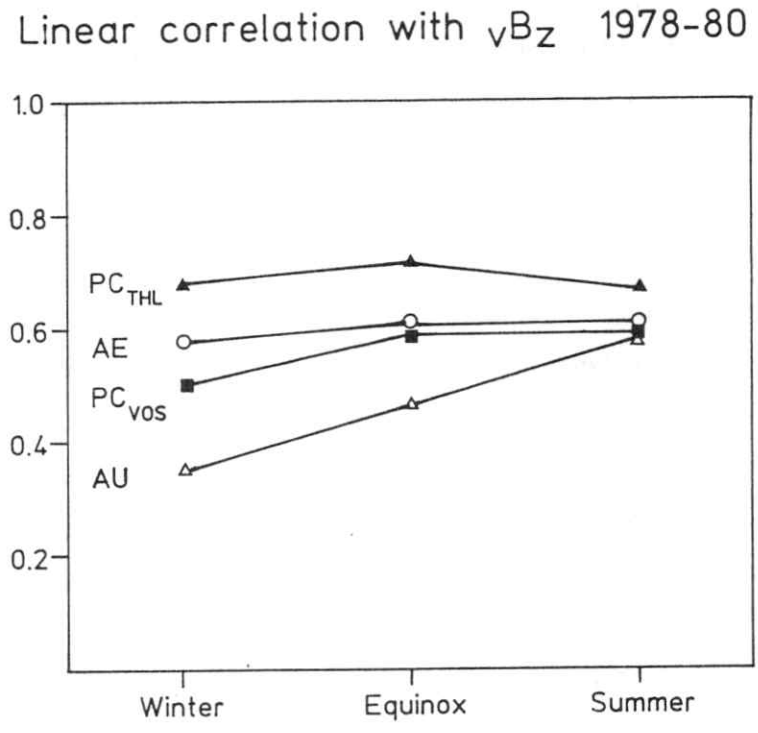

The linear correlation coefficient |R| between the solar wind parameter vB_z as measured by IMP-8 and the various geomagnetic indices as a function of local season in the hemisphere where the index is measured. It is seen that AU shows a stronger seasonal dependence than any of the other indices.

From Figure V.2 it is not possible to determine whether it is the geographic dayside or the magnetic dayside that is most important. In Vostok the minimum in correlation is found between magnetic and geographic noon, and in Thule the minimum is too flat, and magnetic and geographic noon too close together, for anything to be stated. The fact, that the correlation decreases at the dayside during summer, fits well with the discussion of the sources to the PC-index in the last section. The correlation with the auroral zone currents should of course be optimal, when the main source is the field-aligned currents in the oval. During summer at the dayside both "reversed convection events", caused by B_z

positive and B_y controlled currents in the polar cap ionosphere, is known to influence PC, as described in the last sections, and these currents are therefore likely to be the cause of the decrease in correlation.

Figure V.3

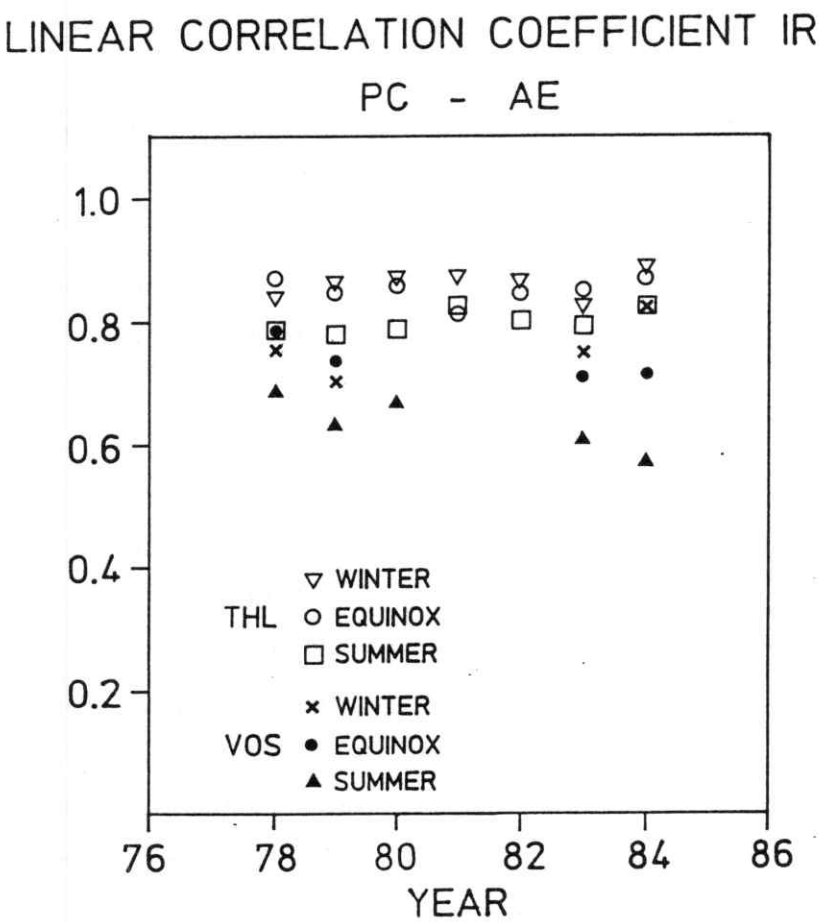

The linear correlation coefficient R between PC and AE for different years. The open symbols indicate the results from Thule and the filled symbols the results from Vostok for different seasons.

The over all correlation with AE and AL is surprisingly high, so it seems reasonable to ask whether there could be any artificial causes, inherent in the way the PC-index is

constructed. The algorithm for the PC-index is empirical and based on observations from the IMS-period 1977-80. The angles and scale factors, used in the algorithm, are, moreover, chosen so as to give the best correlation between PC and the IMF during this time interval. We have, therefore, checked whether the high correlation between PC and AE, obtained during 1977-80, is maintained during 1981-84. Figure V.3 shows the yearly correlation coefficient for Thule and Vostok divided into seasons for the years 1978-84. The open symbols indicate the results from Thule, and the filled symbols the results from Vostok, for different seasons. It is seen that the correlation stays constant, rather than decreases, in the years 1981-84, and we, therefore, conclude that the high correlation is a real physical effect.

It is also obvious from Figure V.3 that the correlation is higher during local winter than during local summer, like we saw in Figure V.1. In Figure V.3 it is seen that this difference is consistent from year to year.

Similarly it is seen that the correlation is significantly lower in Vostok than in Thule. There could be several reasons for this. One explanation could be that both Thule and the stations contributing to AE are measuring the currents in the northern hemisphere, while Vostok is measuring the currents in the southern hemisphere. A second reason could be that Vostok is located further away from the invariant pole than Thule (Vostok: 83.3 degrees inv.lat., Thule: 86.5 degrees inv.lat.), or that the near pole magnetic variations are more peculiar in the southern hemisphere, because the geographic and magnetic pole are much further apart, than in the northern hemisphere. Finally the difference could be caused by different quality of data at the two stations. In Vostok the recordings were changed from analogue to digital only recently, and the equipment used for digitizing and data checking was very old fashioned. From this work we cannot tell which reason is the most important, but from Figure V.2 it is seen, that Vostok also shows a poorer correlation than Thule with the *IMF*. This means that the poorer correlation cannot solely be caused by the fact that Vostok and the AE-stations are in opposite hemispheres, so the quality of data, or location of the stations with respect to the poles, must also have some influence.

The high correlation between PC and AE may be largely influenced by those hours, when both are quiet or only slightly disturbed. In Figure V.4 we have, therefore, shown the correlation computed over ranges of restricted amplitude, ie. for AE > 50nT, AE > 100nT AE > 200nT etc. We see that the correlation gradually decreases with increasing level of activity. This is to be expected, because both indices become more and more inaccurate and difficult to interpret, as the level of activity rises, and more and more sources contribute to the indices, ie. ionospheric currents, field-aligned currents, ring current and wedge currents. Even during moderately disturbed times, however, the correlation stays pretty high.

Figure V.4

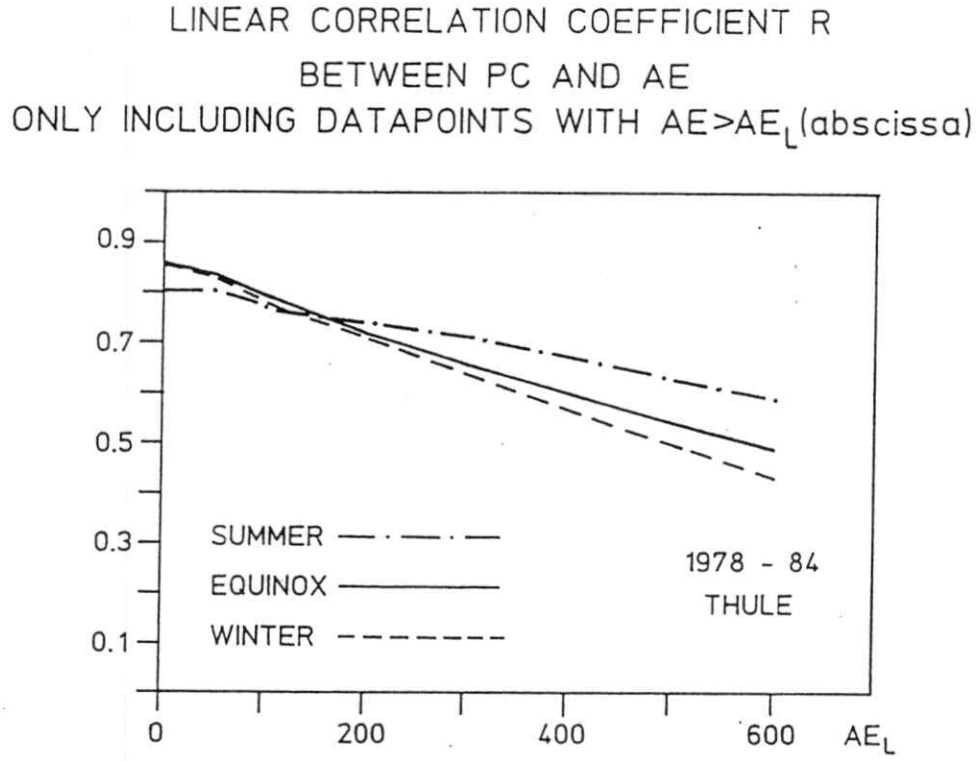

The linear correlation coefficient R between PC_{THL} and AE, computed for data points with AE > AE_L as a function of AE_L.

Figure V.5

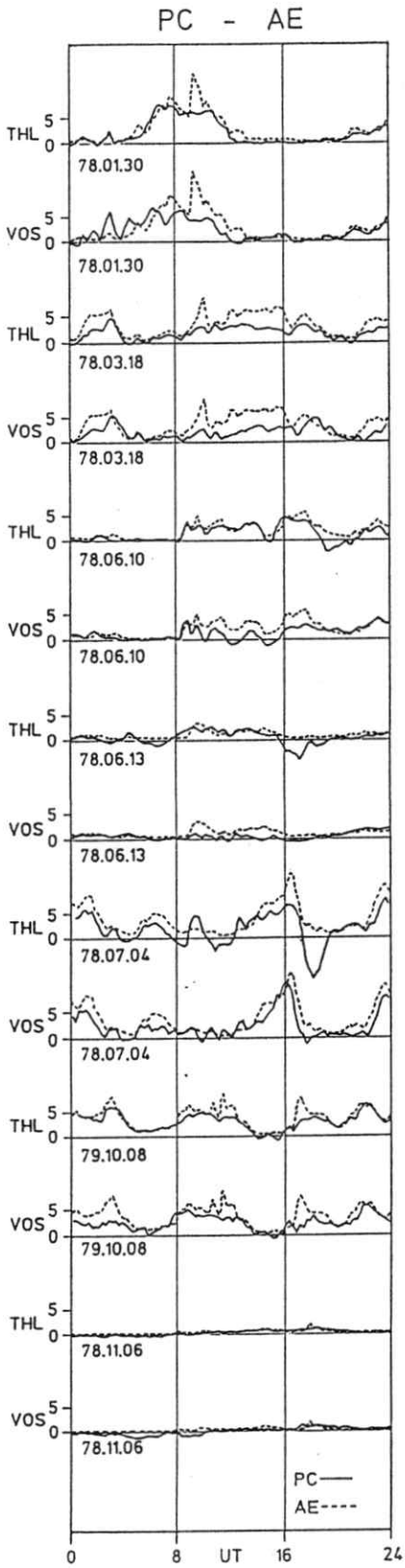

Typical examples of PC-variations in Thule and Vostok together with AE plotted as 15 minute averages. The dashed lines show the AE-index and the solid lines PC. AE is superposed over PC_{THL} and PC_{VOS} for each date.

To give a better idea of what the PC-index looks like compared to AE, and what the differences might be, we have in Figure V.5 plotted some typical examples of PC-variations in Thule and Vostok, together with 15 minute averages of the AE-index. For each day, we have plotted PC in Thule and Vostok as solid lines with AE superposed as a dashed line. The PC-index is obtained by normalization with respect to the solar wind parameter $vB_T\sin^2(\theta/2)$, and a natural unit for PC would, therefore, be "equivalent" mV/m. We want to stress, however, that PC is primarily an index for geomagnetic activity, and only in a statistical sense a measure of the "merging electric field" $vB_T\sin^2(\theta/2)$. In Figure V.5 we, therefore, present PC with a size corresponding to "equivalent" mV/m but as a quantity without unit.

Figure V.6 LINEAR CORRELATION COEFFICIENT IRI

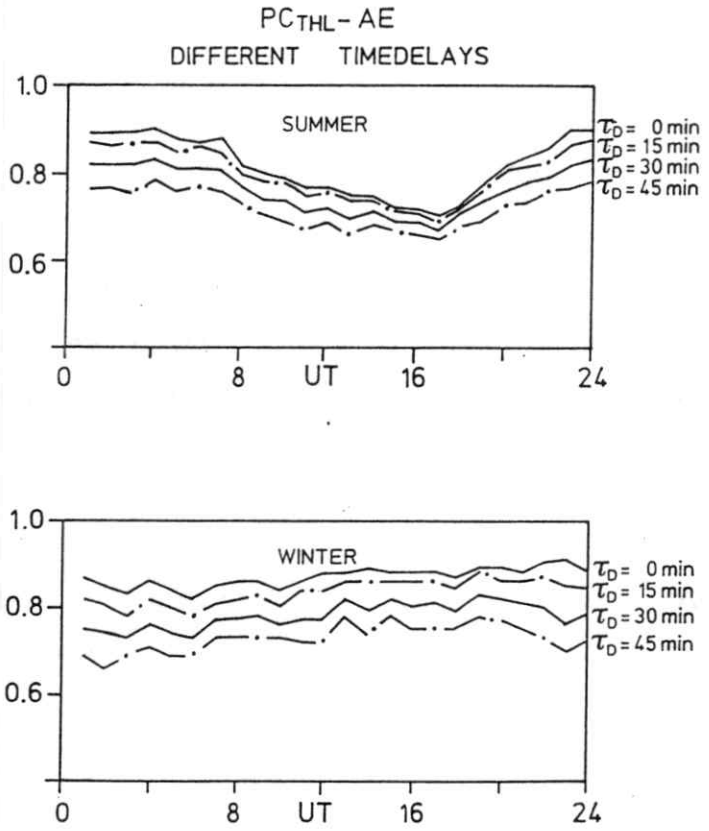

The linear correlation coefficient R between PC_{THL} and AE as a function of UT-hour for different time delays τ_D. The results are shown for summer and winter separately and by letting AE lag with 0, 15, 30 and 45 minutes. It is seen that the best correlation is obtained with no time lag. MLN and GLN indicates magnetic and geographic local noon for Thule.

As the statistical analysis shows, the overall correspondence is seen to be good, especially can it be noted that no significant time delay exists between PC and AE. To investigate this point further, we have in Figure V.6 plotted the correlation coefficient between PC in Thule and AE, using different time delays τ_D. The results were computed for summer and winter separately, letting AE lag with 0, 15, 30 and 45 minutes. It is obvious that the best correlation is obtained with no time delay between the two indices, although 15 minutes time delay is almost as good during summer in the daytime. If the correlation is computed by letting PC lag instead of AE, the correlation also decreases with increasing time lag. One would not expect any time delay if the sources to the two indices were directly connected, so these results are in accordance with the conclusion that the source to the PC-index, during winter or nighttime, is distant field-aligned currents.

V.2 Differences and similarities between PC and AE.

Above we have found a high statistical correlation between PC and AE. This result ensures us that although PC is derived from a single station, it is a good measure of the global activity level, rather than an indicator of local phenomena in the near pole region. An exception is when the station is in the dayside during summer, where the correlation is decreased, because B_z northward and B_y induced local ionospheric currents disturb the PC-index. But even when the correlation is high, there may still be systematic differences between PC and AE, which must be noted if PC is to be used to indicate activity level in the auroral electrojets. In this section we use event studies to describe what we believe is systematic differences, in a qualitative way.

A principal difference is that PC is designed to maximize the correlation with the solar wind parameter $vB_T\sin^2(\theta/2)$, while AE is constructed to measure the maximum current in the auroral electrojet. The auroral electrojet current have been found to consist of at least two components; one directly driven by the solar wind, and one driven by release of energy stored in the geomagnetic tail (see e.g. McPherron and Manka, [1985] and

references therein). Clauer and Kamide [1985] found that the two components could be identified with the geomagnetic variations described as DP1 (substorm intensifications of the westward electrojet) and DP2 (two cell activity) [Obayashi and Nishida, 1968; Nishida, 1968a, 1968b]. The DP1 disturbance is characterized by an intense activation of the westward electrojet, while DP2 is a worldwide two cell disturbance, with a high correlation with the southward component of the IMF. One could therefore hope that PC mainly measured DP2, while AE mainly measured DP1, and that a comparison between PC and AE, therefore, could help to distinguish the driven from the unloading component of the auroral electrojets. The high correlation we find between PC and AE, and the fact that the variations are synchronous, however, indicates that this picture is not correct. Firstly, it has been found that the DP2-system, which originally was thought to be without current concentration in the auroral zone, will have such concentration if the conductivity in the oval is enhanced [Vasyliunas, 1970; Clauer an Kamide, 1985]. DP2 fluctuations will consequently be a significant part of AE. Secondly, a comparison between the proposed DP1 equivalent current system [see e.g. Clauer and Kamide, 1985] and the directions in which PC is measured (Figure 1) shows (see e.g. Table II.2 or Figure IV.1) that the DP1-current must also influence PC. Clauer and Kamide, [1985] have analyzed the substorm of March 22., 1979 using six meridian chains of magnetometers to identify which type of current system, DP1 or DP2, increased and prevailed during the different phases of the substorm. Exactly such analyses are needed if we shall judge the relative importance of DP1 and DP2 on PC and AE. In Figure V.7 we have therefore shown PC and AE on March 22, 1974 with indications of the periods of time, in which increases in DP1 and DP2 current systems were identified by Clauer and Kamide, [1985].

During the first interval, only the DP2 system is found to exist. During the second interval, the increase in AE is caused by a growth of a DP1 type current during substorm expansion. During the third interval, the increase is caused by a growth of the DP2 system, and during the fourth interval both DP1 and DP2 are found to increase. The data from Thule indicates that DP2 has a relatively stronger influence on PC than DP1, compared to AE. This, however, is not confirmed by the data from Vostok, so we feel that more cases of DP1/DP2-identifications are needed, in order to make any conclusions. All we can state here is that both DP2 and DP1 influence both indices significantly.

Figure V.7

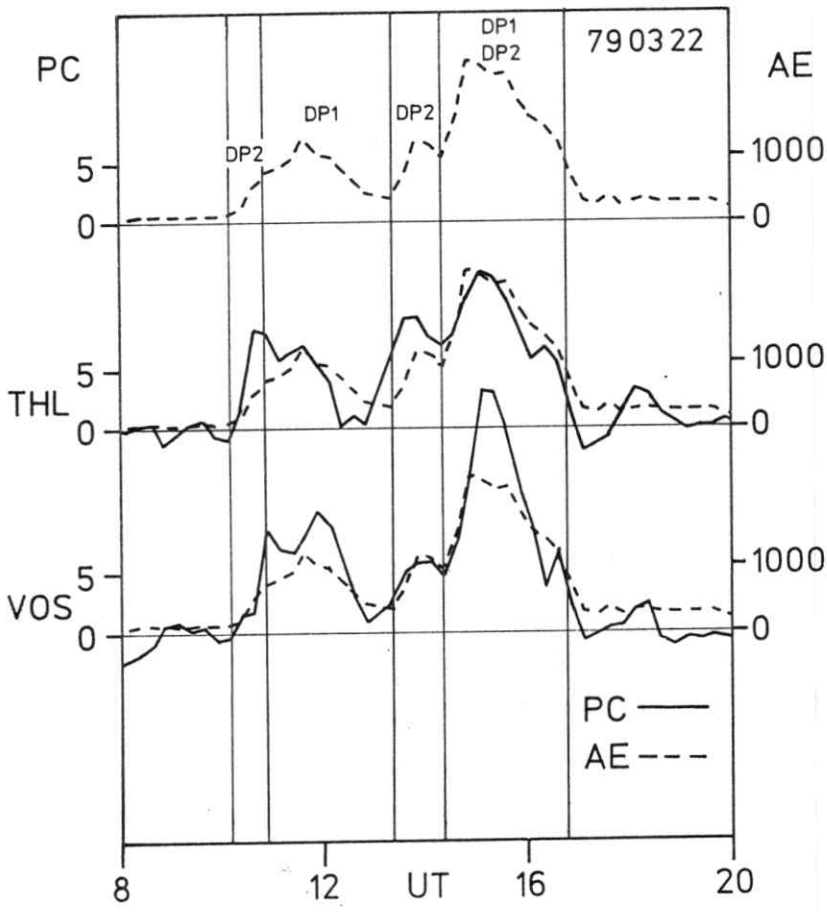

PC and AE on March 22., 1979. AE is plotted in all three panels as a dashed line. The vertical lines indicate the intervals of time where increases in DP1 and DP2 disturbances where identified by Clauer and Kamide [1985].

Another difference between PC and AE is that the AE-index typically shows a lot of spikes, not seen in PC. This is also illustrated by Figure V.8, which shows a typical fo from the meridian chain of magnetometers in Greenland. This chain spans from Thule, in the central polar cap, to Narsarsuaq, in the auroral zone, contributing to the AE-index. It is noted that the perturbations change gradually from being relatively smooth in Thule, to highly fluctuating in Narsarsuaq. So one explanation could be that the spikes are localized features within the auroral oval, which are not seen in the central polar cap. By

always using the perturbation at the station where it is at maximum, AE focuses on local features, rather than the global average.

Figure V.8

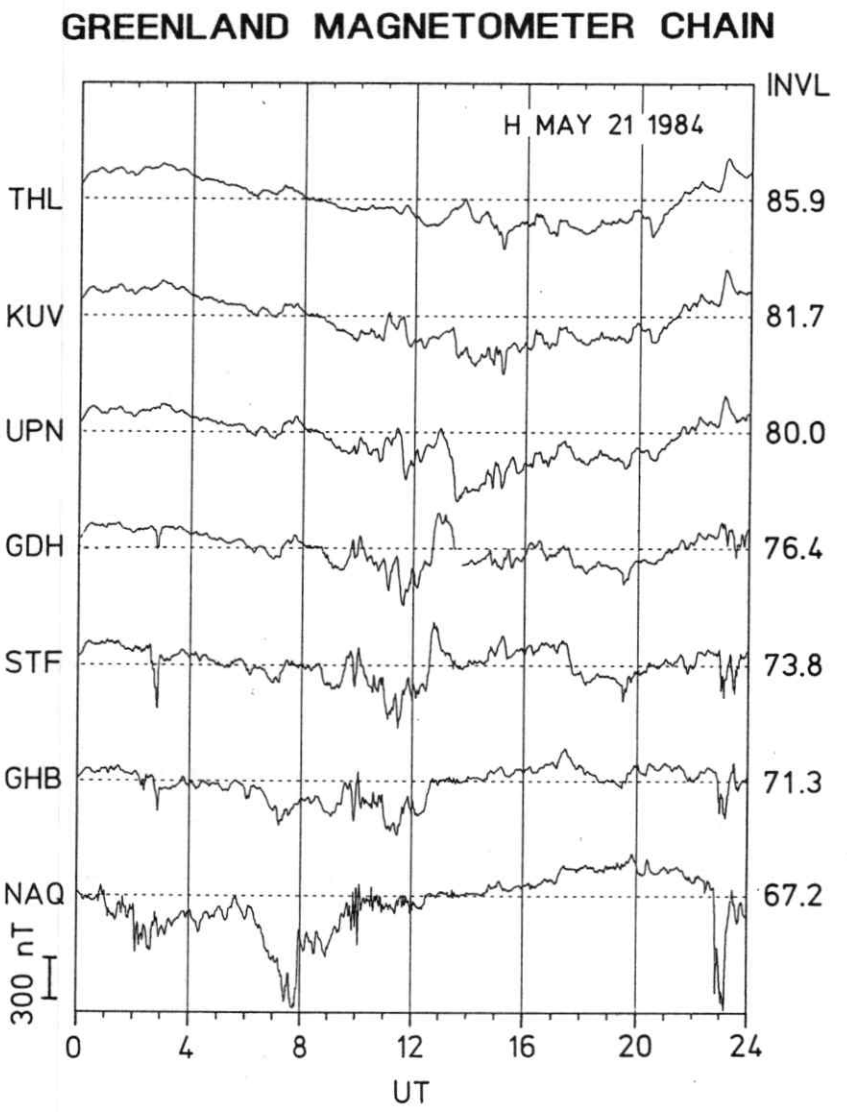

Typical magnetograms from the meridian chain of magnetometers on the west-coast of Greenland.

The local features, described above, can explain spikes of relative short duration, but, as can be seen from Figure V.5, there are also "spikes" of a duration up to an hour or so in AE, which are almost unnoticed in PC, fl. at January 30, 10 UT, and March 18, also at 10 UT. Local features, seen only at one or two AE-stations, can hardly explain these events. Here, we believe, the explanation has to be found in a changing configuration of the field-aligned currents in the oval.

Both the size and the direction of the horizontal magnetic perturbation in the central polar cap would depend upon how the field-aligned currents in the oval are distributed. The region 1 currents, associated with the general two cell convection, downward at the dawnside and upward at the duskside, would give a sunward magnetic perturbation if they were distributed symmetrically with respect to the noon-midnight meridian. If the symmetric picture were somewhat distorted, or a contribution from a sunward Hall-current in the polar cap were added, this might give rise to the observed magnetic perturbations in the central polar cap (Figure III.1). As noted by Maezawa, [1976] the field-aligned currents associated with the intensification of the westward electrojet during substorms, downward in the postmidnight hours and upward in the premidnight hours, could also cause magnetic perturbations in the observed direction (see Figure 4 in Maezawa, [1976]). If the substorm, however, was occurring in the premidnight sector, with a strong westward electrojet in this time sector, the associated magnetic perturbation in the central polar cap would be deflected westward, away from the direction used to compute the PC-index. Consequently PC would not be very sensitive to a DP1 disturbance taking place in the premidnight sector. For the event of March 18, this is in fact the case. March 18, 1978 was analyzed by Kamide et al., [1982] using six meridian chains of magnetometers. Calculating the ionospheric currents they found a strong intrusion of the westward electrojet in the premidnight sector occurring at 10 UT. Their results are reproduced in Figure V.9 together with the observed horizontal perturbation in Thule. The Thule data are rotated to symbolize equivalent current, and are presented in an invariant latitude - MLT diagram. It is seen that the horizontal perturbation is deflected westward at 10 UT, and PC is therefore not sensitive to this DP1-disturbance. Comparing six days of results from the current model taken from Kamide et al., [1982] and Kamide et al., [1983] with PC-indices, we have found it to be a consistent feature that PC is insensitive to DP1 disturbances taking place in the premidnight sector.

Figure V.9

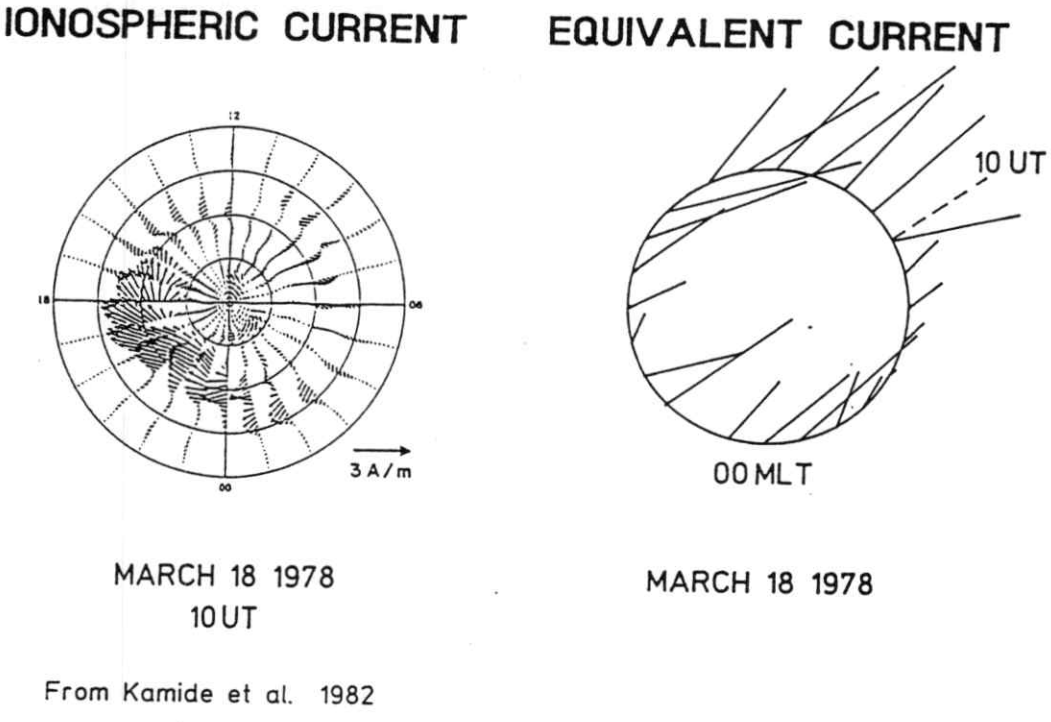

Right: Observed horizontal magnetic perturbations in Thule at March 18. 1978 presented in an invariant latitude - magnetic local time diagram. The vectors have been rotated 90 degrees to symbolize equivalent current. At the indicated times 10 UT at March 18. The perturbation in Thule is seen to be deflected westward.
Left:Ionospheric currents at March 18. 10 UT, modelled from observations from six meridian chains of magnetometers. A strong intrusion of the westward electrojet into the premidnight sector is seen. (Reproduced from Kamide et al., [1982]).

Returning again to Figure V.5, another interesting difference between PC and AE may be noted. Sometimes during summer PC becomes strongly negative, while AE stays close to zero. In Figure V.5 some good examples of this is seen at June 13, and July 4, 1978 in Thule. These events are associated with the earlier mentioned reversed convection events occurring in the polar cap, when B_z becomes positive during summer. It is worth noting that Vostok, having winter, at the same time stays close to zero. Unfortunately, the effect of the polar cap currents during northward IMF are not always to create a negative PC-disturbance. As can be seen from Figure III.2, showing the average horizontal disturb-

ance in Thule for B_z>2nT on top of the PC-directions, it may just as well create a positive PC-disturbance. The sign will depend partly on the local time of the PC-station and partly on the sign of the IMF B_y-component. This point is illustrated further in Figure V.10, where the PC-indices of Thule and Vostok are superposed over AE and together with IMP-8 measurements of the IMF B_y- and B_z-components for June 5, 1979.

Figure V.10

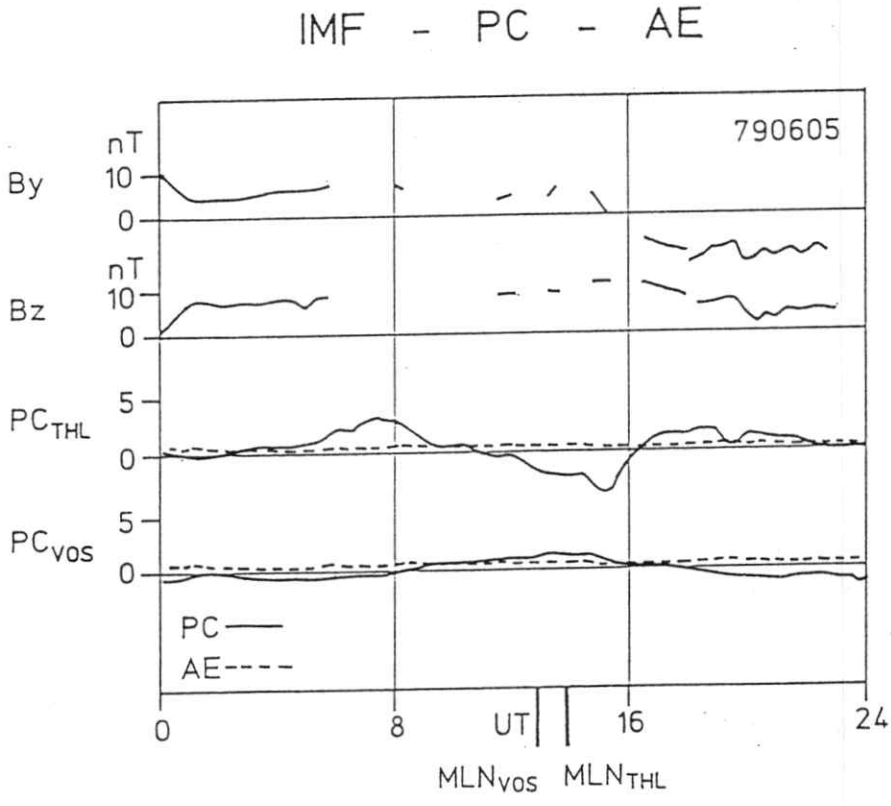

An event illustrating how "reversed convection events" can influence the PC-variations. The two top curves show IMP-8 measurements of the IMF B_y- and B_z-component. The bottom curves show PC_{THL} and PC_{VOS} as solid lines with AE as a dashed line on top. It is seen that such events can cause both positive and negative PC-disturbances in the summer hemisphere, depending on local time and the sign of IMF B_y. MLN indicates magnetic local noon.

The IMF B_z-component is positive throughout the day and both strong positive and strong negative disturbances are observed in Thule while AE stays close to zero. The shift from positive to negative PC in Thule at around 13 UT that occurs during positive B_y is a local

time effect, appearing because the station is moving under a current system in the polar cap, which is far from being homogeneous. This can clearly be seen in Figure III.2 in the panel showing the mean horizontal perturbations when $B_y>0$ and $B_z>2nT$ during summer. The second shift, from negative to positive disturbances around 16.30 UT, is caused by a change in the IMF B_y-component from positive to negative. It is worth noting that in Vostok, where it is winter, PC stays relatively close to zero throughout the day, because the low conductivity in the dark southern polar cap prevents the B_z positive-associated ionospheric currents from being formed. The small deviation from zero actually seen in Vostok is probably caused by the way the baseline was determined. In Vostok the diurnal variation on the five most quiet days of the month was used as baseline, while a constant baseline determined from quiet winter days was used in Thule. Figure V.11 shows another example, where Vostok is measuring $B_z>0$ currents and Thule is in the winter hemisphere.

Figure V.11

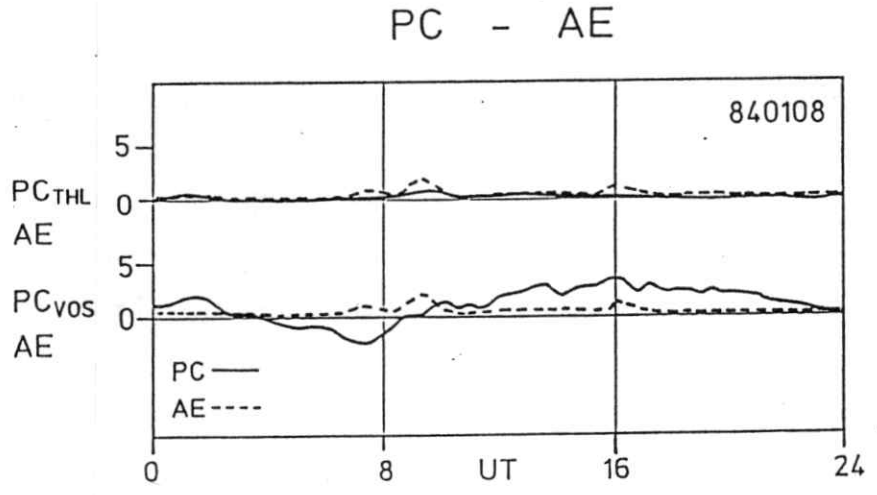

The same as Figure V.10, but on a day where it is winter in Thule and summer in Vostok. Unfortunately no IMF data were available this day, but AE shows that it was a very quiet day. Like in Figure V.10 strong disturbances are observed in PC, but only in the summer hemisphere.

It is obvious that the occurrence of reversed convection events creates a serious problem, if you want to interpret the PC-index during summer, without having access to the IMF or the AE-index. Looking only at the PC-index, there is no way to distinguish between a positive disturbance caused by the current system associated with B_z positive, and a positive disturbance associated with electrojet activity in the oval. The projection procedure used in the algorithm for the PC-index only eliminates part of the NBZ-disturbances, namely the ones giving a negative PC or a PC close to zero. In using the PC-index it is therefore very important to have access to PC-values from both the northern and southern hemisphere. The PC-index from the winter hemisphere will stay close to zero, when the disturbance in the summer hemisphere is caused by the currents associated with the NBZ-currents, thereby enabling you to distinguish between the two effects. It is clear from this that the PC-index not is suited to monitor the currents associated with positive B_z. It is constructed to measure normal two cell disturbances, and not reversed convection events. In our opinion it would require at least two stations in the same hemisphere, and widely separated in local time, to monitor the inhomogeneous currents associated with positive B_z.

The last panel of Figure V.5 shows PC and AE variations on a very quiet day, November 6, 1978. The AE-index have earlier been criticized for not being able to monitor substorms when the oval contracts poleward of 72 degrees invariant latitude because of the location of the AE-observatories [Akasofu et al., 1983; Kamide and Akasofu, 1983]. When the currents in the oval are moving poleward, away from the AE-observatories, they are, however, approaching the PC-observatory in the central polar cap. Therefore, one could hope that by using AE and PC simultaneously, one could distinguish poleward movements of the electrojet from decreasing current intensity, and be able to detect the occurrence of substorms when the oval is contracted. In theory this of course should be possible, but in practice it may show to be of little importance. Substorms occurring at high latitudes are namely normally very weak and localized, and therefore not very likely to be detected by a PC-index measuring the average activity in the oval as a whole. In fact the day November 6, 1978 in Figure 8 was used by Kamide and Akasofu, [1983] as an example of a day, where substorm activity could be seen at a station poleward of the AE-observatories. Around 9-12 UT substorm activity was seen at the station Inuvik at 70.5 degrees

invariant latitude, which was not detected in AE. But, as can be seen from Figure 8, no significant increase is observed in PC at this time.

In summary we have found:

1. There is a high correlation between AE and PC during winter and equinox, the linear correlation coefficient being 0.8-0.9 for Thule and 0.7-0.8 for Vostok.

2. The correlation is better with AE than with AL and especially AU.

3. PC is influenced both by DP2 and DP1 disturbances, but is not sensitive to DP1 disturbances taking place in the premidnight sector.

4. The most likely source to PC during winter is field-aligned currents at the poleward rim of the auroral oval, while Hall-currents in the polar cap ionosphere probably dominates during summer.

5. Existence of "reversed convection events" in the polar cap controlled by the IMF northward and azimuthal components makes an unambiguous interpretation of the PC-index impossible during summer.

We believe that PC can be used as a fast available indicator of auroral electrojet activity, excluding substorm intensifications of the westward electrojet in the premidnight sector. Compared to AE, PC has the limitation that during summer it can only be used for weak or southward B_z due to the effect of the so called "reversed convection events". We therefore stress the importance of having PC available from both hemispheres.

VI. LONG-TERM VARIATIONS

VI. Check of validity of the algorithm

The algorithm of the PC-index is based on the relationship between near pole magnetic variations and the IMF, during a certain time period, namely, the IMS-period 1977-80. In this connection, the question arises whether the relationship between near pole magnetic perturbations and the IMF changes during the course of the solar cycle? The period 1977-80 constitutes the rising part of the solar cycle, and it is therefore necessary to check the validity of the algorithm at other parts of the solar cycle. In this study we have IMP-8 measurements of the IMF available at a time resolution of 15 minutes for the years 1983-85. This period falls within the declining part of solar cycle 21, and we have, therefore, used this data set to make the necessary check. We have simply repeated the investigation, described in section II, which lead to the definition of the algorithm. We have found the optimal angles φ for the parameter $vB_T\sin^2(\Theta/2)$ and the matching linear coefficient of correlation R and orthogonal regression coefficient $\alpha_\perp$. The main difference is that the coefficient of correlation has decreased about 10-20% in 1983-85 compared to 1977-80. The response to the IMF as expressed by $\alpha_\perp$ is also somewhat smaller in 1983-85, while the optimal angle φ is almost unchanged. In the last section, Figure V.3, we saw that the correlation between PC and AE remained unchanged from 1978 to 1984, so it is a puzzle why the correlation with the IMF has decreased. To answer this question, we have computed the yearly correlation coefficients between PC and $vB_T\sin^2(\Theta/2)$ *and* the yearly correlation coefficient between AE and $vB_T\sin^2(\Theta/2)$. The results are shown at Figure VI.1 in a diagram similar to Figure V.3, with different symbols for different seasons.

Figure VI.1

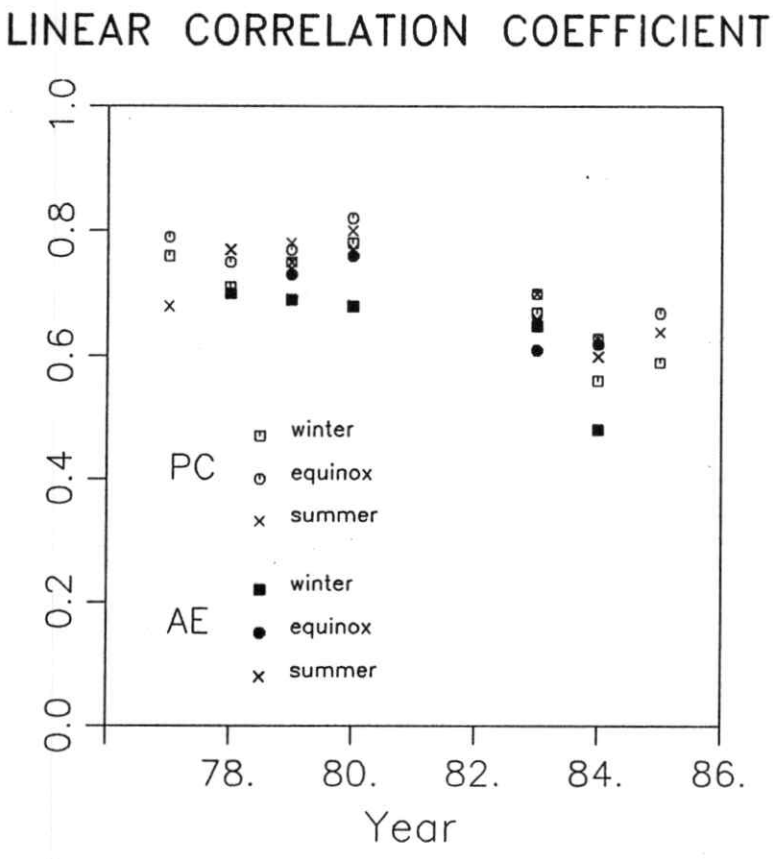

Yearly linear correlation coefficients between PC and the IMF-parameter $vB_T\sin^2(\theta/2)$, compared to the same computed for AE instead of PC. It is seen that the correlation decreases in the years 1983-85 for both PC and AE.

It is seen from the figure that both the correlation with PC and with AE decreases at the falling part of the cycle. This indicates that the reason for the decrease is to be found, not in the definition of the PC-index, but rather in some fundamental change in the solar wind - magnetosphere interaction during the course of the solar cycle.

Figure VI.2 shows annual means of the PC-index for the solar cycle 21 from 1975-85 together with the mean annual sunspot number. It is clear from this that the two parameters show a different solar cycle variation.

Figure VI.2

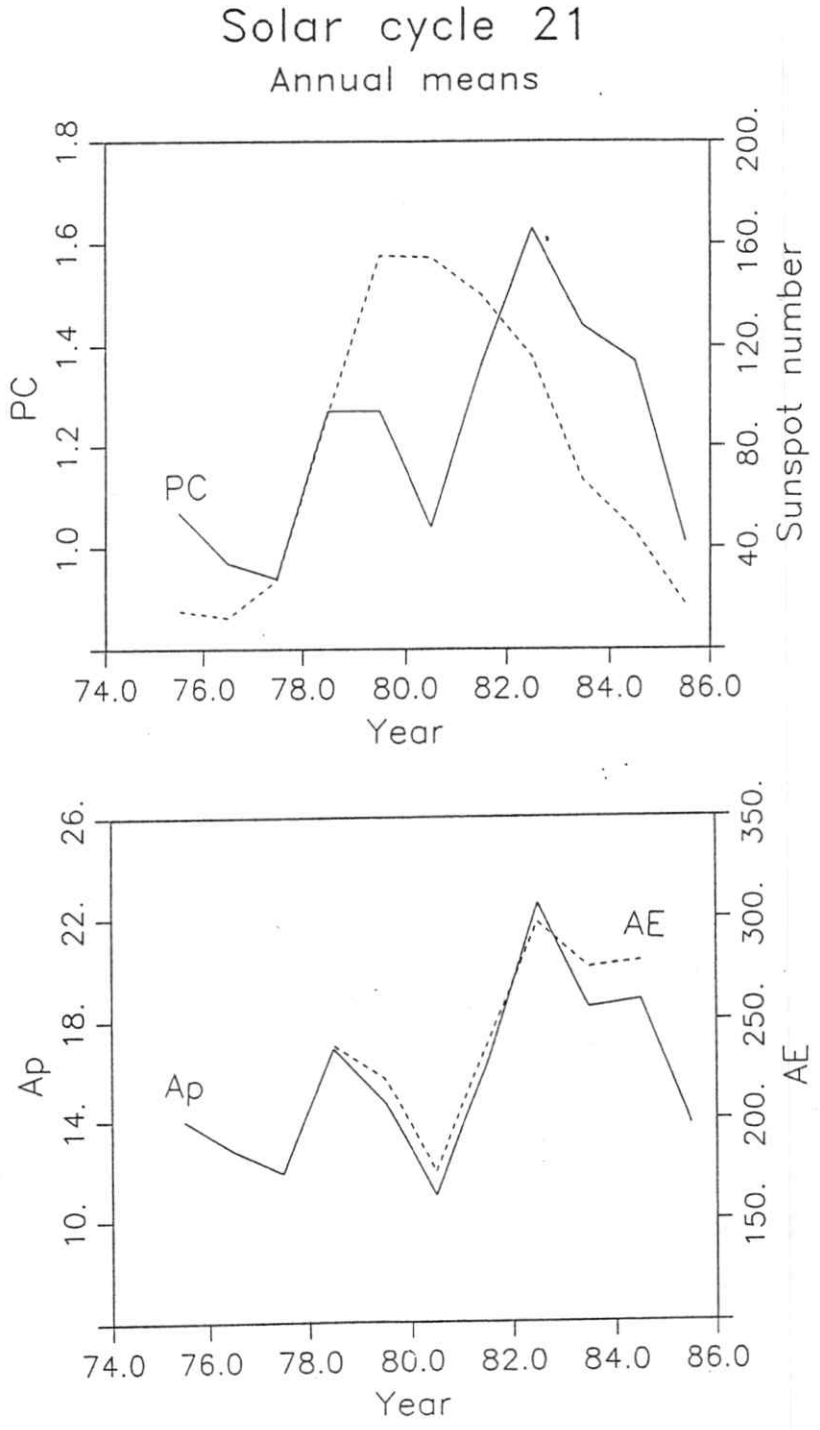

Top: Variations of PC (solid line) and sunspot number (dashed line) during solar cycle 21.
Bottom: The same for the two geomagnetic indices A_p (solid line) and AE (dashed line).
The figure shows annual means of the four parameters.

The difference between the solar cycles of sunspot number and geomagnetic activity has been discussed by many authors [e.g. Bartels 1963, Ol' 1971, Crooker et al. 1977, Feynman 1980, Legrand and Simon 1989]. Each cycle shows individual features, but, in general, geomagnetic activity rise with the sunspot c. During maximum and decline of the sunspot cycle the activity continues, although it often shows a local minimum close to sunspot maximum. In the late part of the decline, the activity peaks a second or third time, in connection with fast streams of solar wind created by solar coronal holes. After this, the activity quickly decreases to a minimum together with sunspot minimum. The bottom part of Figure VI.2 shows annual means of two other geomagnetic indices AE and A_p. A_p is a daily planetary index derived from the index K_p. K_p measures averages from 14 selected midlatitude (subauroral) observatories of 3 hour ranges of the activity. The difference between A_p and K_p is, that A_p is given as a daily index, and in a linear scale, while the scale of K_p is quasi-logarithmic.

The important thing to note is that all three indices, PC from the polar cap, AE from the auroral zone, and A_p from the midlatitude, show the same variation: A rise with the sunspot number, a local minimum in 1980 close to solar maximum, a second and larger peak in 1982, and traces of a third peak in 1984. The close similarity between the three indices indicates that the long-term variations in PC are representative for a rather broad range of geomagnetic activity.

Many works have shown that there is a close correlation between long-term variations in geomagnetic activity and the solar wind velocity (e.g. Snyder et al. [1963], Hirshberg [1973], Svalgaard [1977], Crooker et al. [1977]). On shorter time-scales, like and hour or so, it is, as we have seen in section II, well established that the southward component of the IMF is an effective generator of geomagnetic activity. On such time-scales B_s even seems to dominate the variations in activity, because the solar wind velocity normally varies very slowly. On long time-scales, at the other hand, the opposite has been the case: While it is well established that the solar wind velocity plays a role, it has been more difficult to document the influence of B_z. Siscoe et al. [1978] who studied the solar cycle variation of IMF, and especially B_z, during solar cycle 20, found that it was distinctly different from the variation of geomagnetic activity as described by A_p.

Figure VI.3

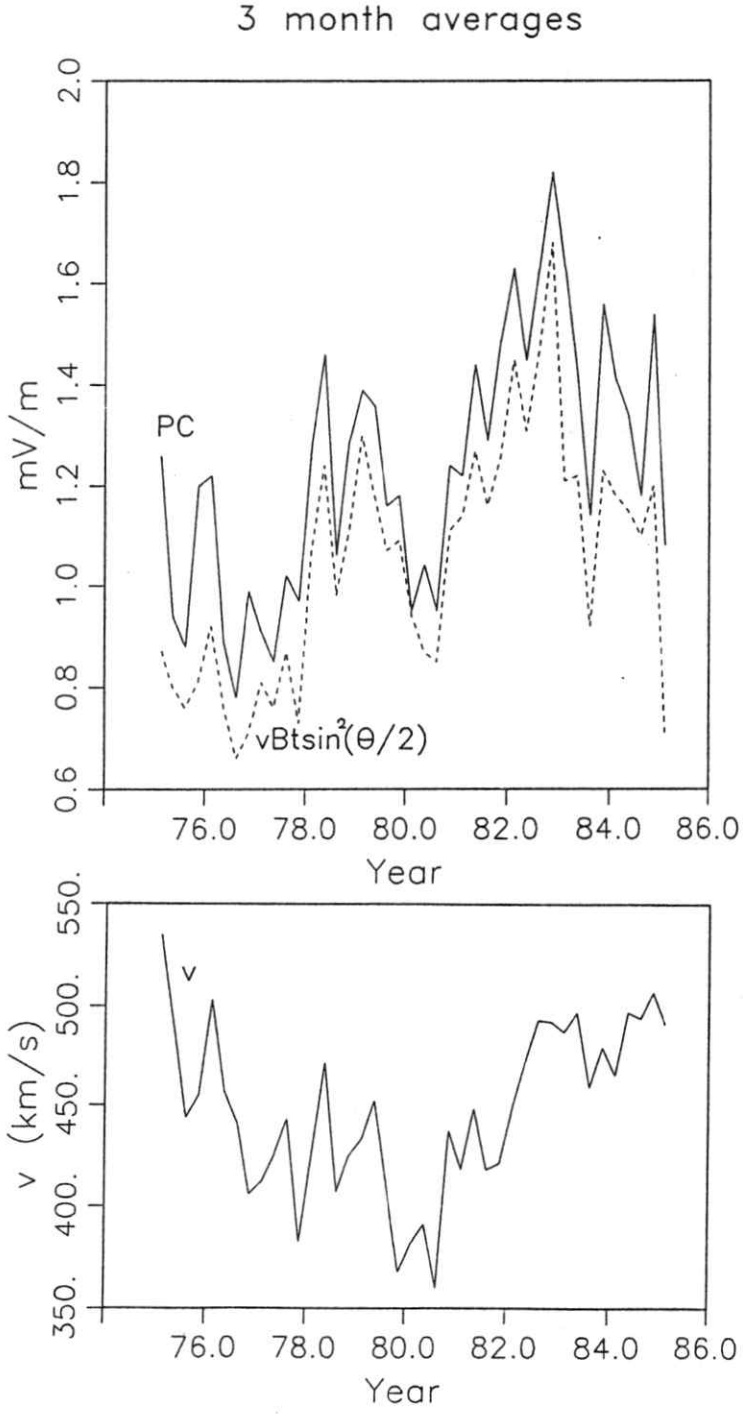

Top: Variations of PC (solid line) and the IMF-parameter $vB_T\sin^2(\theta/2)$ (dashed line) during solar cycle 21.
Bottom: The same for the solar wind velocity.
The figure shows three month averages.

Crooker et al. [1977] examined the correlation between v and B_z, and A_p during solar cycles 19 and 20, and found a much better similarity between v and A_p than between B_z and A_p, and concluded that the data set was insufficient, to establish whether B_z had any influence on the long-term variations of A_p or not. Feynman [1980] examined the same cycles, but used the midlatitude magnetic activity index aa and the equatorial index Dst. She concluded that aa was controlled solely by v but Dst was controlled by vB_z.

In order to investigate this point for solar cycle 21 and the PC-index, we have computed three month averages of PC and the solar wind parameter $vB_T\sin^2(\theta/2)$ for the years 1975-85. The computation of the solar wind parameter was based on hourly averages of v, B_z, and B_y. Figure VI.3 shows the result. The Figure shows a striking similarity between the two curves, both for the variations with a period of several years, also seen in Figure VI.2, and for variations on shorter time-scale within a year. It should be noted, at this place, that the reason for the similarity is not to be found in the rather complicated appearance of the parameter $B_T\sin^2(\theta/2)$. A computation of the averages of the parameter vB_s produces very similar results.

The lower part of Figure VI.3 shows three month averages of the solar wind velocity. By comparison with the upper part of the figure, it is obvious that the inclusion of the IMF-parameter $B_T\sin^2(\theta/2)$ (or B_s) improves the correlation with PC considerably. We believe that these data leave no doubt that the IMF and especially the southward component influence geomagnetic activity considerably, on long, as well as on short, time-scales. The reason that this was less obvious in the studies of cycles 19 and 20, is probably that the long-term variations of B_z was much less in the previous cycles.

Figure VI.4 shows annual averages of the solar wind parameters v and B_s together with the A_p-index, for cycle 20 (lower panel) as well as for cycle 21 (upper panel). In cycle 20 the similarity between v and A_p is much better than in cycle 21, but the variation of B_s was also much smaller.

Figure VI.4

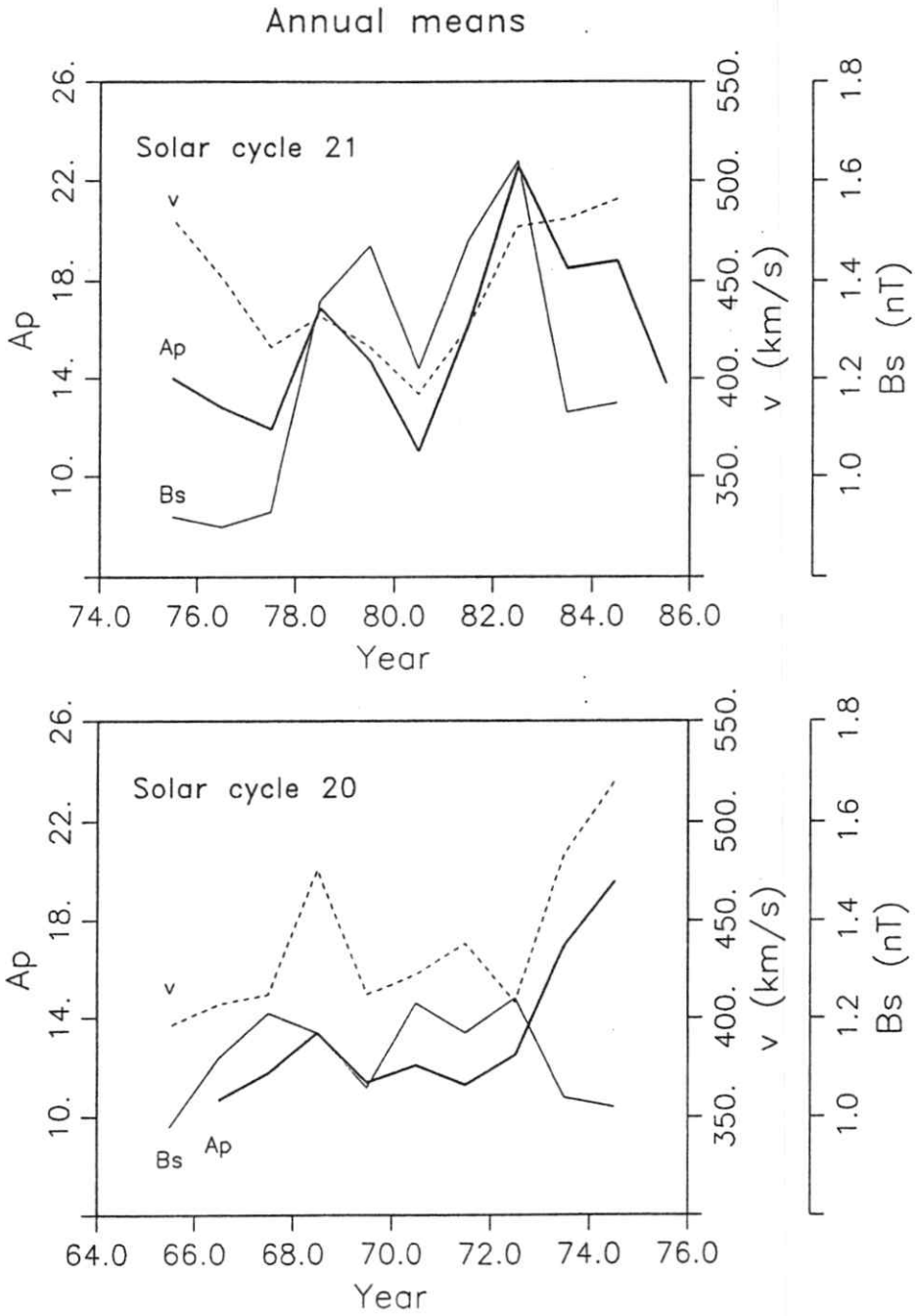

Top: Variations of A_p (broad solid line), the solar wind velocity v (dashed line) and the southward component of the IMF B_s (thin solid line) during solar cycle 21.
Bottom: The same, but for solar cycle 20.
The figure shows annual means.

The close correspondence between PC and the solar wind parameter $vB_T\sin^2(\theta/2)$ on long, as well as short, time-scales indicates that this parameter is well suited to normalize the PC-index. It does, however, not explain why the correlation between the solar wind parameters and geomagnetic activity is less in 1983-85 than in 1977-80. The key to the answer of this question probably lies in the understanding of the solar sources to the interplanetary medium. One of the best described relations between solar and interplanetary phenomena is the fast solar wind streams created in solar coronal holes. This phenomenon shows up in geomagnetic activity in the late part of the declining phase of the solar cycle, and is rather easy to identify in the magnetograms, because it is a recurrent, with a recurrence time of about one solar rotation. The peak of this type of activity is rather sharp, normally lasting around two or three years. Legrand and Simon [1989] have identified this and other types of solar wind streaming by their geomagnetic signature. In solar cycle 21 they find that the recurrent activity peaks in 1984. We therefore believe that the solar coronal holes is the cause of the third peak in geomagnetic activity in 1984, in solar cycle 21, seen in Figures VI.2 and VI.4. It seems plausible that this type of solar activity is responsible for the decrease of correlation between the solar wind parameters and geomagnetic activity in 1983-85.

Apart from the strong geomagnetic activity in the late part of the declining phase, there is one other difference between solar and geomagnetic activity, which deserves to be mentioned. There is generally a local minimum in geomagnetic activity very close to solar maximum. At Figures VI.2 and IV.3 it is seen that in solar cycle 21 this happened in the first half of 1980. By comparing with Figure VI.4 it is seen that both B_s and the solar wind velocity show a similar minimum. Very little work has been done in understanding the cause of variations in B_z and its variation with the solar cycle. Siscoe et al. [1978], investigated the long-term variations of $|B_z|$ during solar cycle 20 and found that $|B_z|$ was stronger during solar maximum than during solar minimum, but that it showed a *double peak* during maximum. This double peak with a minimum in 1969 can be inspected at Figure VI.4 (note that at an annual scale we have $<|B_z|> = <B_s>$). In solar cycle 21 the variations of B_z are larger than in cycle 20 and the double peak, therefore, more obvious.

A crude model of the heliospheric magnetic field can be constructed from measurements of the large scale magnetic field in the solar photosphere, by using the so called Potential field - Source Surface approximation. By assuming that the coronal field is approximately a potential field, and that the field at some height above the photosphere is completely radial (the source surface), the field configuration can be determined solely from photospheric measurements. Daily magnetogram observations of the large-scale photospheric field have made at the John M. Wilcox Solar Observatory at Stanford since May 1976. The resulting source surface field has been computed for each solar rotation, for the years 1976 through 1985 (Hoeksema and Scherrer [1986]). A close inspection of these data reveals that during the approach to maximum the field configuration becomes increasingly complex, and that the minimum in geomagnetic activity roughly coincides, with the reversal of the polarity of the large scale solar magnetic field. (The development of the source surface field has been reproduced in Appendix B.) It is therefore tempting to suggest that the two phenomena are related. Much more work on the relationship between solar and interplanetary phenomena, however, seems to be needed in order to fully understand the differences between long-term variations in geomagnetic and solar activity.

VII. CONCLUSIONS

We have examined the horizontal magnetic perturbation at the station Thule and its relationship with various solar wind parameters and the auroral electrojet indices AE, AL, and AU. We have found that several different sources contribute to the perturbation.

(1) The well-known two cell equivalent current system, made up partly by ionospheric Hall-currents and partly distant field-aligned currents, and generated mainly by B_s and v.

(2) A current system generated by B_y, which may, or may not, be an integrated part of the two cell system, but which can be flowing in other directions than the normal two cell current, depending on the sign of B_y.

(3) An ionospheric Hall-current system generated at very high latitudes when B_z is northward and existing almost exclusively during sunlit conditions. During B_z positive conditions the B_y generated current (2) is dominating the picture.

(4) Distant field-aligned currents in the auroral oval associated with substorm intensifications of the westward electrojet, especially if the intensification occurs in the postmidnight sector.

The measured horizontal perturbation shows a high correlation with B_s and v and can therefore be used as a single station index to monitor current system (1) generated by these parameters. During northward IMF the polar cap magnetic perturbations are too inhomogeneous, and variable in direction with B_y, to be monitored by a single station index.The correlation between the measured horizontal perturbation and the northward component of the IMF, B_N, is consequently very low.

The measured perturbation changes direction with the sign of the azimuthal component B_y, but B_y also gives a contribution to the total current, which is about half the size of the contribution of B_s. The B_y induced currents are rather similar for B_z positive and negative conditions, but are dominating the total picture when B_z is positive, while the B_s induced currents are dominating, when B_z is negative. Because the contribution from the B_y induced currents changes direction with sign of B_y they can only partly be monitored by the PC-index. This is done by using the composite solar wind parameter $v(B_y^2+B_z^2)^{\frac{1}{4}}\sin^2\theta/2$ to define PC. The earlier reported seasonal asymmetry in the relation between B_y and the auroral zone index AL (Murayama et al. [1980]) is also observed in PC but only as a second order effect. The asymmetry is absent in AU, which during all year shows a larger response to B_y negative than to B_y positive. We therefore object to an interpretation of the seasonal asymmetry in terms of merging site asymmetry. Our results rather indicate that the reason for the B_y positive effect is to be found in the night side processes, and the reason for the B_y negative effect in the dayside processes.

Also the field-aligned currents in the auroral oval associated with substorm intensifications of the westward electrojet during substorm expansion phase can be detected in the near pole region. This has been seen through examination of specific events, but also through a linear correlation analysis between PC and the auroral zone indices AE, AL, and AU showing a very high correlation, especially with AE and AL. The correlation between PC and AU is found to be very seasonal dependent, with a rather poor correlation during northern winter. By including measurements from the near pole station Vostok in Antarctica in the examination it can, however, be seen, that the cause is a seasonal effect on the AU index rather than on the PC-index.

Because of the high correlation between PC and AE we propose to use PC as an indicator of auroral electrojet activity, excluding substorm intensifications of the westward electrojet occurring in the premidnight sector. PC can not be used as a total replacement of AE, but has three main advantages:

(1) It can be made fast available.
(2) It can be derived from both hemispheres.
(3) It can be computed for many periods where AE is not available.

The PC-index, as an indicator of auroral electrojet activity, is disturbed by polar cap currents induced by the northward and azimuthal components. These currents make an unambiguous interpretation of PC impossible. The polar cap currents are, however, confined to the summer hemisphere, and the problem can therefore be solved by having simultaneous access to PC-indices from both hemispheres.

In the detailed derivation of the PC-index the following items was examined:

(1) The direction of the measured perturbation.
(2) Diurnal and seasonal variations of the measured perturbation.
(3) The effect of B_y.
(4) The effect of smoothing of the empirically determined coefficients in the algorithm.

The direction of optimal correlation with various solar wind parameters show diurnal and seasonal variations, but is similar for all solar wind parameters that are dominated by B_s. The correlation is highest with the parameter $vB_T\sin^2(\theta/2)$.

The size of the horizontal perturbation likewise shows both diurnal and seasonal variations. This is taken into account by normalizing the horizontal perturbation with respect to $vB_T\sin^2(\theta/2)$. This also has the effect of making PC-indices from different stations directly comparable. The normalization coefficients are found to be different if they are

computed for B_y positive and negative separately. The difference can, however, for practical reasons, not be implemented in the algorithm for PC, and is also found not to be very large. A smoothing procedure has to be applied to the normalization coefficients in order to avoid jumps in PC, caused by statistical uncertainty. This procedure has been found to introduce a small but detectable seasonal and diurnal variation.

Finally we have examined the long-term variations of PC, and find that they are well correlated with $vB_T\sin^2(\theta/2)$. Both v and $B_T\sin^2(\theta/2)$ (or B_s) are needed in order to understand the PC variations during solar cycle 21. The PC variations are furthermore very similar to the long-term variations in both AE and A_p. The activity as measured by all three indices shows a local minimum right at solar maximum which could be associated with the shift of polarity of the magnetic field of the sun. In the late part of the declining phase all three indices show a local maximum probably caused by fast solar wind streams from solar coronal holes, and associated with a decrease in the computed correlation between the solar wind parameters and PC and AE.

For future examination we especially suggest two points:

1) For the interpretation of PC it would be valuable with a further clarification of the relative contribution of the distant field-aligned currents and the ionospheric Hall-current and also of the DP1 and DP2 currents.

2) We have examined PC during solar cycle 21, but we are now entering a new solar cycle with a much larger level of activity. Our latest PC computations (see appendix A) indicate that this may have the effect of introducing a diurnal variation in PC. So the difference between PC in different solar cycles ought to be examined.

In summary we believe that PC can be a very useful tool for scientists, e.g. to sort their data or select interesting periods for investigations. In the future it may even be used as

a real time indicator during experiments. Like any other index PC has its limitations and problems. The most serious may well show up to be that several sources contribute to the index, and the difficulties in distinguishing between them.

Acknowledgements. I would like to thank B. Pedersen for his help in providing the observatory data from Thule, A. Hetmar and P. Kristensen for their help in preparing the manuscript and E. Friis-Christensen for many useful discussions. The IMP-8 satellite data were provided through World Data Centre A for Rockets and Satellites in Boulder, the AE-indices through World Data Centre C2 in Kyoto, and the data from Vostok through World Data Centre B in Moscow.

References

Akasofu, S.-I., Interplanetary energy flux associated with magnetospheric substorms, Planet. Space Sci., 27, 425-431, 1979

Akasofu S.-I., B.-H. Ahn, Y. Kamide, and J.H. Allen, A note on the accuracy of the auroral electrojet indices, J. Geophys. Res. 88, 5769-5772, 1983

Allen, J.H., and H.W. Kroehl, Spatial and temporal distributions of magnetic effects of auroral electrojets as derived from AE indices, J. Geophys. Res., 80, 3667-3677, 1975

Baker, D.N., R.D. Zwickel, S.J. Bame, E.W. Hones, Jr., B.T. Tsurutani, E.J. Smith, and S.-I. Akasofu, An ISEE 3 high time resolution study of interplanetary parameter correlations with magnetospheric activity, J. Geophys. Res. 88, 6230-6242, 1983

Bartels, J., Discussion of time-variations of geomagnetic activity indices K_p and A_p, 1932-1961, Annales Geophysicae, 19, 1-20, 1963

Clauer, C.R., and E. Friis-Christensen, High-latitude dayside electric fields and currents during strong northward interplanetary magnetic field: Observations and model simulations, J. Geophys. Res., 93, 2749-2757, 1988

Clauer, C.R., and Y. Kamide, DP1 and DP2 current systems for the March 22., 1979 substorms, J. Geophys. Res., 90, 1343-1354, 1985

Crooker, N.U., Dayside merging and cusp geometry, J. Geophys. Res., 84, 951-959, 1979

Crooker, N.U., J. Feynman, and J.T. Gosling, On the high correlation between long-term averages of solar wind speed and geomagnetic activity, J. Geophys. Res., 13, 1933-1937, 1977

Crooker, N.U., J.G. Luhmann, J.R. Spreiter, and S.S. Stahara, Magnetopause merging site asymmetries, J. Geophys. Res., 90, 341-346, 1985

Davis T.N., and M. Sugiura, Auroral electrojet activity index AE and its universal time variations, J. Geophys. Res., 71, 785-801, 1966

Fairfield, D.H., and L.J. Cahill,Jr., Transition region magnetic fields and polar magnetic disturbances, J. Geophys. Res., 71, 155, 1966

Fairfield, D.H., Polar magnetic disturbances and the interplanetary magnetic field, Space Research, 8, 107, 1967

Feynman, J., Implications of solar cycles 19 and 20 geomagnetic activity for magnetospheric processes, Geophys. Res. Lett., 7, 971-973, 1980

Friis-Christensen, E., and J. Wilhjelm, Polar cap currents for different directions of the interplanetary magnetic field in the Y-Z plane, J. Geophys. Res., 80, 1248-1260, 1975

Friis-Christensen, E., Polar cap current systems, Magnetospheric currents, ed. T.A. Potemra, Geophysical Monographs, Vol. 28, 86-95, 1983

Friis-Christensen, E., Y. Kamide, A.D. Richmond, and S. Matsushita, Interplanetary magnetic field control of high-latitude electric fields and currents determined from Greenland magnetometer data, J. Geophys. Res. 90, 1325-1338, 1985

Friis-Christensen, E., Solar wind control of the polar cusp, Solar wind Magnetosphere coupling, ed. Y.K. Kamide and J.A. Slavin, 423-440, 1986

Gizler, V.A., B.M. Kuznetsov, V.A. Sergeev, and O.A. Troshichev, The sources of polar cap and low latitude bay-like disturbances during substorms, Planet. Space Sci., 24, 1133-1139, 1976

Hald, A., Statistiske metoder, Akademisk Forlag, København, 1968

Heelis, R.A., The effect of interplanetary magnetic field orientation on dayside high-latitude ionospheric convection, J. Geophys. Res., 89, 2873-2880, 1984

Heppner, J.P., J.D. Stolarik, and E.M. Wescott, Electric field measurements and the identification of currents causing magnetic disturbances in the polar cap, J. Geophys. Res., 76, 6028-6053, 1971

Heppner, J.P., Polar cap electric field distributions related to the interplanetary magnetic field direction, J. Geophys. Res., 77, 4877-4887, 1972

Heppner, J.P., Empirical models of high-latitude electric fields, J. Geophys. Res., 82, 1115-1125, 1977

Heppner, J.P., and N.C. Maynard, Empirical high-latitude electric field models, J. Geophys. Res., 92, 4467-4489, 1987

Hirshberg, J., The solar wind cycle, the sunspot cycle and the corona, Astrophys. Space Sci., 20, 473-481, 1973

Hoeksema, J.T., and P. Scherrer, The solar magnetic field 1976 through 1985, report UAG-94, World Data Centre A for Solar-Terrestrial Physics, 1986

Iijima, T., T.A. Potemra, L.J. Zanetti, and P.F. Bythrow, Large-scale Birkeland currents in the dayside polar region during strongly northward IMF: A new Birkeland current system, J. Geophys. Res., 89, 7441-7452, 1984

Kamide, Y., and S.-I. Akasofu, Notes on the auroral electrojet indices, Rev. Geophys. Space Phys., 21, 1647-1656, 1983

Kamide, Y., H.W. Kroehl, A.D. Richmond, B.-H. Ahn, S.-I. Akasofu, W. Baumjohann, E. Friis-Christensen, S. Matsushita, H. Maurer, G. Rostoker, R.W. Spiro, J.K. Walker, and A.N. Zaitsev, Changes in the global electric fields and currents for March 17-19, 1978 for six meridian chains of magnetometers, Report UAG-87, World Data Centre A for Solar-Terrestrial Physics, 1982

Kamide, Y., H.W. Kroehl, B.A. Hausman, R.L. McPherron, S.-I. Akasofu, A.D. Richmond, P.H. Reiff, and S. Matsushita, Numerical modeling of ionospheric parameters from global IMS magnetometer data for the CDAW-6 intervals, Report UAG-88, World Data Centre A for Solar-Terrestrial Physics, 1983

Kan, J.R. and L.C. Lee, Energy coupling function and solar wind-magnetosphere dynamo, Geophys. Res. Lett., 6, 577-580, 1979

Kokubun S., Polar substorms and interplanetary magnetic field, Planet. Space Sci., 19, 697-714, 1971

Kokubun S., Relationship of interplanetary magnetic field structure with development of substorm and storm main phase, Planet. Space Sci., 20, 1033-1049, 1972

Kroehl H.W., and Y. Kamide, High-latitude indices of electric and magnetic variability during the CDAW 6 intervals, J. Geophys. Res., 90, , 1367-1374, 1985

Kuznetsov, B.M., and O.A. Troshichev, On the nature of polar cap magnetic activity during undisturbed periods, Planet. Space Sci., 25, 15-21, 1977

Legrand, J.-P., P.A. Simon, Solar cycle and geomagnetic activity: A review for geophysicists, Annales Geophysicae, 7, 565-594, 1989

Maezawa, K., Magnetospheric convection induced by the positive and negative Z components of the interplanetary magnetic field: Quantitative analysis using polar cap magnetic records, J. Geophys. Res., 81, 2289-2303, 1976

Mayaud, P.N., Derivation, meaning and use of geomagnetic indices, Geophysical Monograph, 22, 112-115, AGU, Washington DC, 1980

McPherron, R.L., and R.H. Manka, Dynamics of the 10.54 UT March 22. 1979 substorm event: CDAW 6, J. Geophys. Res., 90, 1175-1190, 1985

Mikkelsen, I.S., T. Stockfleth Jørgensen, and M.C. Kelley, Observations and interpretation of plasma motions in the polar cap ionosphere during magnetic substorms, J. Geophys. Res., 80, 3197-3204, 1975

Mozer, F.S., W.D. Gonzales, F. Bogott, M.C. Kelley, and C. Schutz, High-latitude electric fields and the three-dimensional interaction between the interplanetary and terrestrial magnetic fields, J. Geophys. Res., 79, 56-63, 1974

Murayama, T., T. Akoi, H. Nakai, and K. Hakamada, Empirical formula to relate the auroral electrojet intensity with interplanetary parameters, Planet. Space Sci., 28, 803-813, 1980

Nishida, A., Geomagnetic DP2 fluctuations and associated magnetospheric phenomena, J. Geophys. Res., 73, 1795-1803, 1968a

Nishida, A., Coherence of geomagnetic DP2 fluctuations with interplanetary magnetic field variations, J. Geophys. Res., 73, 5549-5559, 1968b

Nishida, A., and K. Maezawa, Two basic modes of interaction between the solar wind and the magnetosphere, J. Geophys. Res., 76, 2254-2264, 1971

Obayashi, T., and A. Nishida, Large scale electric fields in the magnetosphere, Space Sci. Rev., 8, 3-31, 1968

Ol', A.I., Physics of the 11-year variation of magnetic disturbances, Geomag. Aeron., 11, 549-551, 1971

Olesen, J.K., F. Primdahl, F. Spangslev, E. Ungstrup, A. Bahnsen, U.V. Fahleson, C.-G. Fälthammar, and A. Pedersen, Rocket borne wave fields and plasma observations in unstable polar cap E-region, Geophys. Res. Lett., 3, 399-402, 1976

Primdahl, F., and F. Spangslev, Cross-polar cap horizontal E-region currents related to magnetic disturbances and to measured electric fields, J. Geophys. Res., 82, 1137-1143, 1977

Rostoker G., Geomagnetic indices, Rev. Geophys. Space Phys., 10, 935, 1972

Siscoe, G.L., N.U. Crooker, and L. Christopher, A solar cycle variation of the interplanetary magnetic field, Solar Phys., 56, 449-461, 1978

Snyder, C.W., M. Neugebauer, and U.R. Rao, The solar wind velocity and its variation with cosmic ray variations and with geomagnetic activity, J. Geophys. Res., 68, 6361-6370, 1963

Sonnerup, B.U.Ö, Magnetopause reconnection rate, J. Geophys. Res., 79, 1546-1549, 1974

Svalgaard, L., Polar cap magnetic variations and their relationship with the interplanetary magnetic sector structure, J. Geophys. Res., 78, 2064-2078, 1973

Svalgaard, L., Geomagnetic activity: dependence on solar wind parameters, in coronal holes and high speed wind streams, ed. J.B. Zirker, Colorado Ass. Univ. Press, Boulder, 371-432, 1977

Troshichev, O.A., V.G. Andrezen, S. Vennerstrøm, and E. Friis-Christensen, Magnetic activity in the polar cap - a new index, Planet. Space Sci., 36, 1095-1102, 1988

Troshichev, O.A., and V.G. Andrezen, The relationship between interplanetary quantities and magnetic activity in the southern polar cap, Planet. Space Sci., 33, 415-419, 1985

Troshichev, O.A., N.P. Dmitrieva, and B.M. Kuznetsov, Polar cap magnetic activity as a signature of substorm development, Planet. Space Sci., 27, 217-221,1979

Ungstrup, E., A. Bahnsen, J.K. Olesen, F. Primdahl, F. Spangslev, W.J. Heikkila, D.M., Klumpar, J.D. Winningham, U.V. Fahleson, C.-G. Fälthammar, and A. Pedersen, Rocket borne particle field and plasma observations in the cleft region, Geophys. Res. Lett., 2, 345-348, 1975

Vasyliunas, V.M., Mathematical models of magnetospheric convection and its coupling to the ionosphere, Particles and fields in the magnetosphere, ed. B.M. McCormac, 60-71, D. Reidel, Dordrecht, Netherlands, 1970

Vennerstrøm, S., and E. Friis-Christensen, On the role of IMF B_y in generating the electric field responsible for the flow across the polar cap, J. Geophys. Res., 92, 195-202, 1987

Vennerstrøm, S., E. Friis-Christensen, O.A. Troshichev and V.G. Andrezen, Comparison between the polar cap index PC and the auroral electrojet indicies AE, AU and AL, In press, 1990

Appendix A:

From the observatory in Qaanaaq digital data are available from 1975 till today with 1 minute time resolution. We have used these data to compute PC_{THL} by means of the algorithm described in section IV. These data are now available in digital as well as in the form of plots in World Data Centre C1 for Geomagnetism in Copenhagen. Here we show summary plots, containing one year per page of all the data. Futhermore, we show examples of daily variation plots of data from 1990. In the first and last months of 1990 a systematic diurnal variation can bee seen at the summary plots.

PC-INDEX

Thule **1975**

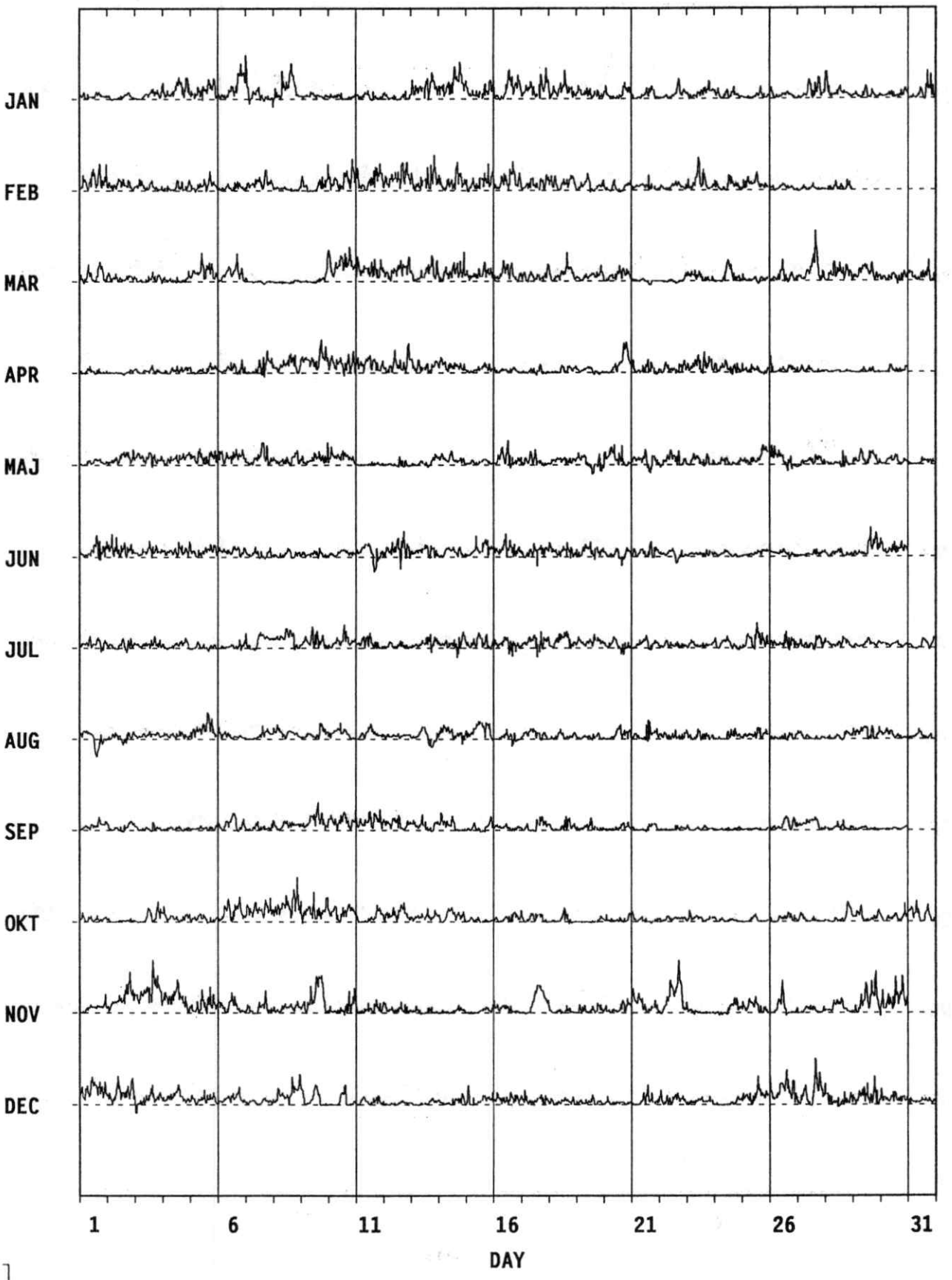

20

Div. Geophys. D M I

PC-INDEX

Thule **1976**

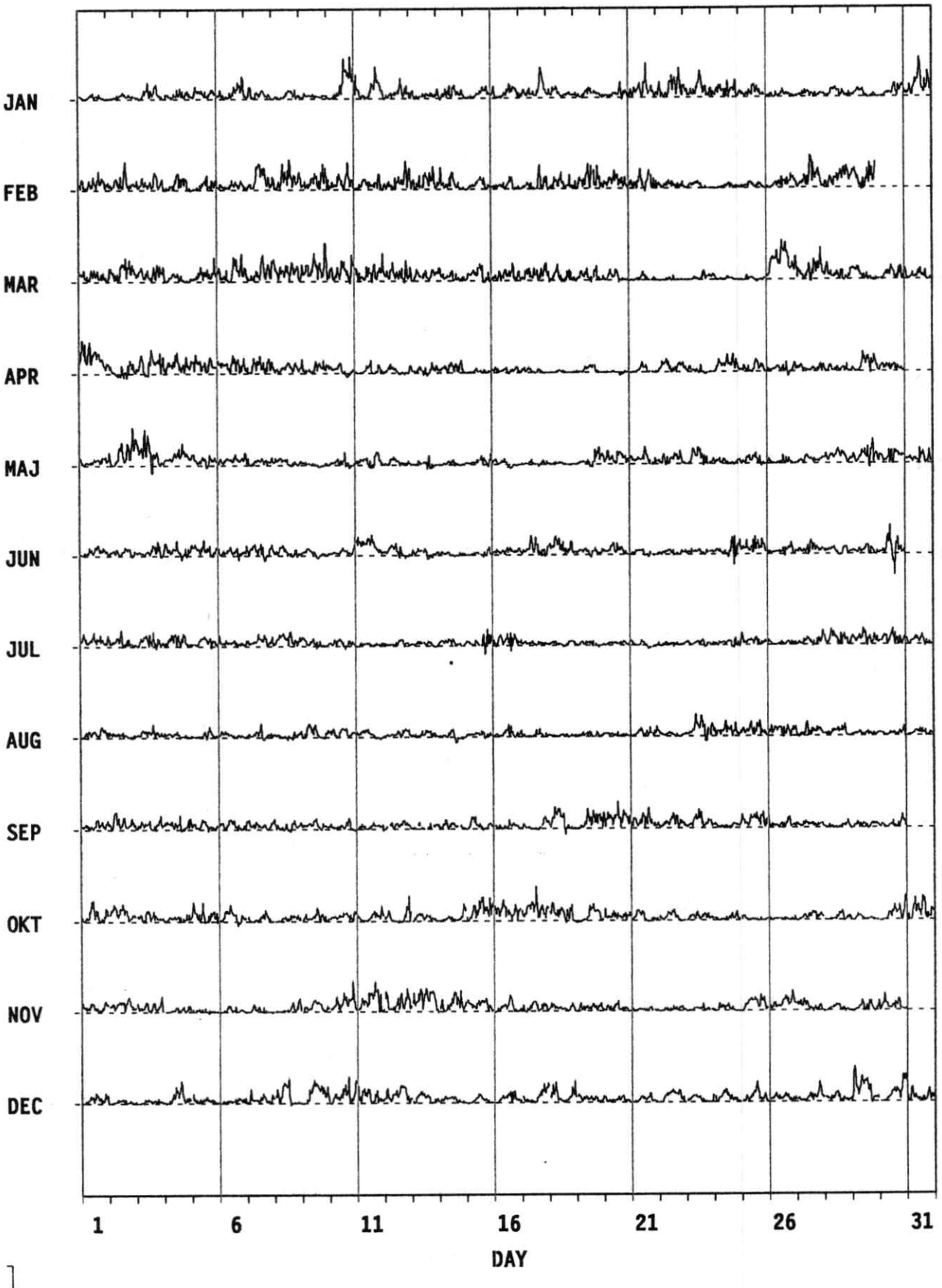

Div. Geophys. D M I

PC-INDEX

Thule **1977**

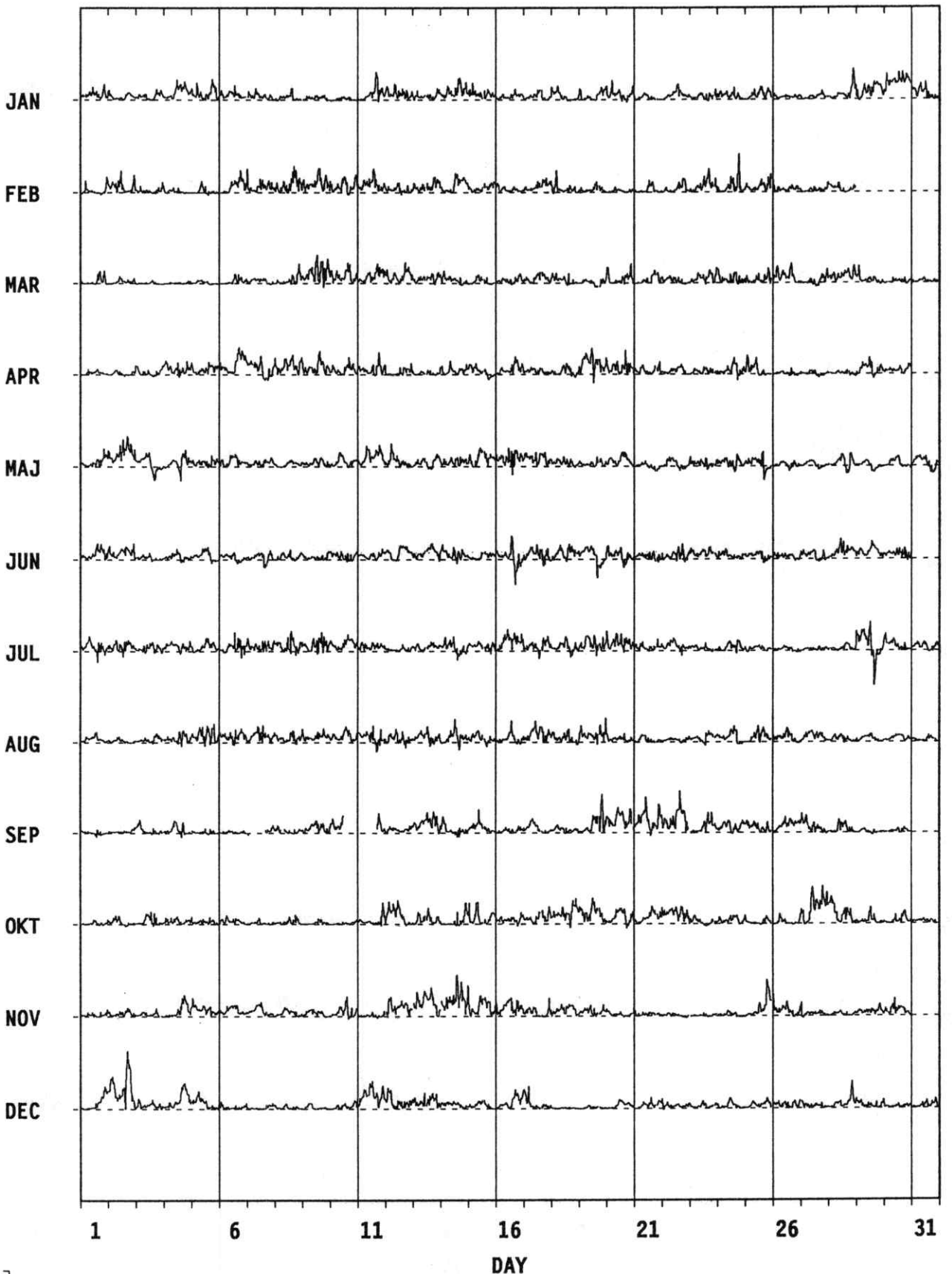

20

Div. Geophys. D M I

PC-INDEX

Thule

1978

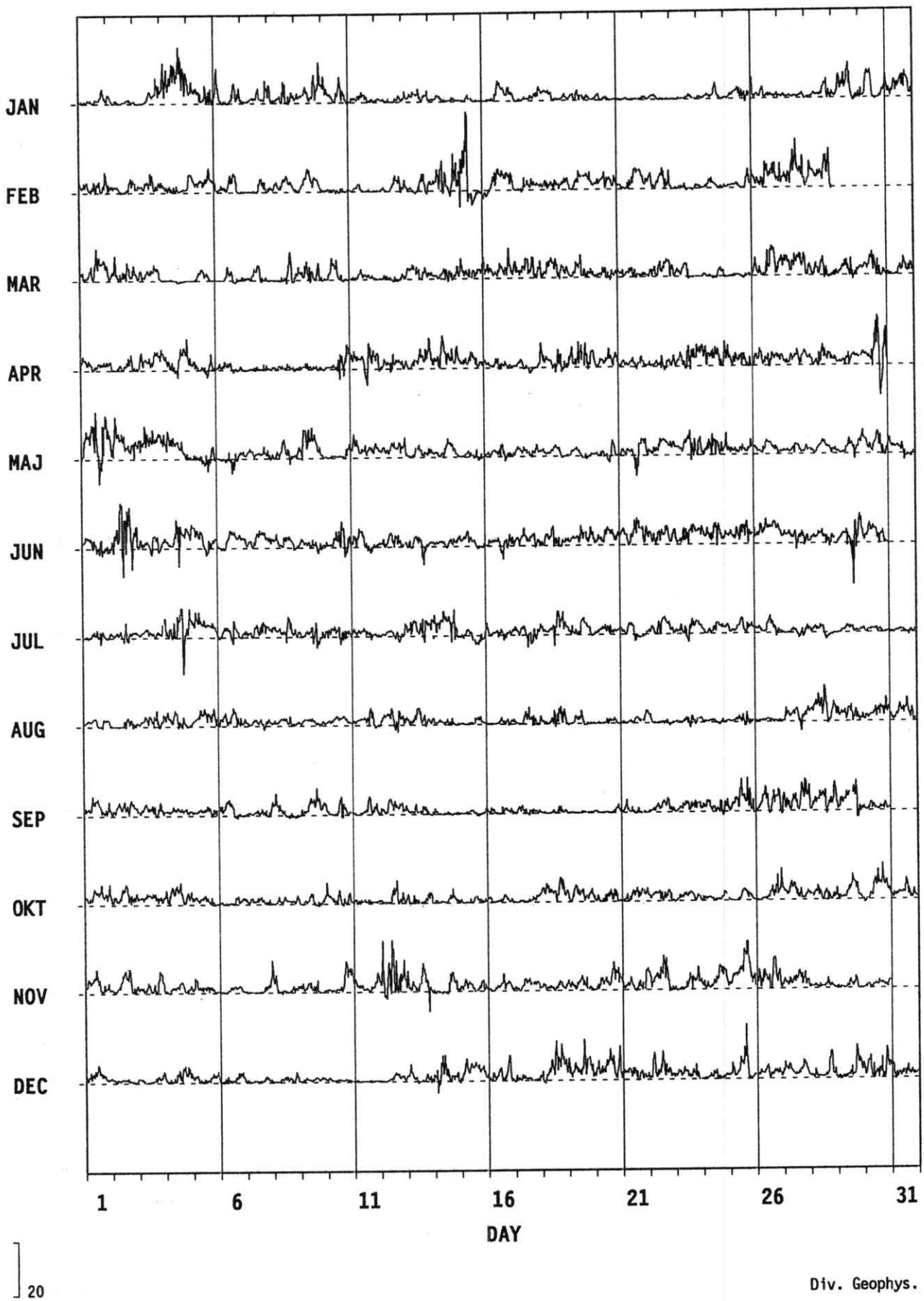

Div. Geophys. D M I

PC-INDEX

Thule **1979**

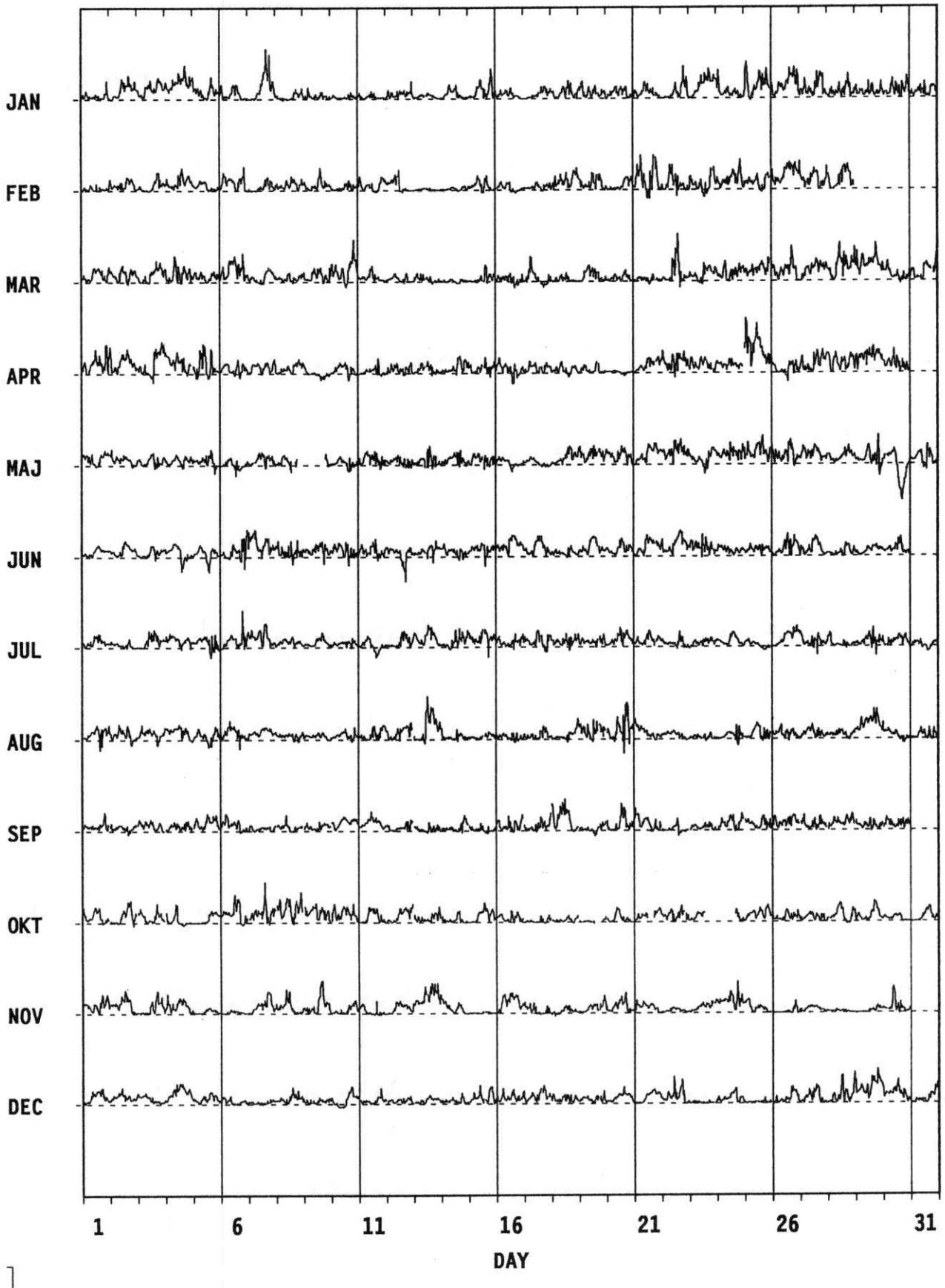

20

Div. Geophys. D M I

PC-INDEX

Thule **1980**

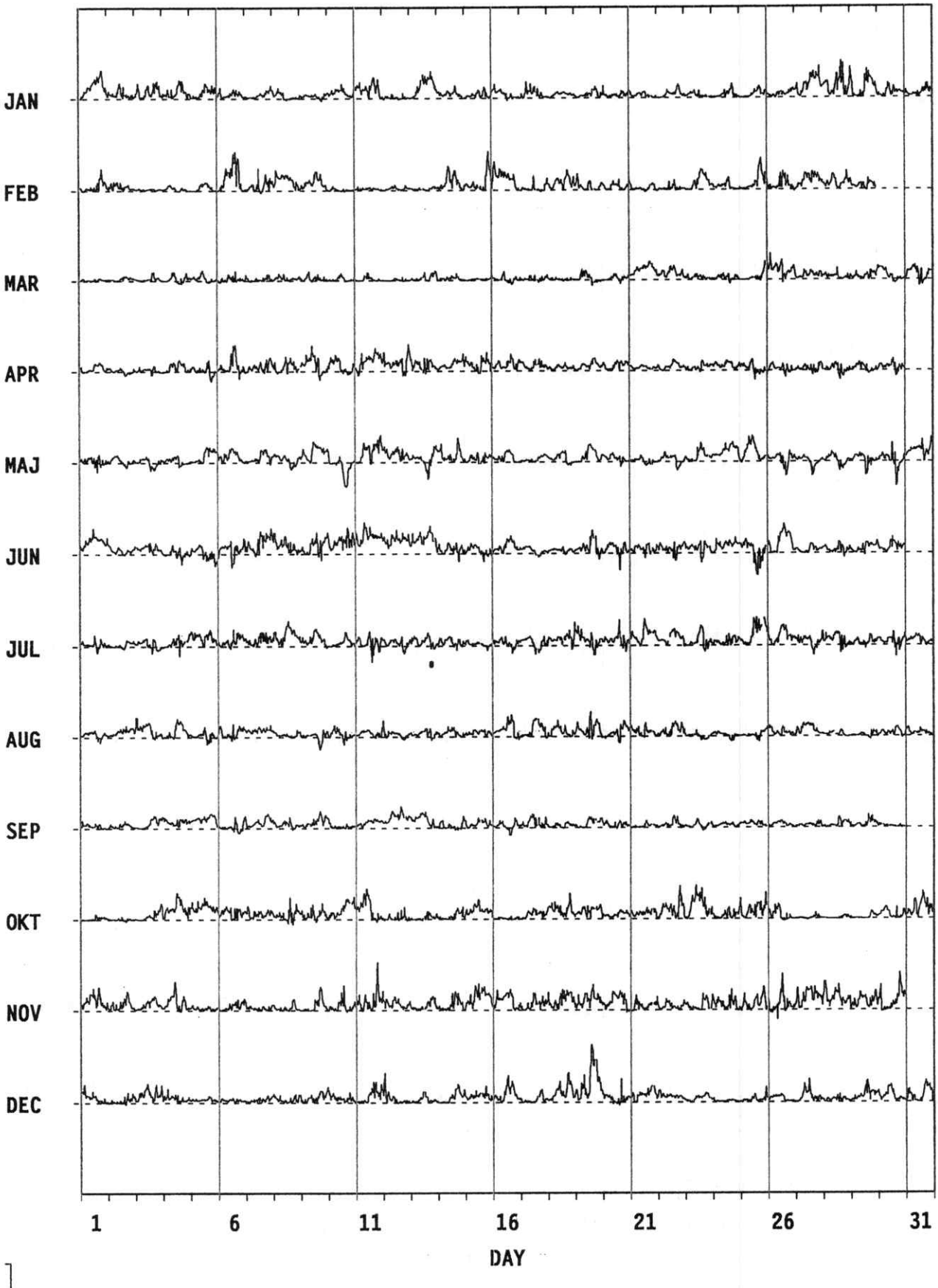

20

Div. Geophys. D M I

PC-INDEX

Thule **1981**

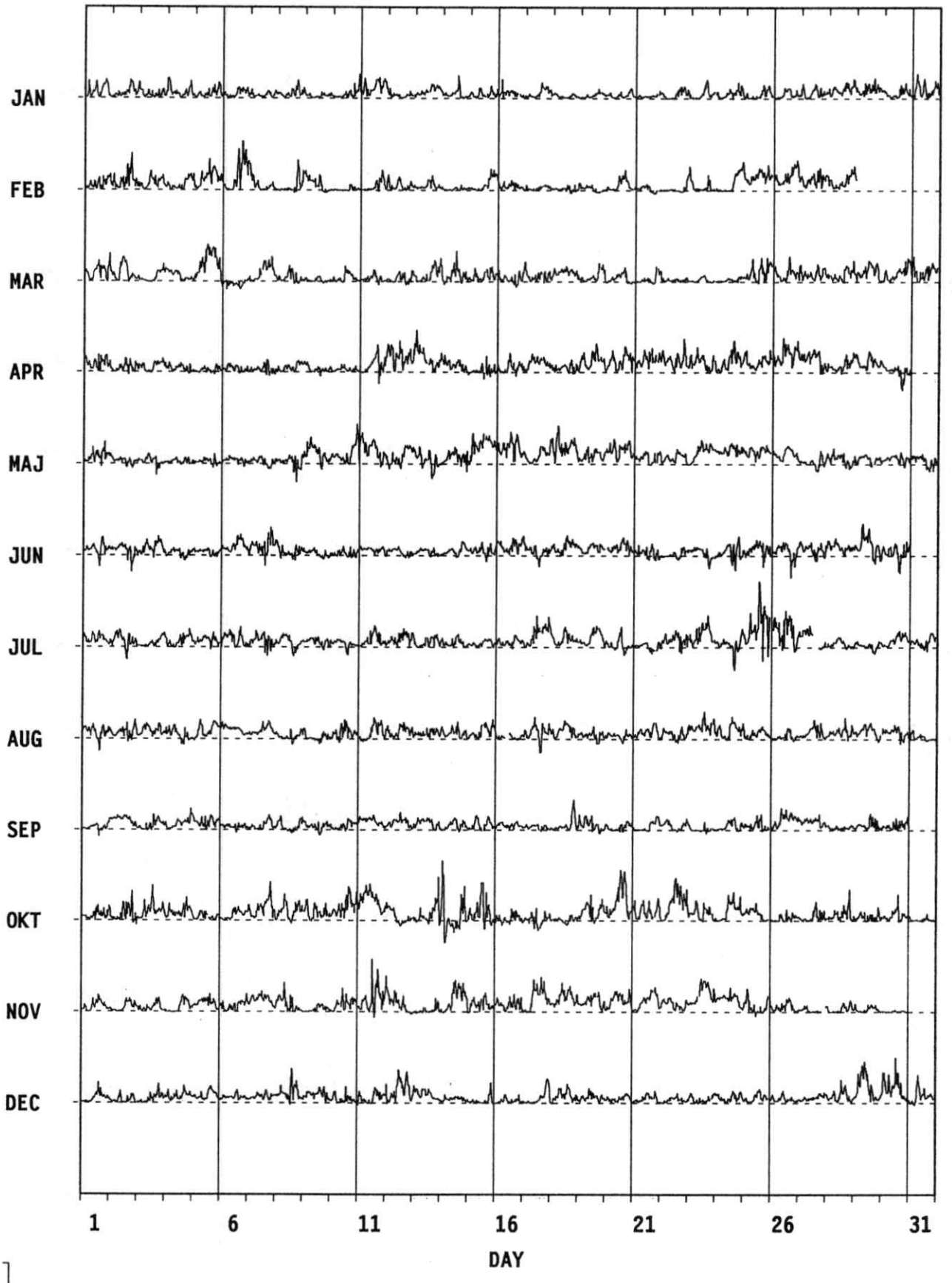

20

Div. Geophys. D M I

PC-INDEX

Thule **1982**

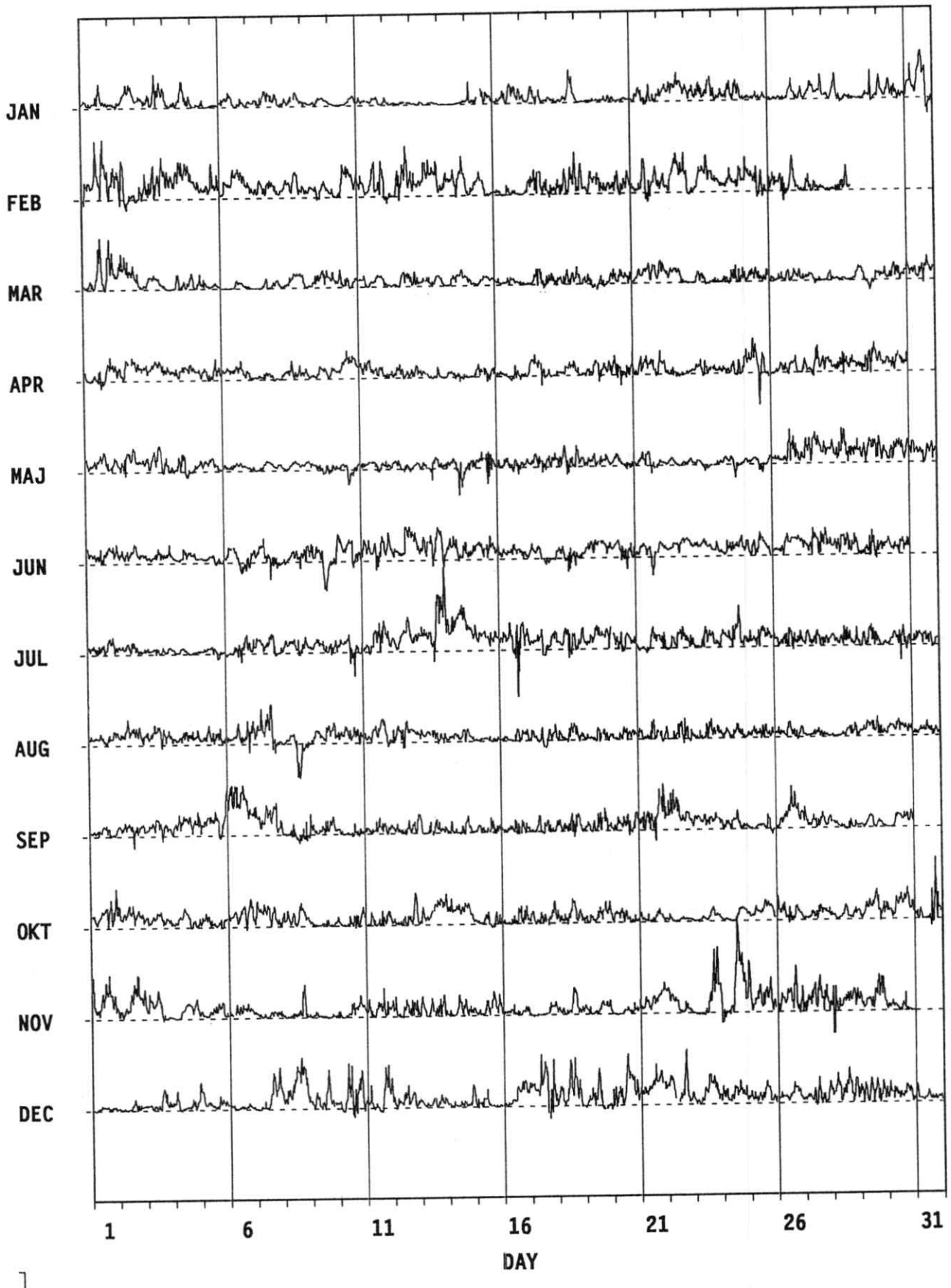

Div. Geophys. D M I

PC-INDEX

Thule **1983**

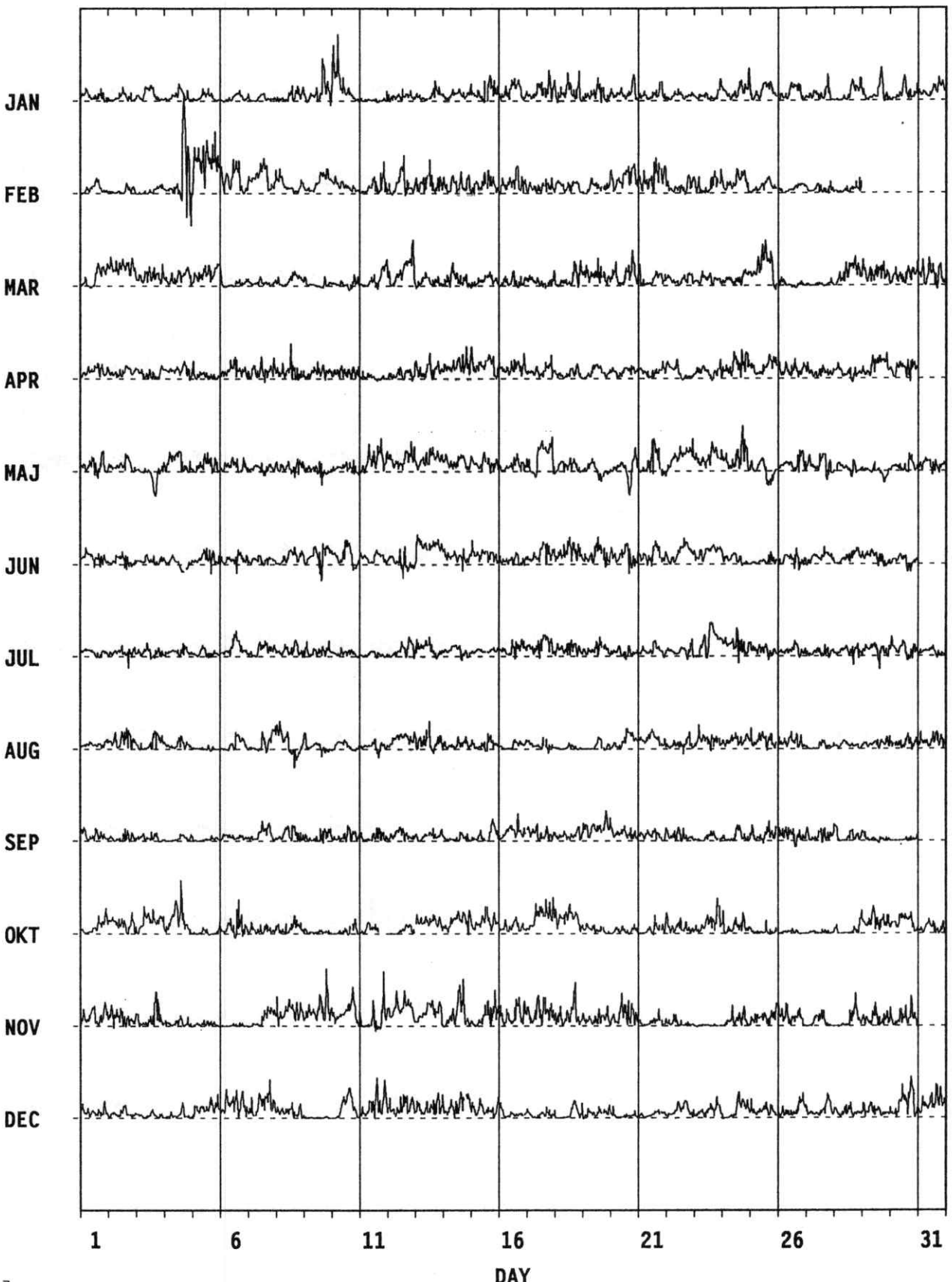

20

Div. Geophys. D M I

PC-INDEX

Thule **1984**

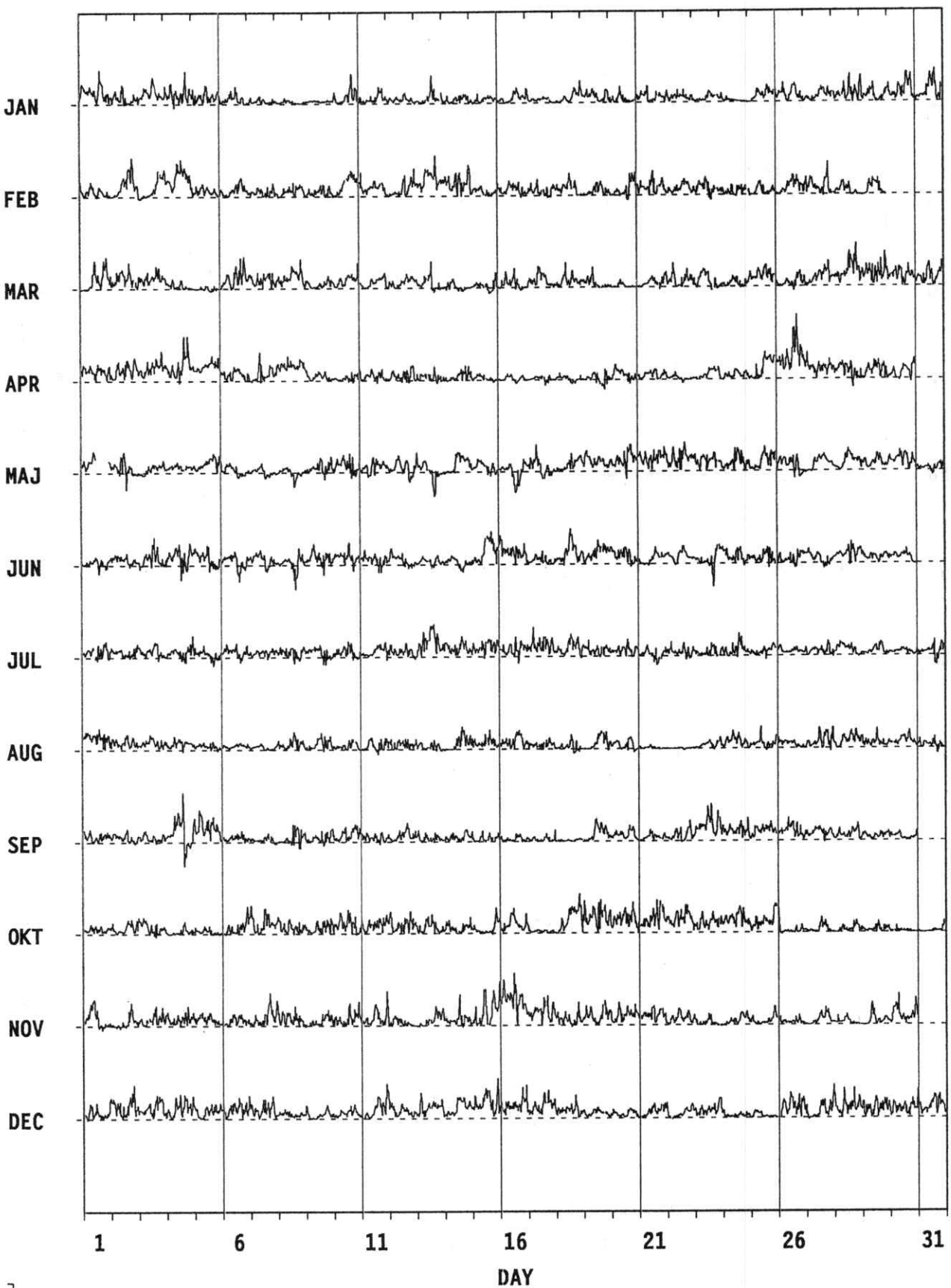

Div. Geophys. D M I

PC-INDEX

Thule **1985**

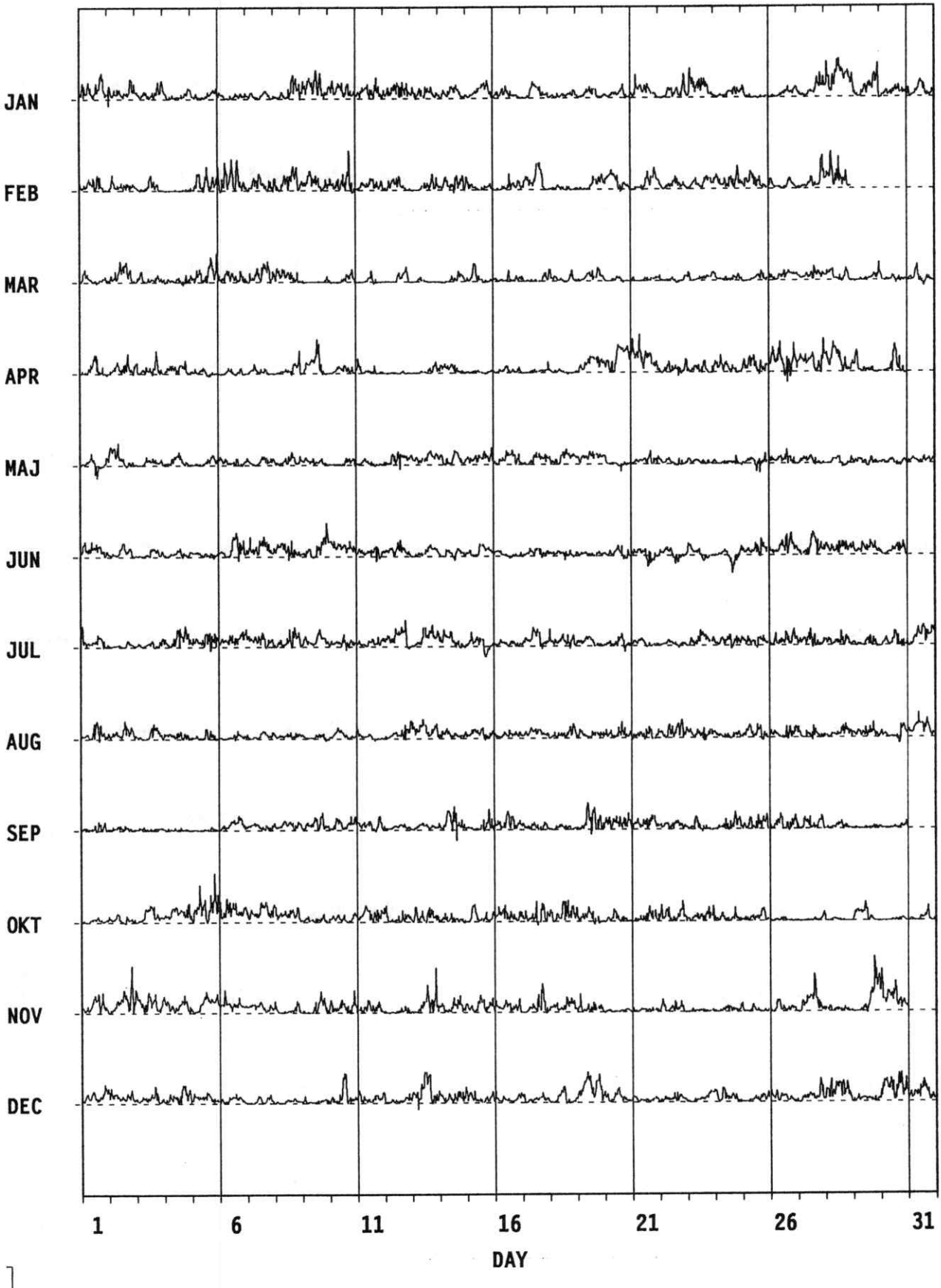

20

Div. Geophys. D M I

PC-INDEX

Thule

1986

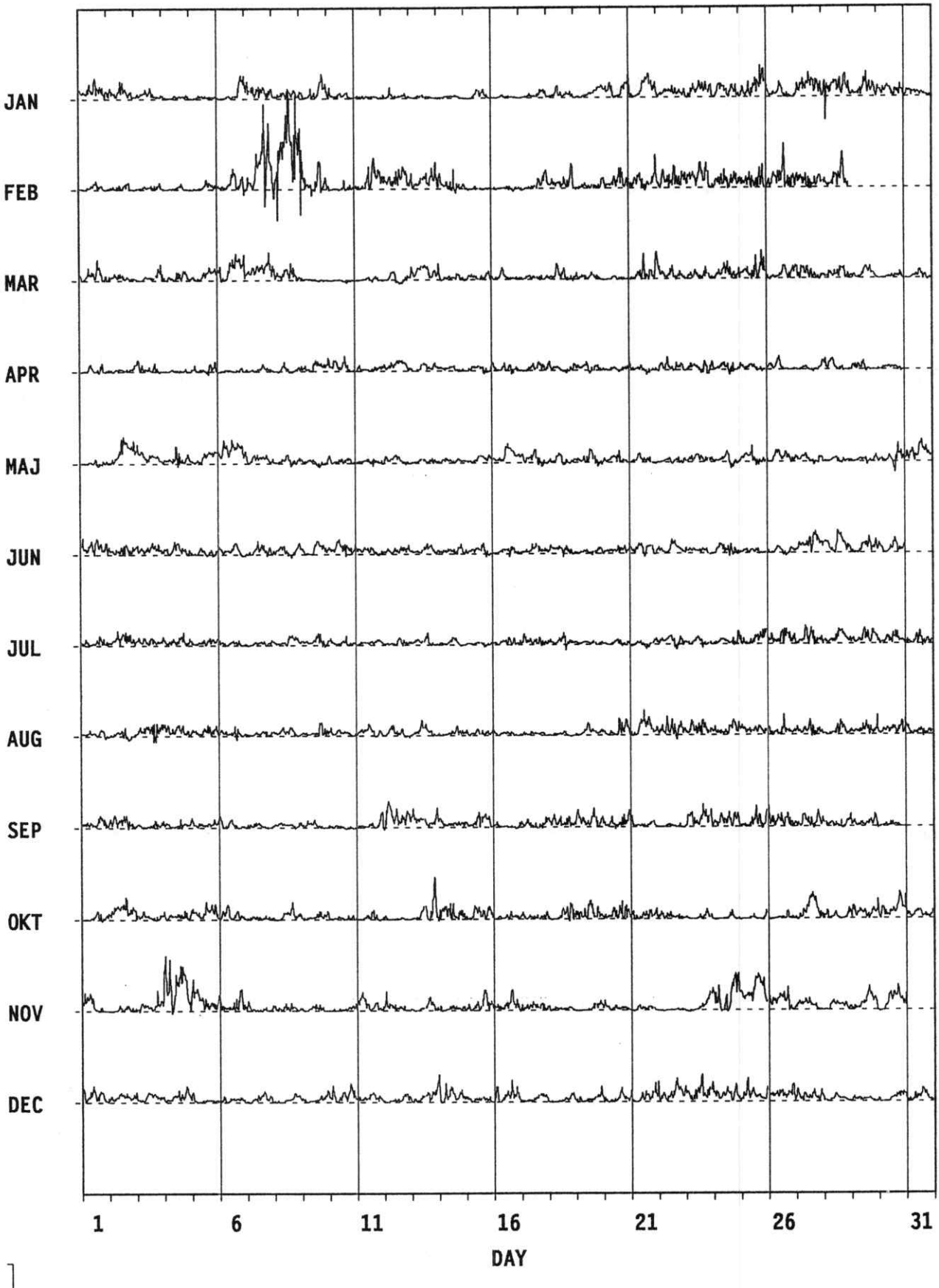

Div. Geophys. D M I

PC-INDEX

Thule 1987

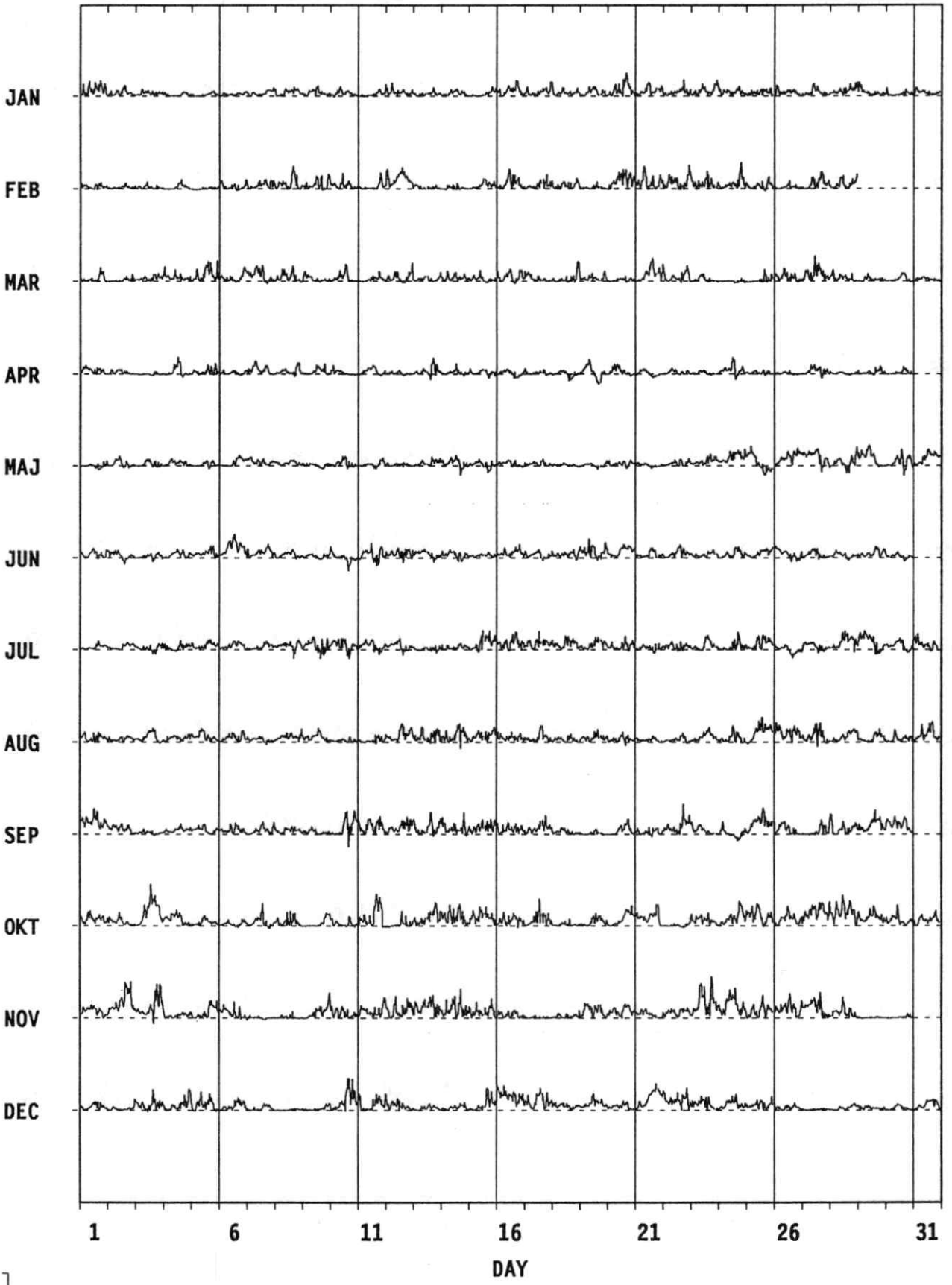

Div. Geophys. D M I

PC-INDEX

Thule **1988**

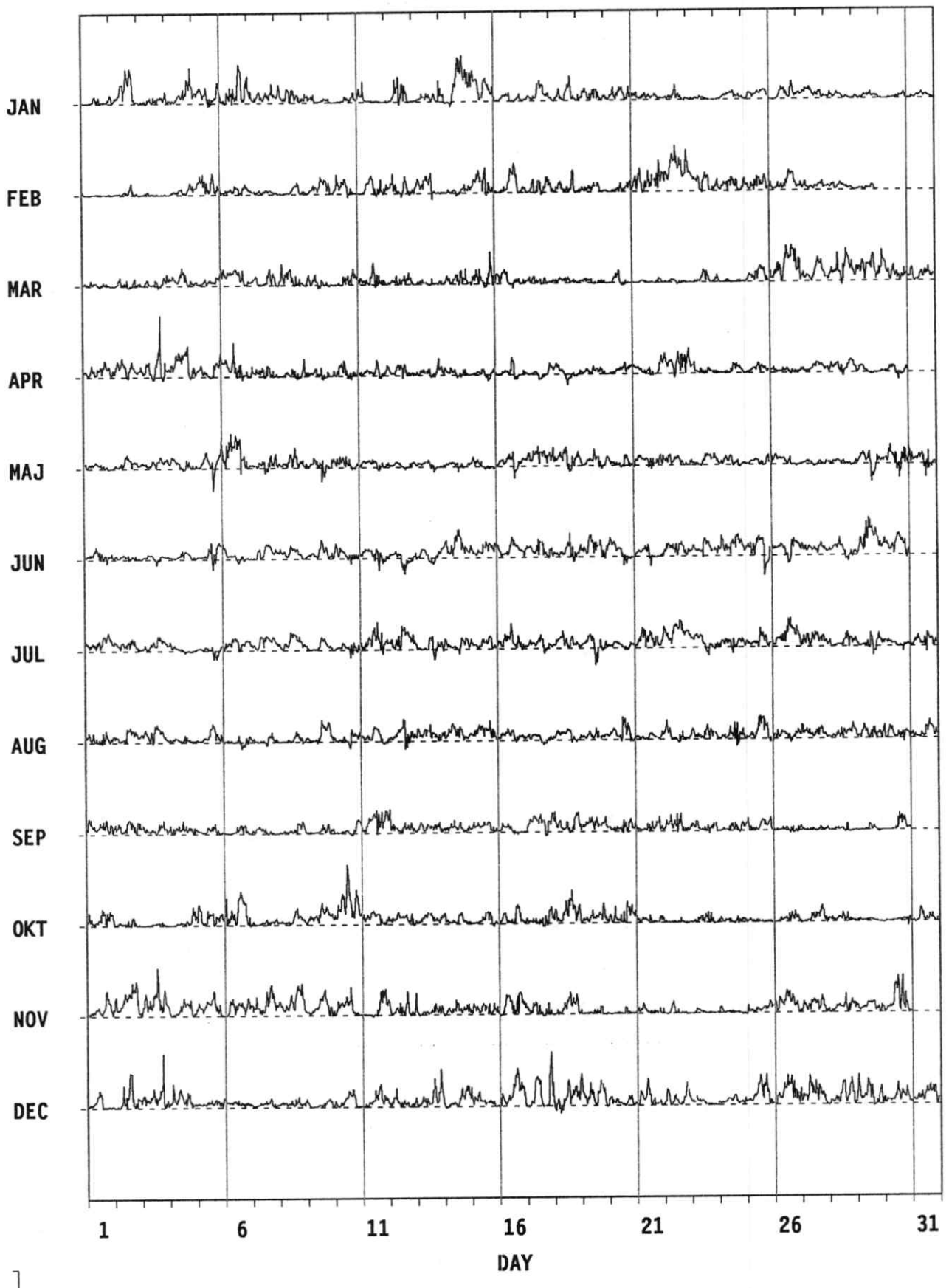

Div. Geophys. D M I

PC-INDEX

Thule **1989**

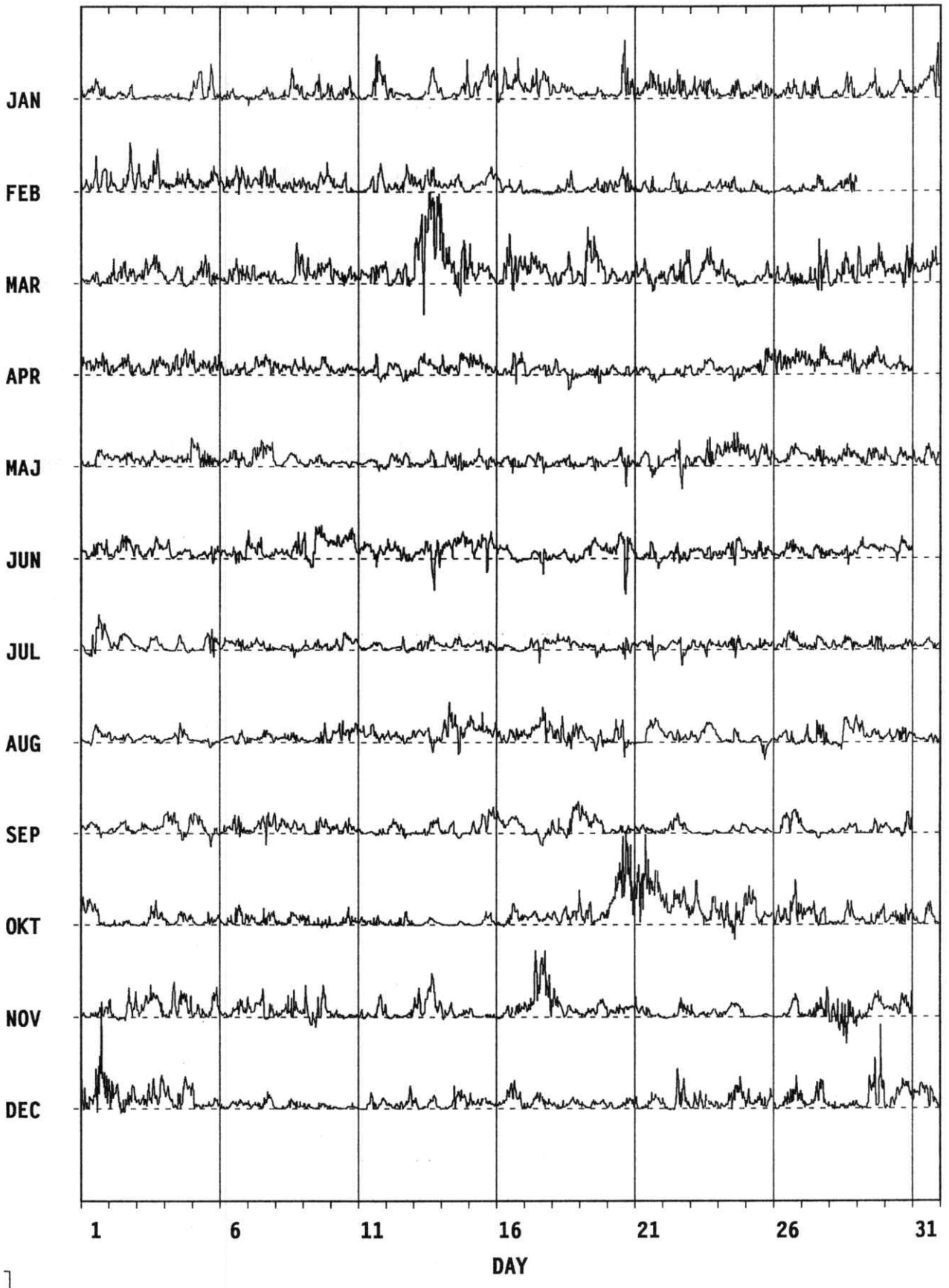

20

Div. Geophys. D M I

PC-INDEX

Thule **1990**

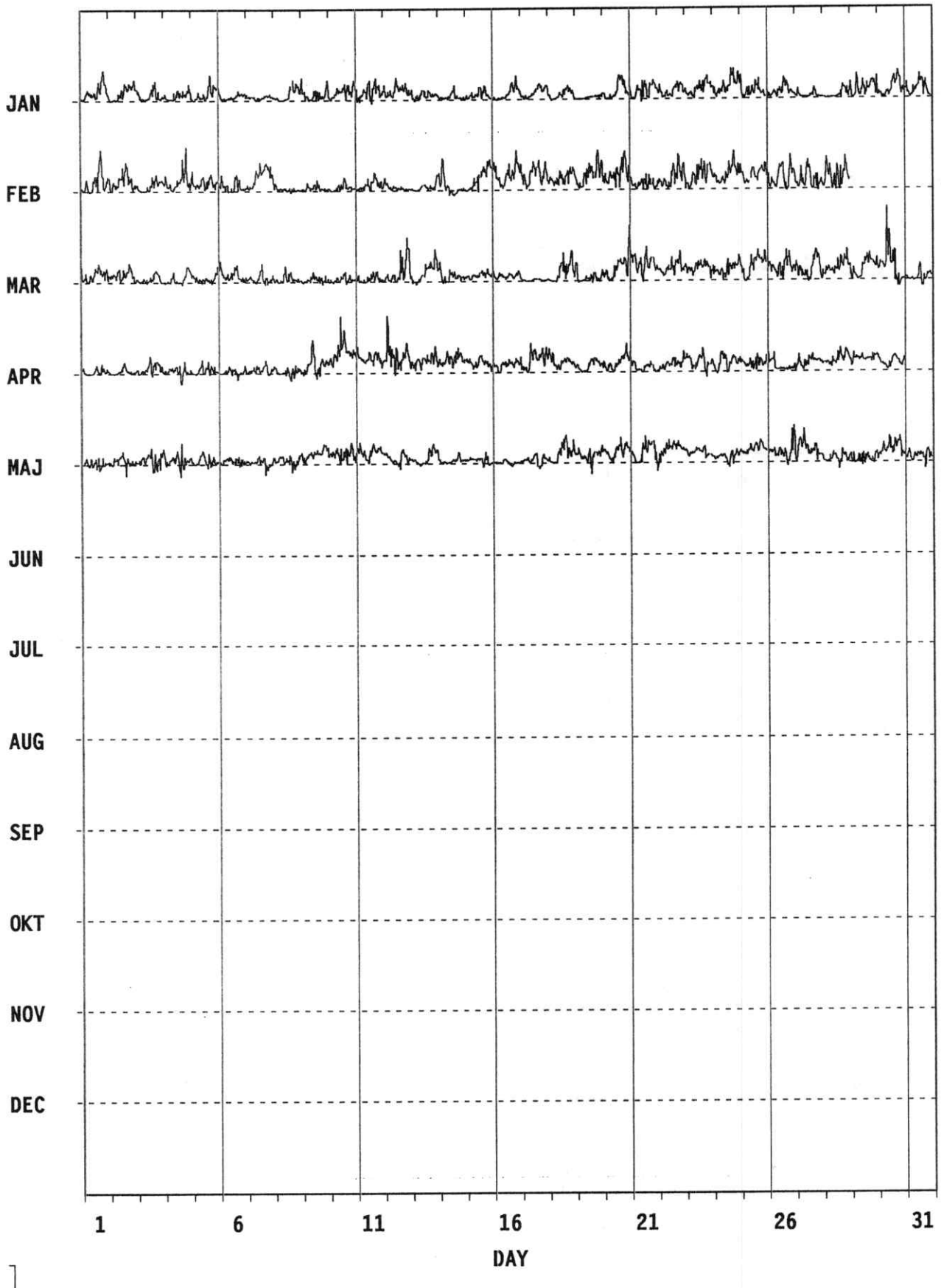

20

Preliminary Values.

Div. Geophys. D M I

PC-INDEX

Thule **January, 1990**

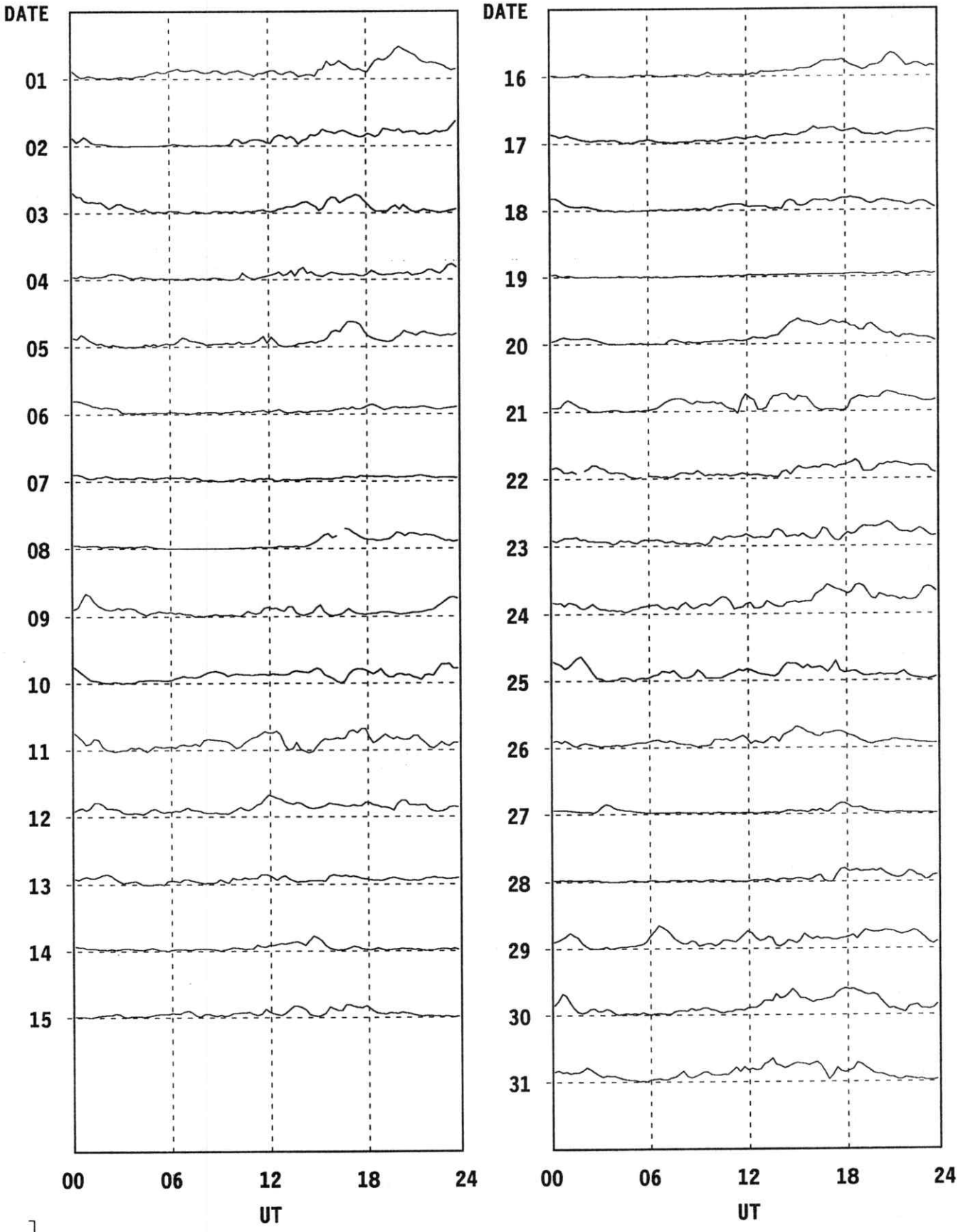

20

Preliminary Values.

15-min. Values.

Div. Geophys. D M I

PC-INDEX

Thule **February, 1990**

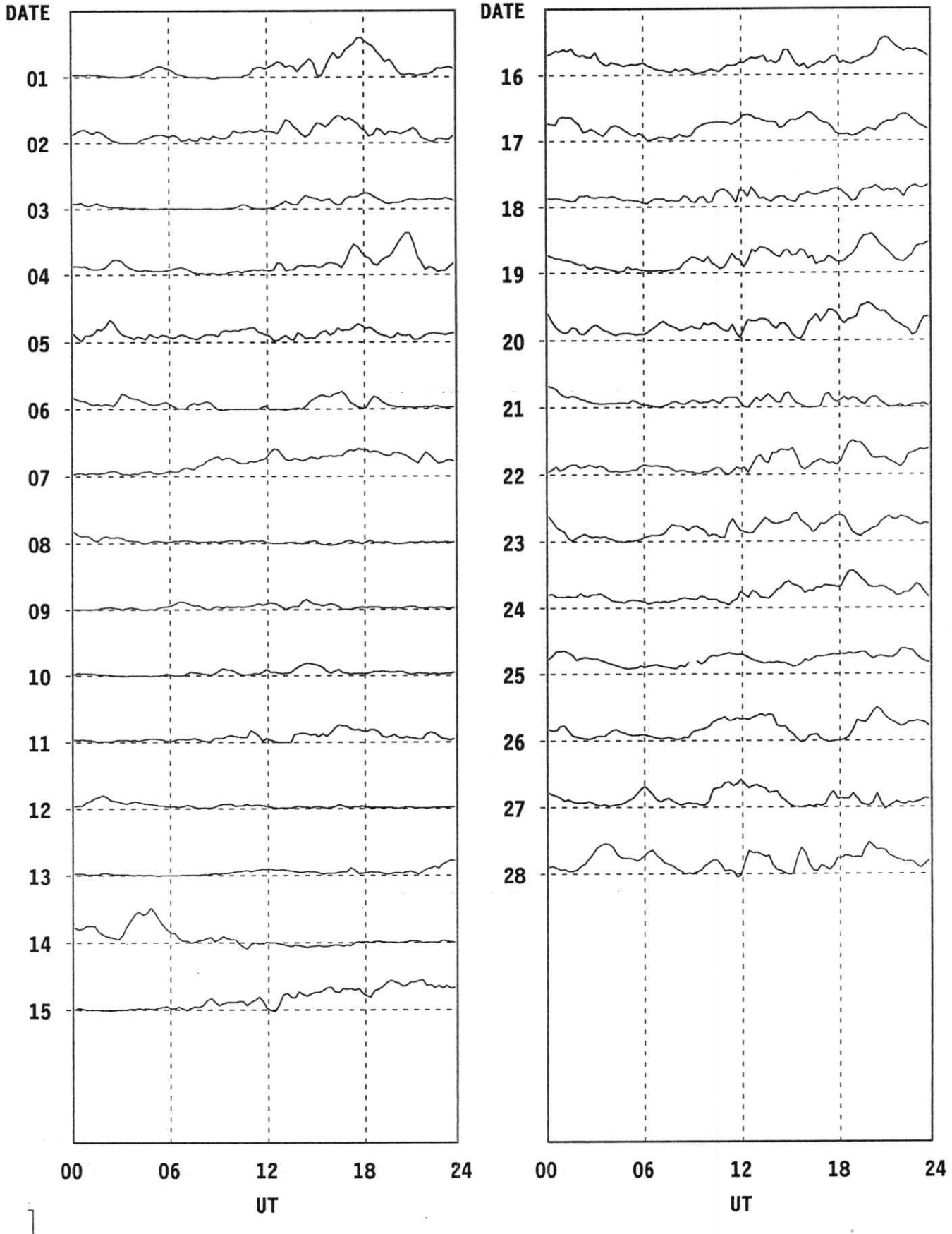

20

Preliminary Values.

15-min. Values.

Div. Geophys. D M I

PC-INDEX

Thule **March, 1990**

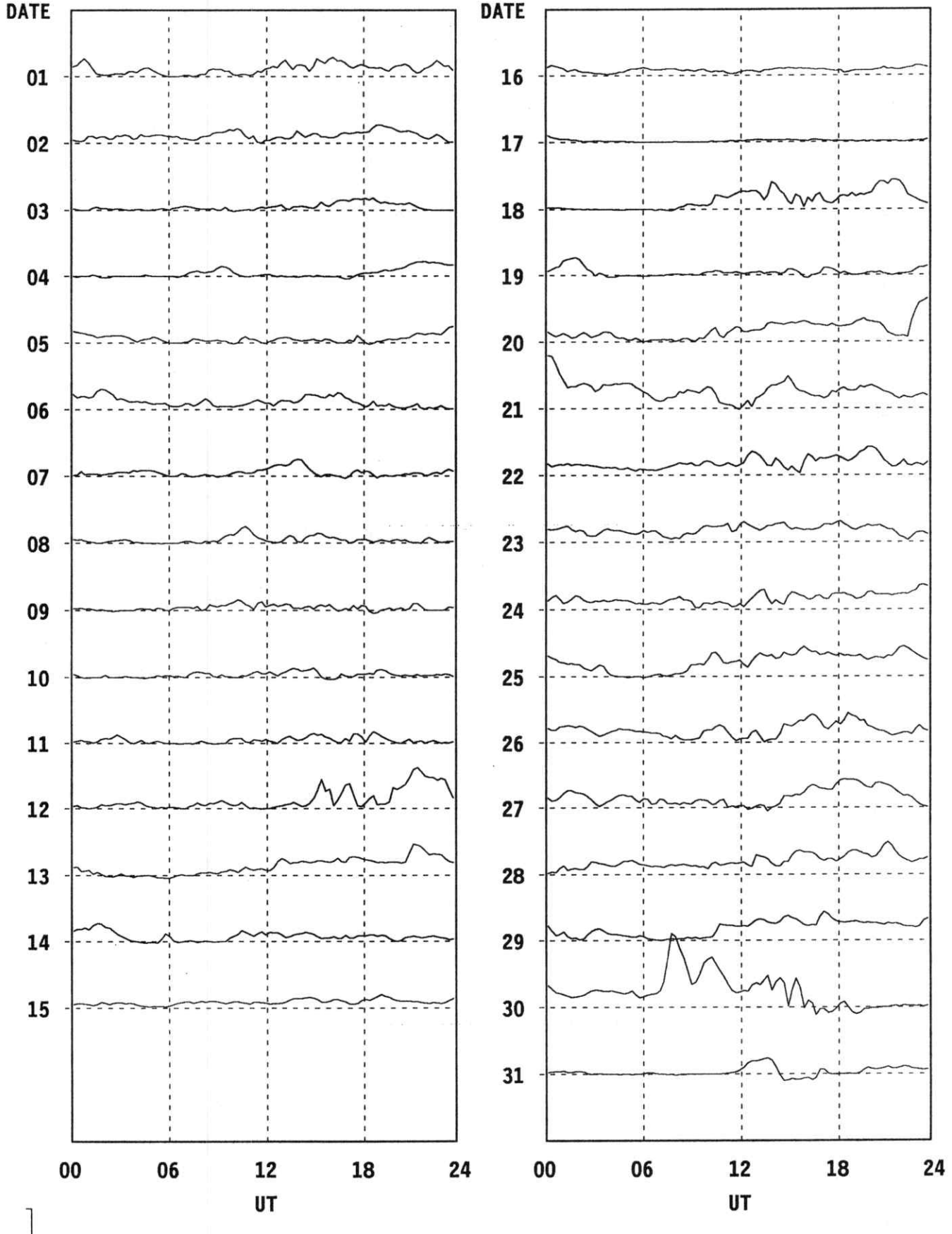

20

Preliminary Values.

15-min. Values.

Div. Geophys. D M I

PC-INDEX

Thule

April, 1990

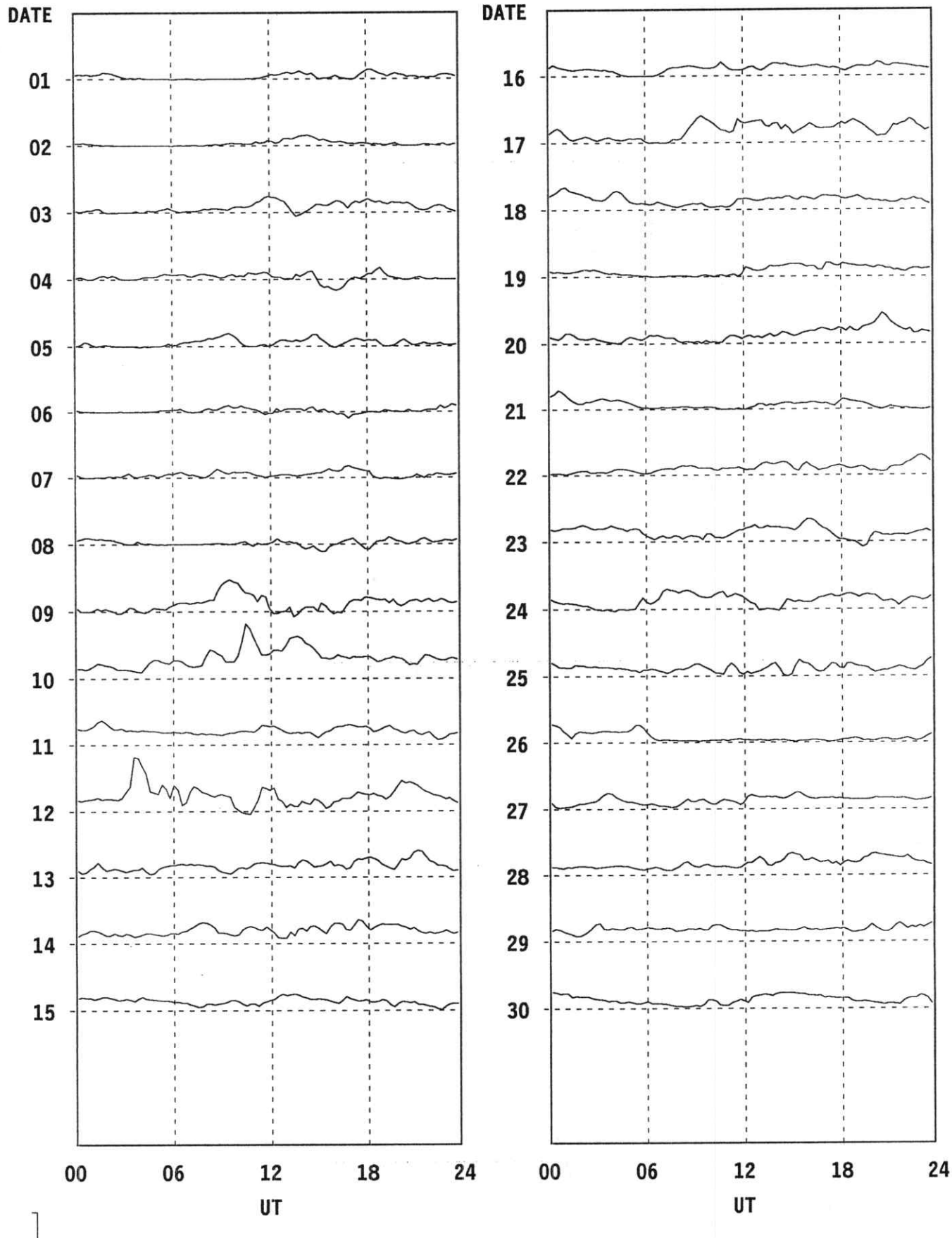

20

Preliminary Values.

15-min. Values.

Div. Geophys. D M I

PC-INDEX

Thule **May, 1990**

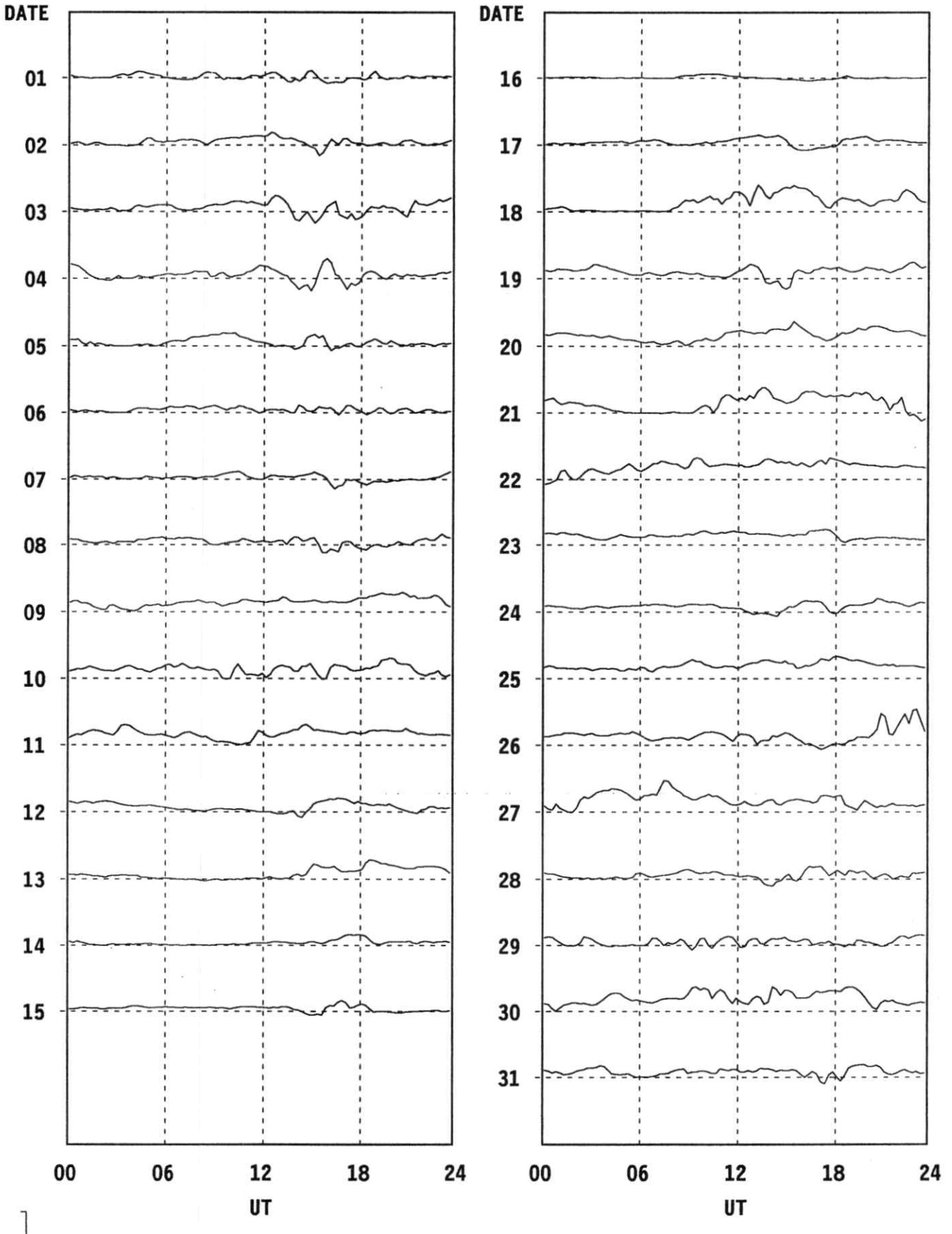

20

Preliminary Values.

15-min. Values.

Div. Geophys. D M I

Appendix B:

The magnetic field filed at the solar source surface, shown as contour maps. Each panel shows one solar rotation plus an additional half rotation appended to each side. The numbers indicated are Carrington rotation numbers. The horizontal lines denote ±70 degrees and the equator. Rotations that include Jan. 1 are labelled in the center with the new year. Regions of negative polarity, where the field is directed in to the sun are shaded and indicated with dashed contour lines. The thinner solid lines identify positive field regions and the broad solid contour is the neutral line. Reproduced from Hoeksema and Scherrer [1986].

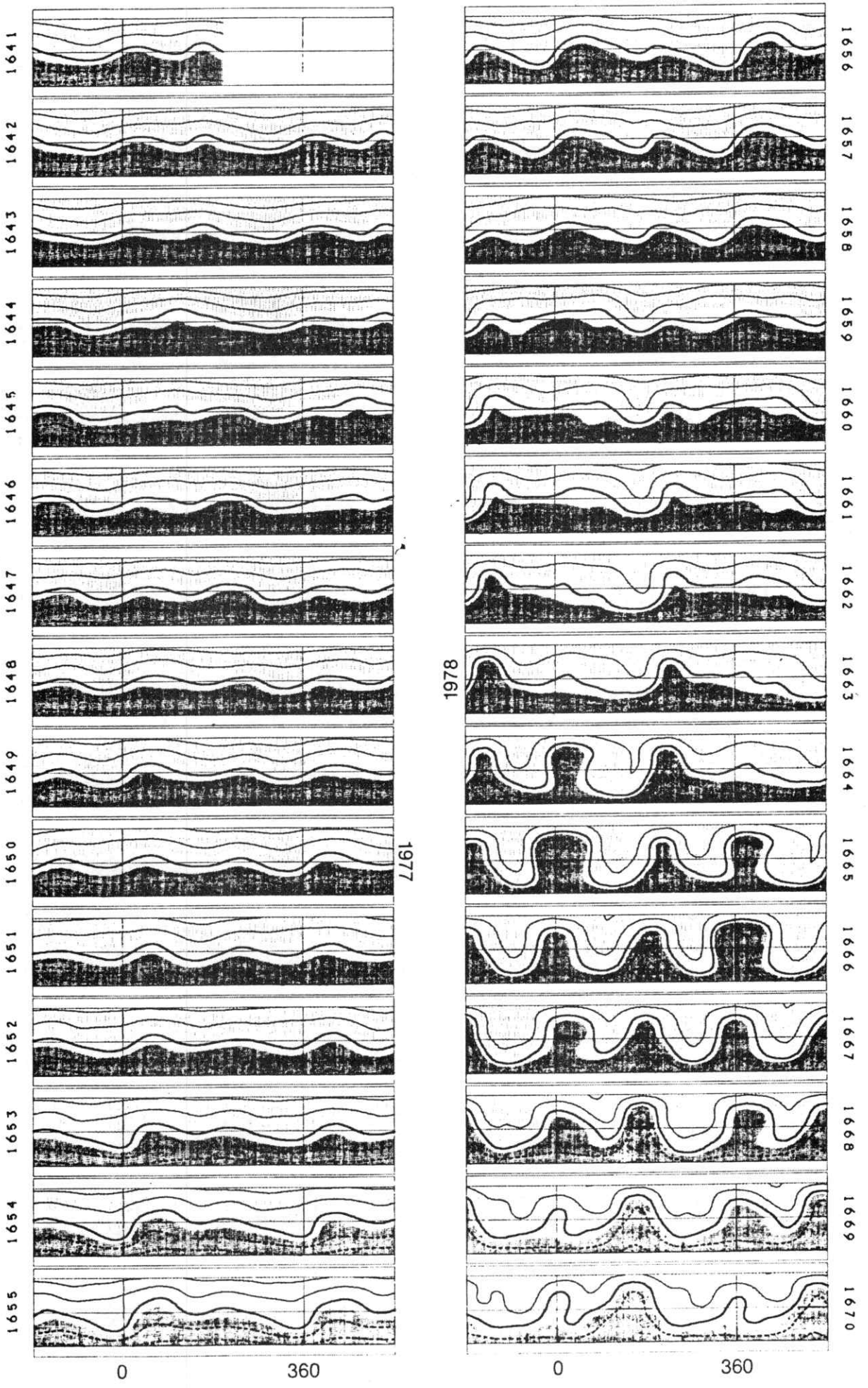
THE FIELD AT THE SOURCE SURFACE: 1976-1978
1641
1642
1643
1644
1645
1646
1647
1648
1649
1650
1651
1652
1653
1654
1655
1977
0
360
1978
1656
1657
1658
1659
1660
1661
1662
1663
1664
1665
1666
1667
1668
1669
1670
0
360

THE FIELD AT THE SOURCE SURFACE: 1978-1980

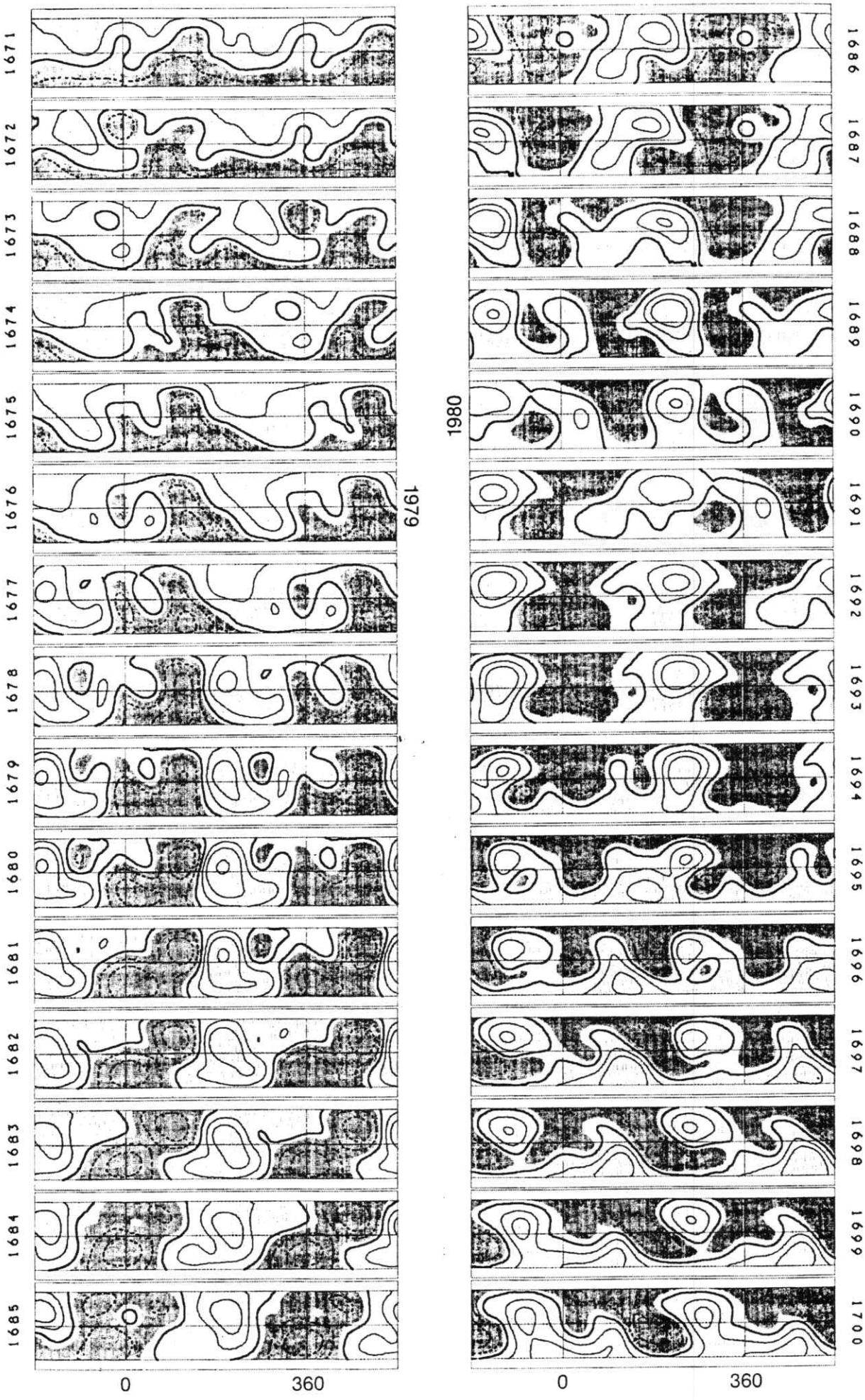

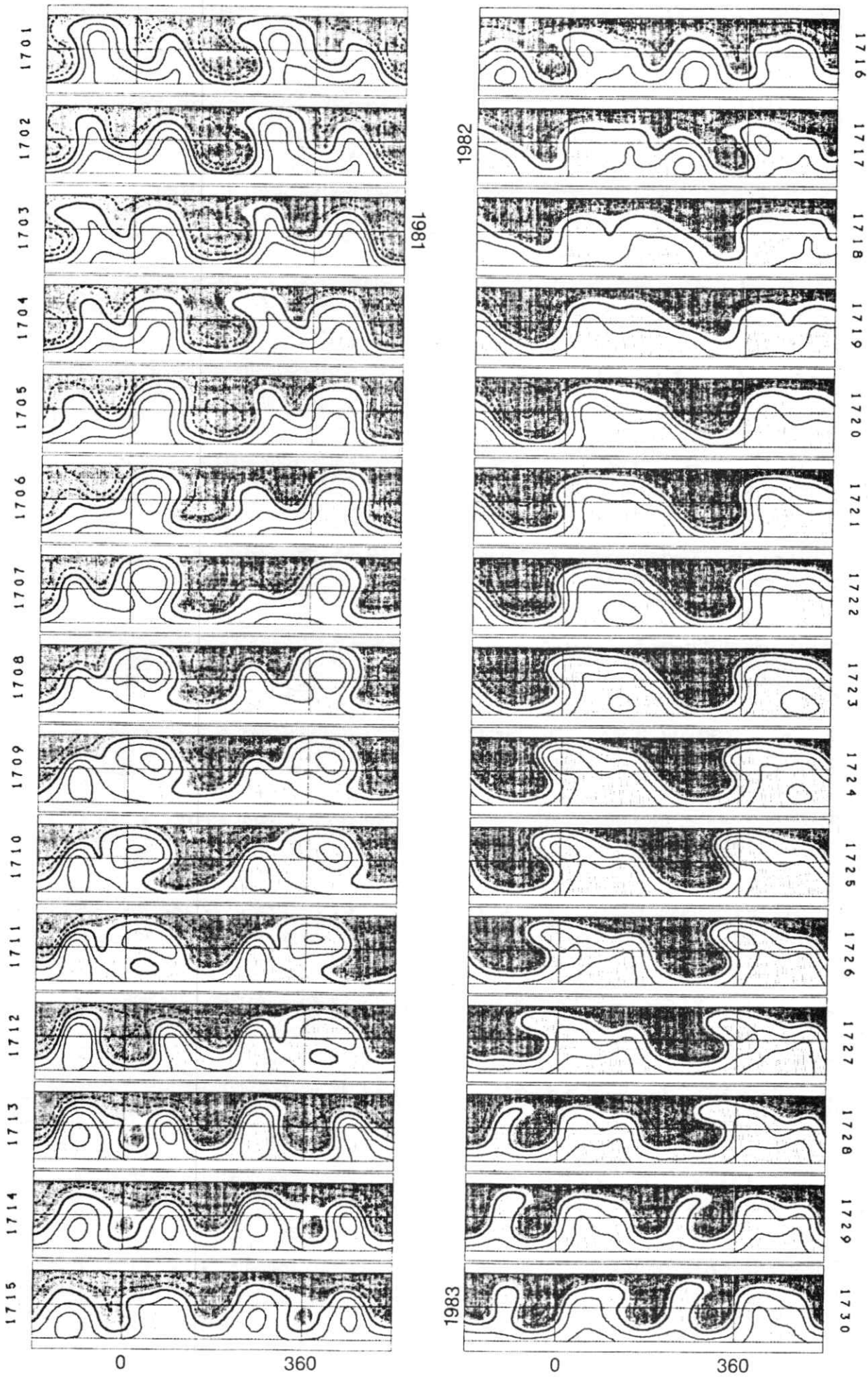
THE FIELD AT THE SOURCE SURFACE: 1980-1982
1981
1982
1983
1701
1702
1703
1704
1705
1706
1707
1708
1709
1710
1711
1712
1713
1714
1715
1716
1717
1718
1719
1720
1721
1722
1723
1724
1725
1726
1727
1728
1729
1730
0
360
0
360

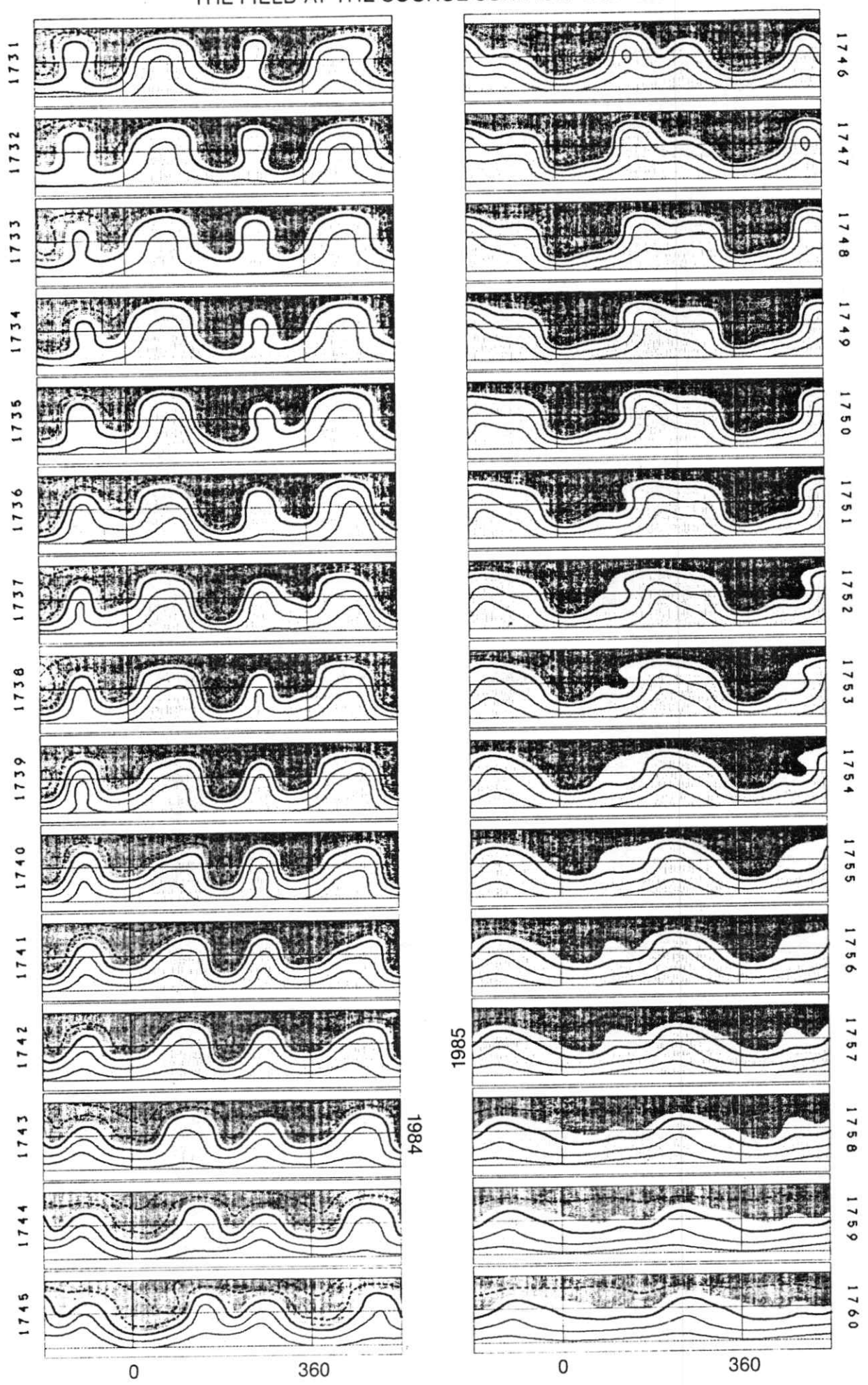
THE FIELD AT THE SOURCE SURFACE: 1983-1985
1731
1732
1733
1734
1735
1736
1737
1738
1739
1740
1741
1742
1743
1744
1745
1984
0
360
1746
1747
1748
1749
1750
1751
1752
1753
1754
1755
1756
1757
1758
1759
1760
1985
0
360